



Norwegian University of
Science and Technology

Experimental weathering of microplastic under simulated environmental conditions

Method development and characterization of
pristine, photodegraded and mechanically
weathered microplastic

Marion Olsen Hepsø

Environmental Toxicology and Chemistry

Submission date: March 2018

Supervisor: Rudolf Schmid, IKJ

Co-supervisor: Andy M. Booth, SINTEF

Iurgi Imanol Salaverria-Zabalegui, IBI

Norwegian University of Science and Technology
Department of Chemistry

Marion Olsen Hepsø

Experimental weathering of microplastic under simulated environmental conditions

Method development and characterization of
pristine, photodegraded and mechanically
weathered microplastic

Environmental Toxicology and Chemistry

Trondheim, March 2018

Supervisor: Rudolf Schmid, IKJ

Co-supervisor: Andy M. Booth, SINTEF

Iurgi Imanol Salaverria-Zabalegui, IBI

Norwegian University of Science and Technology

Faculty of Natural Sciences

Department of Chemistry



NTNU – Trondheim
Norwegian University of
Science and Technology

Abstract

The aim of this master thesis was to investigate the physico-chemical changes of microplastic (MP) weathered under simulated environmental conditions: floating on the ocean surface and in the intertidal zone. Polyethylene (PE) and polystyrene (PS) of two different sizes (10 and 100 μm) were weathered in rotating seawater for 80 days under two different conditions: (1) photodegradation equivalent to ≤ 616 average days in Trondheim and (2) mechanical degradation with sediment. Sample extraction involved NaCl density separation, filtration and drying. Surface morphology and size was examined by light- and scanning electron microscopy (SEM), while chemical analysis was conducted using Fourier Transform infrared spectroscopy (FTIR) and pyrolysis-gas chromatography-mass spectrometry (Pyr-GC/MS).

Analyses revealed <1 % w/w residual sediment in the MP samples, likely due to heteroaggregation with fragmented sediment (clay), which also coated the MP particles and accumulated in gaps. A temporal trend in surface roughness was observed for the photodegraded MP. Oxidation was apparent in PS after 80 days of photodegradation, and a range of oxidation products and polymer fragments were desorbed by Pyr-GC/MS at 250 $^{\circ}\text{C}$. Pyrolysis (600 $^{\circ}\text{C}$) chromatograms of both PE and PS changed with weathering time, indicating chain scission and/or leaching of polymer oligomers. Fragmentation did not occur for the 10 μm MP particles, while the size of the 100 μm mechanically degraded MPs changed with weathering time. The size of potential MP fragments could not be assessed due to an overlapping size range with the residual sediment. Loss of small nanoplastic (NP) fragments from the MP surface is likely, but the analysis methods were not applicable to the nm-range.

The experimental challenges demonstrate the need for qualitative analysis; NaCl density separation is ineffective on inorganic particles <39 μm and visual identification of MP particles is insufficient. The use of spherical, pristine MP particles in abiotic media limits the environmental relevancy of the experiments. It can be concluded that degradation is largely initiated and accelerated by photooxidation, and PS is more susceptible to photodegradation than PE. While no reports of MP heteroaggregation with clay were found in published literature, it is a plausible sedimentation mechanism. Oxidation and heteroaggregation has implications for e.g. the interaction between MP and microorganisms, chemical adsorption/desorption, fragmentation, transport and ultimate fate in the environment.

Sammendrag

Målet i dette masterprosjektet var å simulere forvitring av mikroplast (MP), flytende på havoverflaten og i tidevannssonen, og undersøke de fysiske og kjemiske endringene over tid. To forskjellige størrelser (10 og 100 μm) av polyetylen (PE) og polystyren (PS), ble eksponert i roterende sjøvann i 80 dager, under to forskjellige forhold: (1) fotodegradering tilsvarende ≤ 616 gjennomsnittlige dager i Trondheim, og (2) mekanisk forvitring med sediment. Mikroplast-ekstrahering involverte gravitativ separasjon, filtrering og tørking. Overflatemorfologi og partikkelstørrelse ble undersøkt ved hjelp av lys- og skanningelektronmikroskop (SEM), mens kjemiske analyser ble utført med Fourier Transform infrarød spektroskopi (FTIR), og pyrolyse gaskromatografi massespektrometri (Pyr-GC/MS). MP-prøvene inneholdt sedimentrester, sannsynligvis på grunn av heteroaggregering med fragmentert sediment (leire). MP-partiklene hadde også et belegg av sediment, som i tillegg akkumulerte i fordypninger på MP-partiklene. Overflateujevnheten på de fotodegraderte MP-partiklene økte med forvitringstid. Fotodegradert PS var tydelig oksidert etter 80 dager, og en rekke oksidasjonsprodukter og polymerfragmenter ble desorbert ved Pyr-GC/MS (250 °C). Både PE og PS pyrolysekromatogram (600 °C) forandret seg med forvitringstid, noe som indikerer kjedefragmentering og/eller utlekking av polymeroligomerer. Fragmentering ble ikke observert for de minste MP-partiklene (10 μm), mens størrelsen på de største (100 μm) mekaniske forvitrede MP-partiklene endret seg med forvitringstid. Størrelsen på potensielle MP-fragmenter kunne ikke vurderes på grunn av et overlappende størrelsesområde med gjenværende sediment. Tap av nanoplast (NP) fragmenter fra MP-overflaten er sannsynlig, men analysemetodene var ikke anvendelig for partikler mindre enn 3 μm .

De eksperimentelle utfordringene understreker behovet for kvalitative analyser; gravitativ separasjon med NaCl er ineffektivt på uorganiske partikler $< 39 \mu\text{m}$, og visuell identifisering av MP-partikler er utilstrekkelig. Bruken av sfæriske, nye MP-partikler i abiotiske media begrenser eksperimentenes miljømessige relevans. Det kan konkluderes med at nedbrytning i stor grad settes i gang og akselereres av fotooksidering, og PS blir lettere fotooksidert enn PE. Ingen publisert litteratur ble funnet ang. heteroaggregering av MP og leire i havmiljøet, som er en tenkelig sedimenteringsmekanisme. Oksidering og heteroaggregering har implikasjoner for bl.a. samspillet mellom MP og mikroorganismer, kjemisk adsorpsjon/desorpsjon, fragmentering, transport og endelig skjebne i havmiljøet.

Preface

This master's thesis was written as a part of the Environmental Chemistry and Toxicology program at NTNU in the period August 2015 – March 2018, with a delay due to leave of absence. As the project was a collaboration with SINTEF it was jointly funded by SINTEF and NTNU. Weathering experiments were carried out at SINTEF Sealab, while sample analysis was carried out at both SINTEF Sealab and NTNU (Sealab and Gløshaugen). Preliminary results of this thesis were presented at the SETAC Europe conference in Brussels, May 2017.

Acknowledgements

I would like to thank the following persons for supporting me both practically, theoretically and morally during the production of this master's thesis:

My external supervisor, Andrew Booth, for granting me an exciting project and guiding me through it with clear objectives. I appreciate your effectiveness and style of supervision - challenging me to critical thinking and decision-making.

My internal supervisor, Rudolf Schmid, for training and guiding me through the pyrolysis-GC/MS analysis, and for valuable input and feedback throughout the project. Your positive attitude, patience and dedication never failed to cheer up my day.

NTNU staff, including Yingda Yu for electron microscopy training and support, Tora Bardal for light microscopy training and support, Jon Erik Aaseng for support with ATR-FTIR issues, Martin Wagner for input on biological aspects and Alexandros Asimakopoulos for thesis feedback.

Staff at SINTEF Ocean, including Kristin Bonaunet for guidance in the laboratory and help with risk assessment, Roman Netzer for Coulter Counter training, Julia Farkas for experimental input and Lisbeth Sørensen for input and Pyr-GC/MS training. I would also like to thank the rest of the laboratory staff for a welcoming and friendly environment, showing me laboratory procedures and helping me find necessary equipment.

Fellow students and friends, for procrastination coffee-breaks, laughter and competitive comparison of experimental failures that helped us realize that things are "not so bad after all".

My family, for moral support, significant share of household duties and love during the challenging periods of this project.

Table of contents

ABBREVIATIONS AND ACRONYMS	XIII
1 INTRODUCTION	1
1.1 THE USE OF PLASTIC	1
1.2 PLASTIC WASTE	1
1.3 PLASTIC MARINE DEBRIS.....	3
1.4 ENVIRONMENTAL IMPACT OF PLASTIC.....	4
1.5 STUDY AIM AND OBJECTIVES.....	7
2 BACKGROUND	9
2.1 SYNTHETIC POLYMERS	9
2.1.1 <i>Common types of synthetic polymers</i>	9
2.1.2 <i>Polymer additives</i>	11
2.2 (MICRO)PLASTIC IN THE MARINE ENVIRONMENT – CURRENT STATUS OF KNOWLEDGE	13
2.2.1 <i>Occurrence</i>	13
2.2.2 <i>Distribution</i>	15
2.3 DEGRADATION	16
2.3.1 <i>Physical degradation</i>	16
2.3.2 <i>Photodegradation</i>	18
2.3.3 <i>Release of associated substances</i>	21
2.4 ANALYSIS OF MICROPLASTICS.....	22
2.4.1 <i>Chemical characteristics</i>	22
2.4.2 <i>Size</i>	26
2.4.3 <i>Morphology</i>	27
2.4.4 <i>Experimental considerations</i>	28
3 EXPERIMENTAL	31
3.1 EQUIPMENT AND MATERIALS	31
3.2 CONTAMINATION CONTROL	32
3.3 WEATHERING EXPERIMENTS.....	33
3.3.1 <i>Photodegradation</i>	34
3.3.2 <i>Mechanical degradation</i>	36
3.4 SAMPLE ANALYSIS.....	39
3.4.1 <i>Light microscopy</i>	39
3.4.2 <i>Scanning electron microscopy</i>	39
3.4.3 <i>Fourier Transform infrared spectroscopy</i>	40
3.4.4 <i>Pyrolysis-gas chromatography-mass spectrometry</i>	41
3.4.5 <i>Coulter Counter</i>	42
3.4.6 <i>Data processing</i>	42

3.5	METHOD DEVELOPMENT	43
3.5.1	<i>Separation of microplastics from sediment</i>	43
4	RESULTS	49
4.1	CHARACTERIZATION OF PRISTINE MICROPLASTIC MATERIALS	49
4.2	RECOVERIES	55
4.3	PHOTODEGRADED MICROPLASTIC	56
4.3.1	<i>Discolouration</i>	56
4.3.2	<i>Shape and morphology</i>	57
4.3.3	<i>Chemical characteristics</i>	60
4.3.4	<i>Size distribution</i>	67
4.4	MECHANICALLY WEATHERED MICROPLASTIC.....	68
4.4.1	<i>Shape and morphology</i>	68
4.4.2	<i>Chemical characteristics</i>	73
4.4.3	<i>Size distribution</i>	79
5	DISCUSSION.....	85
5.1	PHOTODEGRADATION.....	85
5.1.1	<i>Exposure conditions and extraction procedure</i>	85
5.1.2	<i>Chemical changes</i>	85
5.1.3	<i>Fragmentation</i>	90
5.2	MECHANICAL DEGRADATION	90
5.2.1	<i>Exposure conditions and extraction procedure</i>	90
5.2.2	<i>Interaction with sediment particles</i>	91
5.2.3	<i>Fragmentation</i>	93
5.2.4	<i>Chemical changes</i>	94
5.3	EVALUATION OF THE METHOD	95
5.3.1	<i>Experimental design</i>	95
5.3.2	<i>Contamination</i>	95
5.3.3	<i>Analysis methods</i>	98
5.4	SUMMARY	100
5.5	IMPLICATIONS AND SUGGESTIONS FOR FUTURE RESEARCH.....	102
5.5.1	<i>Toxicity</i>	104
5.5.2	<i>Fate of microplastic in the marine environment</i>	102
5.5.3	<i>Nanoplastic, fibres and plastic debris in terrestrial/freshwater ecosystems</i>	104
	CONCLUSION	107
	REFERENCES	109
	APPENDIX	121

Abbreviations and acronyms

ATR	Attenuated total reflectance
CI	Confidence interval
DI	De-ionized
EDS	Energy dispersive X-ray spectroscopy
EPS	Expanded polystyrene
FE-SEM	Field emission scanning electron microscopy
FTIR	Fourier transform infrared spectroscopy
GC	Gas chromatography
HDPE	High-density polyethylene
IR	Infrared
LDPE	Low-density polyethylene
LOD	Limit of detection
MP	Microplastic
MS	Mass spectrometry
MW	Molecular weight
NP	Nanoplastic
PE	Polyethylene
PE-10	10 μm polyethylene microspheres
PE-100	100 μm polyethylene particles
PP	Polypropylene
PS	Polystyrene
PS-10	10 μm polystyrene microspheres
PS-100	100 μm polystyrene particles
Pyr-GC/MS	Pyrolysis-gas chromatography-mass spectrometry
SA/V	Surface area to volume ratio
SD	Standard deviation
SEM	Scanning electron microscopy
SW	Seawater
UV-Vis	Ultraviolet and visible light
X_A	Area equivalent diameter

1 Introduction

1.1 The use of plastic

Polymers, from the Greek words *poly* (“many”) and *mer* (“parts”), are high molecular weight substances made up of macromolecules of repeating units. They can be grouped into natural and synthetic polymers, depending on whether the macromolecules are sourced from plants/animals or synthesized from smaller molecules, respectively. Wool, cellulose and DNA are examples of natural polymers, while synthetic polymers include polyethylene, nylon and Teflon. The majority of synthetic plastic products are produced from oil and gas resources, of which 5 % of is allocated to plastic manufacturing in Europe (PlasticsEurope, 2016). In between there are semi-synthetic polymers, which are chemically processed natural polymers (e.g. cellulose rayon) (Nic et al., 2006). Of the global plastic production in 2015, bio-based and bio-degradable polymers made up <1 and <0.3 %, respectively (Geyer et al., 2017, European Bioplastics, 2016). Synthetic polymers, commonly referred to as plastic, are ubiquitous in contemporary society. To name a few, plastic is used to make vehicle parts, building materials, microelectronics, workplace equipment, furniture, prostheses, glasses, food equipment, recreational equipment, general household items and as packing material. The use of synthetic polymers can perhaps be explained by low cost relative to alternative materials, and in some cases superior properties. Astonishing developments include conducting and light-emitting polymers (Zhang et al., 2015), and synthesis of a wide range of biopolymers used in e.g. drug delivery (Misra and Shahiwala, 2014). Plastic production also plays a key role in many countries; in Europe the plastic industry employs 1.5 million, with an annual turnover of 350 billion (PlasticsEurope, 2016). The terms plastic and synthetic polymers will be used interchangeably in this thesis.

1.2 Plastic waste

Synthetic plastic products are designed to be durable and do not decompose easily in the environment compared to natural polymers, leading to accumulation. It is estimated that 8.3 billion tons plastic has been produced since the 1950s, of which 79 % has ended up in landfills or the natural environment. Of this, 12 % is fibres of polyester, polyamide and polyacrylonitrile. In 2015, 380 million tons of plastic was produced (not including fibrous plastic), of which 93

million tons (24 %) ended up in landfills or the environment instead of being incinerated or recycled (Geyer et al., 2017). Although plastic waste management has improved since the 1950s, 24 % is far from a negligible number. Improvement of the current state of plastic pollution is however challenging due to a growing global population, habitual use of plastic consumables, and overall insufficient waste-management.

In Europe, packaging accounts for 40 % of the plastic demand (PlasticsEurope, 2016); i.e. material that is only used once before it is discarded. On the other hand, plastic waste only comprises about 10 % of total waste generated. One of the aims of the latest EU proposal, the *Circular Economy Action Plan*, is that by 2030 all plastic packaging should be either reusable or recyclable, and a 75 % recycling target. The proposed four-fold increase in plastic sorting and recycling is expected to create 200,000 new jobs (EU, 2018). A global change in the direction of a circular plastic economy is however not as straightforward; in addition to conflicting interests between industry, consumers, scientists and policymakers, waste management is not prioritized (or non-existent) in the most populated countries. Plastic products are readily available and affordable, and although consumer awareness of the problems related to plastic (waste) has increased in the last decade, plastic production is still exponentially increasing and thought to reach 1.2 billion tons in 2050 (EU, 2017). An improvement of today's plastic culture might be driven by economic interests; The World Economic Forum aims for alternative sources, better design and re-use of plastic. Such changes will enable a decrease of the current value loss of 95 % due to the low rate and yield of recycling (WEF, 2016).

The main sources of plastic waste in the UK is household packaging (41 %), commercial and industrial packaging (17 %), building and construction (10 %), electrical/electronics (7 %) and furniture/housewares (7 %) (Hopewell et al., 2009). Of the plastic waste that is not incinerated or recycled, 87 % resides in landfills, terrestrial and freshwater environments (unknown distribution), while 13 % ends up in the marine environment. In addition to the abovementioned mega- and macroplastic waste that can fragment to form secondary sources of microplastic (MP), it has been estimated that 84 million tons of primary MP is released annually. Main sources of primary MP is vehicle tire dust, primary polymer beads spills, paint and synthetic textiles; a polyester garment can produce more than 1900 fibres per wash (Browne et al., 2011). Although synthetic fibres are efficiently removed by wastewater treatment plants, sewage sludge commonly ends up in agricultural or forest soils. Most primary MP therefore end up in the natural environment, either directly or indirectly (Ziajahromi et al., 2016).

1.3 Plastic marine debris

The amount of plastic in the ocean as of 2013 has been estimated to be 86 million tons (Jang, 2015), with between 4.8 and 12.7 million tons entering the ocean only in 2010. Estimates indicate that the majority of marine plastic debris originate from coastal populations, 17 % is transported by rivers from inland populations and 14 % is comes from fishing and shipping activities and (Lebreton et al., 2017). The countries with the highest contribution to plastic marine debris are not those with the highest plastic waste production per capita, but those with greatest percentage of mismanaged plastic waste. Along with a large coastal population, this makes China the greatest contributor, followed by other coastal Asian and African countries, with Brazil, EU and the United States ranked 16th, 18th and 20th, respectively (Jambeck et al., 2015). The Northern Hemisphere holds more of the plastic marine debris than the Southern Hemisphere, and the fraction that resides in coastal waters is concentrated around populated areas and river mouths (Barnes et al., 2009)

Figure 1.1 illustrates the input of plastic waste to the marine environment and where in the ocean it is likely to reside; astonishingly only 1 % floats on the sea surface (Eunomia, 2016). From ocean trawling data and oceanographic modelling, the mass of plastic floating on the ocean surface has been estimated to 270 000 tons. Plastic concentrations on shorelines are still increasing, but the quantity of meso- and macroplastic (5-20 and >20 mm, respectively) on open ocean surfaces has stabilized. The quantity MP (<5 mm) is significantly less than what is expected from fragmentation modelling, indicating a loss of this fraction from the surface to the water column or ocean floor (Eriksen et al., 2014, Barnes et al., 2009). Several studies indicate that a substantial fraction of MP and perhaps also nanoplastic (NP) particles end up in ocean sediments (Woodall et al., 2014, Van Cauwenberghe et al., 2013). Systematic sampling of the whole ocean is however impossible, causing significant uncertainties in distribution modelling of marine plastic debris. Challenging sampling and quantification of plastic in the lower micron- and nano range also contribute to uncertainties. The plastic not residing on the surface, along shorelines or in sediments is often referred to as the “missing fraction” (Woodall et al., 2014).

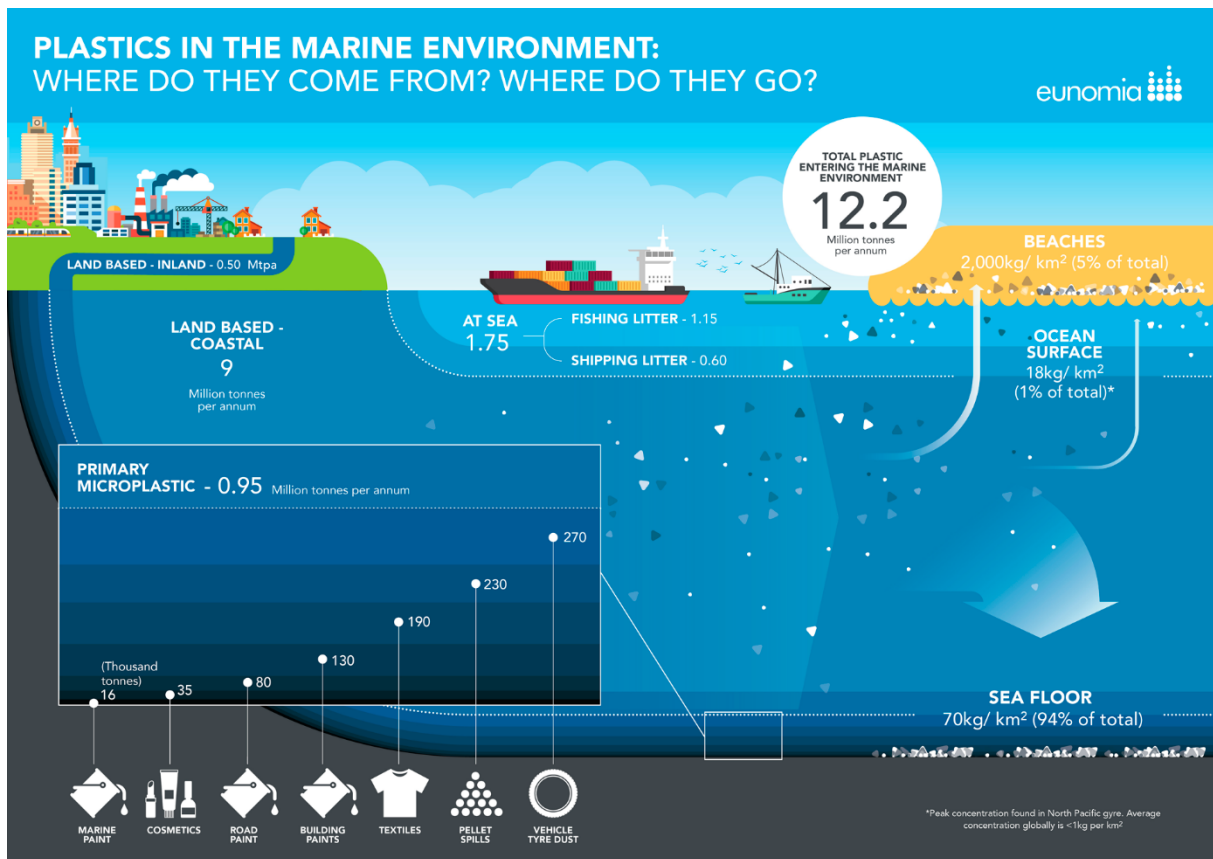


Figure 1.1: *Plastics in the marine environment: Where do they come from? Where do they go?*(Eunomia, 2016).

1.4 Environmental impact of plastic

Despite their versatility, synthetic polymers, like many other materials and consumables, impact the environment in numerous ways. Figure 1.2 displays a number of environmental impact categories, and the relative contribution of different finished materials, including plastic (data from 27 European countries plus Turkey in 2000) UNEP (2010). Interestingly, the main contributor to the category *Human Toxicity* is plastic, with a relative contribution of more than 25 %, followed by coal and metals, likely due to our continuous exposure to plastic materials in modern society. Toxicity to organisms other than humans are not included in the figure. The last category in Figure 1.2, *Environmentally Weighted Material Consumption* (EMC), is an indicator which in simple terms is the product of the total environmental impact (including i.a. CO₂ emissions and eco-toxicity) of a material throughout its life cycle, and the mass of material flow. The relative EMC score of plastic is in the lower range, explained by the negligible land use and low relative mass consumption. Nevertheless, the toxic effects of plastic on organisms is an area of importance and public concern, whether direct or indirect.

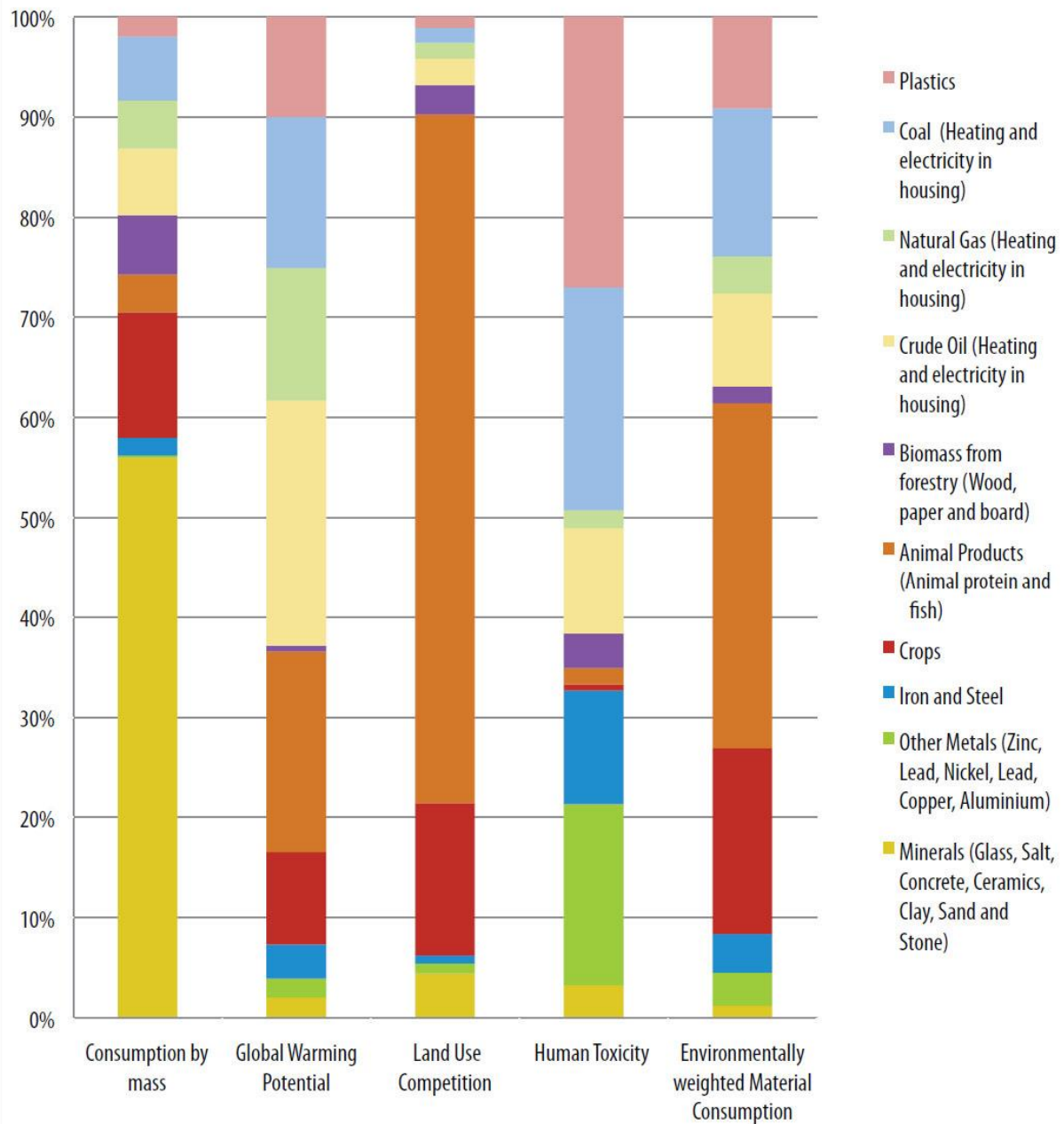


Figure 1.2: The relative contribution of different finished materials to various environmental impact categories, in the 27 European countries plus Turkey, 2000 (UNEP, 2010).

While environmental toxicity during production is often overlooked, the aspects of plastic toxicity during use and after disposal has gained great attention in both science and public media in the last decade(s). A classic example of plastic toxicity concern during use includes the potential leaching of polymer additives such as bisphenol-A from plastic food and water containers. As an endocrine disruptor, bisphenol-A is possibly correlated with a range of effects in humans (Seachrist et al., 2016).

The potential toxicity of synthetic polymers after disposal is the rationale behind assessing the degradation and fate of plastic waste ending up in the natural environment: the incentive for this study. The public awareness of issues associated with plastic waste has increased in the last decade, mainly due to media reports of large masses of plastic floating in the ocean and plastic ingested by animals, such as the image in Figure 1.3.



Figure 1.3: *Plastic in stomach contents of a dead albatross chick (Jordan, 2009).*

The slow degradation rate of synthetic polymers results in a longer lifetime in the environment during which they potentially can cause harmful effects on biota. Adverse environmental effects can be classified as either physical or chemical: examples of physical effects are accumulation in natural habitats, entanglement and gastrointestinal obstruction due to ingestion. Chemical effects are due to the polymer itself and/or associated substances. In the marine environment, plastic can enter the ecosystem through ingestion, either through seawater filtering, accident or selectively - several species mistake micro- and mesoplastic for food, including several seabird, cetacean and fish species (Sigler, 2014). Other routes are through trophic transfer and external adhesion. Microplastic has been detected in a large range of marine species, including zooplankton, fish and blue mussels (Frias et al., 2014, Collard et al., 2015, Phuong et al., 2017). Although a large portion of ingested MP is egested for some species, laboratory experiments

have shown various effects on growth, behaviour and reproduction, as well as trophic transfer (Chae and An, 2017). MP has also been found to be taken up in the circulatory system of blue mussels (Browne et al., 2008).

Although the types of plastic that account for the bulk mass are considered non-toxic in themselves (Lithner et al., 2011), there are toxicity concerns due to the range of incorporated additives. In addition to the potential leaching of additives, plastic debris, especially in the marine environment, might act as vectors for environmental pollutants and pathogens (Wright et al., 2013, Vethaak and Leslie, 2016, Ivar do Sul and Costa, 2014). Although there is a current “boom” in research on the fate and potential adverse effects of plastic debris, there are numerous knowledge gaps that need to be filled regarding plastic degradation. This is particularly true for plastic debris ending up in the ocean; a dynamic environmental compartment where the transportation, break-down and ultimate fate of plastic waste is largely dependent upon factors such as the local ecosystem, ocean currents and climate.

1.5 Study aim and objectives

Background research revealed limited published literature regarding the weathering of plastic in the micron size range. To potentially increase the knowledge on weathering of common types of plastic in the marine environment, the following study aim and objectives were composed:

Aim	<i>Develop and carry out a method for assessing the weathering of microplastic in the marine environment</i>
Objectives	<ol style="list-style-type: none">(1) <i>Simulate photodegradation at the sea surface through UV-Vis light irradiation of suspended microplastic particles</i>(2) <i>Simulate mechanical degradation in the intertidal zone through microplastic-sediment interaction</i>(3) <i>Investigate the temporal changes (physical and chemical) of the experimentally weathered microplastic in Objectives (1) and (2)</i>

It was hypothesised that UV-Vis irradiation would cause oxidation and desorption of polymer-associated substances (e.g. additives) and that physical impact with sediment at shorelines would cause fragmentation. Weathering was expected to depend on factors such as polymer type and size, and particularly on the surface area to volume ratio.








2 Background

2.1 Synthetic polymers

2.1.1 Common types of synthetic polymers

An overview of the most common synthetic polymers (excluding fibres) is shown in Table 2.1, listed in order of global annual production quantity. Combined, low- and high-density polyethylene (LDPE and HDPE) make polyethylene (PE) the most prevalent polymer, making up 34.4 % of the demand (PlasticsEurope, 2016, Ellis and Smith, 2008)

Table 2.1: Overview of the most common synthetic polymers.

Name	Acronym	Density (g/cm ³)	Symbol	Present uses
Polypropylene	PP	0.90		Food containers
Low-density polyethylene	LDPE	0.92		Soft bottles, toys
Poly(vinyl chloride)	PVC	1.39		Pipes, lawn chairs, non-food containers
High-density polyethylene	HDPE	0.94		Hard bottles, plastic bags
Polystyrene	PS	1.05		Disposable cutlery, food containers, building isolation, styrofoam
Poly(ethylene terephthalate)	PET	1.38		Bottles, food packaging, tape
Others: Polyurethanes, other thermoplastics, ABS/ASA/SAN, polycarbonate, polyacrylates				Fishing lines, food packaging, tooth brushes, foams, adhesives, industrial applications

Most synthetic polymers (including PE, PP, PVC, PS and PET) are thermoplastics: polymers that can be repeatedly heated to a softening point and cooled to solidify. Intermolecular forces hold the polymer chains together, as opposed to thermosets in which polymer chains are covalently bonded and decompose upon heating. Figure 2.1 shows the chemical structure of the two polymer types used in this study, PE and PS, and illustrates the degree of polymer chain branching in PE that separates LDPE from HDPE. The minimal branching in HDPE allows the polymer chains to pack closer together, making it a harder and less flexible polymer than LDPE. Other sub-categories of PE also exist, e.g. linear low-density (LLDPE), ultra-high molecular weight (UHMPE) and crosslinked (XLPE).

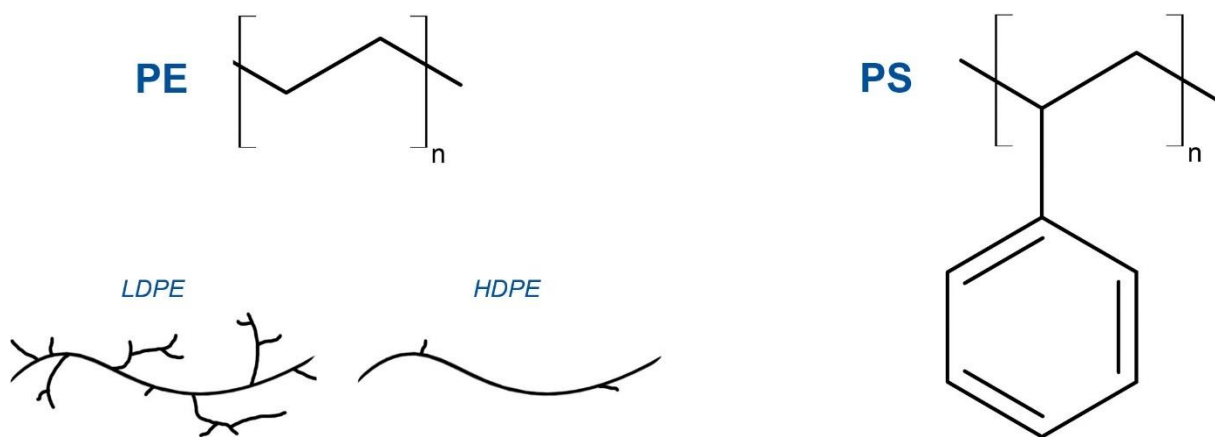


Figure 2.1: Chemical structure of polyethylene (PE) and polystyrene (PS), and an illustration of the polymer chain branching differences of low- and high-density polyethylene (LDPE and HDPE).

The molecular weight (MW) of commercial PE and PS is typically 10,000-1,000,000 and 100,000-300,000 Da, respectively. The polymers are highly customizable; the molecular weight, branching, orientation (tacticity) of the polymer chain and blend (mixture of e.g. LDPE and HDPE) can be optimized for the desired product. The popularity of HDPE can be attributed to its low density, high durability and biological and chemical resistance – it is only decomposed by strong oxidizing agents. Chemical resistance is lower for LDPE, but its greater flexibility makes it a convenient packaging material. As the melting points of LDPE, HDPE and PS are 80-115, 105-135 and 210-270 °C, respectively. PS is superior to PE when a higher operating temperature or transparency is necessary, and foamed PS (expanded and extruded polystyrene; EPS and XPS) is widely used in light-weight, shock absorbing and insulating products (Robertson, 2016).

The chemical toxicity of the most common polymers (except PVC) is low: in a chemical health ranking of 55 polymers, PE, PP, PS, and PET were all on the bottom of the list, while PVC was ranked 6th mainly due to its toxic monomer (Lithner et al., 2011). The toxicity assessment did not include endocrine disrupting properties (of e.g. the styrene monomer) or incorporated additives, which can significantly affect the actual safety of plastic products. Residential burning is not considered safe, as the decomposition products formed at intermediate temperatures (300 - 1000 °C) include polycyclic aromatic hydrocarbons (PAHs), in addition to the polymer-characteristic pyrolysis products: low-MW hydrocarbons for PE, and styrene monomer and oligomers for PS. Combustion at incineration plants (>1000 °C) yields primarily CO and H₂O (Ellis and Smith, 2008, Bolgar et al., 2015).

2.1.2 Polymer additives

A large variety of additives can be added to polymers to optimize physical properties and increase product lifetimes. On average, additives constitute 7 % of non-fibre plastic materials (Geyer et al., 2017). Table 2.2 presents an overview of polymer additives commonly added to PE and PS. The name of the different additive categories indicates its purpose. Plasticizers are however added to improve flexibility, extensibility and/or workability, while fillers either act as reinforcement or reduce the production cost (Wang, 2000). Plasticizers are widely used in PE, but not as greatly in PS as some negatively affect the mechanical properties. Although most additives are not chemically bonded, some are incorporated into the polymer chain to avoid leaching/volatilization, such as methacrylamide antioxidants (Ellis and Smith, 2008, Chalmers and Meier, 2008, Crompton, 2006).

In addition to additives, polymers often contain impurities from the manufacturing process, such as unreacted monomer, catalysts, solvents and lubricants. PS contains unreacted monomer, which should not exceed 1 % if used as food packaging. Side-reaction products are also common, e.g. incorporation of (hydro)peroxide groups in the polymer chain by reactions with O₂, which are believed to be initiators of photooxidation in otherwise UV-stable polymers such as PE (Ellis and Smith, 2008). Risk assessment of polymers must therefore include the potential toxicity of the polymer itself, additives and manufacturing impurities and their leaching potential. For polymers that end up in the environment, the leaching potential is relevant prior to polymer degradation, but all additives (or additive degradation products) will eventually be

released due to fragmentation and eventually mineralization, the complete breakdown of the polymer.

Table 2.2: Common additives in polyethylene (PE) and polystyrene (PS).

Additive category	Examples	Toxicity^a	Leaching^b
Antioxidants	Butylated hydroxytoluene (BHT)		x
	Bumetrizole		
	Irgafors (e.g. 168, TNPP)	x	x
	Irganox (e.g. 1010, 1076)		x
	Isoprene 1680		
Biocides	Arsenic (compounds)	x	
	Triclosan	x	x
Colorants	Azo colorants	x	
	Inorganic (Pb, Cr, Cd)	x	x
Flame retardants	Boric acid	x	
	Brominated flame retardants (e.g. HBCDD)	x	
Plasticizers	Phthalates (e.g. DEHP, DBP, DIBP)	x	x
	Benzyl benzoate		
Fillers	Glass		
	Carbon black		
UV stabilizers	Benzophenones		x
	Benzotriazoles		x
	Hindered amines		
	TiO ₂ pigment		

^a On the REACH Candidate list of substances of very high concern or Norwegian Priority List of hazardous substances.

^b Has been detected in leachates (Crompton, 2006, Suhrhoff and Scholz-Böttcher, 2016).

2.2 (Micro)plastic in the marine environment – current status of knowledge

2.2.1 Occurrence

The type, size and quantities of MP found in the marine environment vary greatly on location. Concentrations are generally higher close to populated areas but are also highly dependent on ocean currents and seawater density. As seen in Figure 2.2, the density of surface seawater in the North Atlantic Ocean is approximately 1.025 g/cm^3 , while it is significantly lower around equator and generally lower closer to land (NASA, 2009). Due to the differences in surface SW density, the relative abundance of different types of MP and their fate will differ in e.g. the North Atlantic and the Indian Ocean. In addition, ocean currents result in gyres in which plastic debris accumulate on the surface: the main ones located between the continents just above and below the equator. The highest surface concentration (up to 10 kg/km^2) is found in the North Pacific gyre, in which plastic debris from east coast of Asia and west coast of North America is accumulated (Bergmann et al., 2015). In the last two decades, the concentration of plastic on the surface has stabilized or even decreased in certain locations (van Franeker and Law, 2015). In addition, the mean size of plastic debris in the western North Atlantic Ocean decreased from 11 to 5 mm from the early 1990s to the mid-2000s (Morét-Ferguson et al., 2010). These findings indicate that the plastic debris is fragmented and mechanisms that removed the MP from the surface.

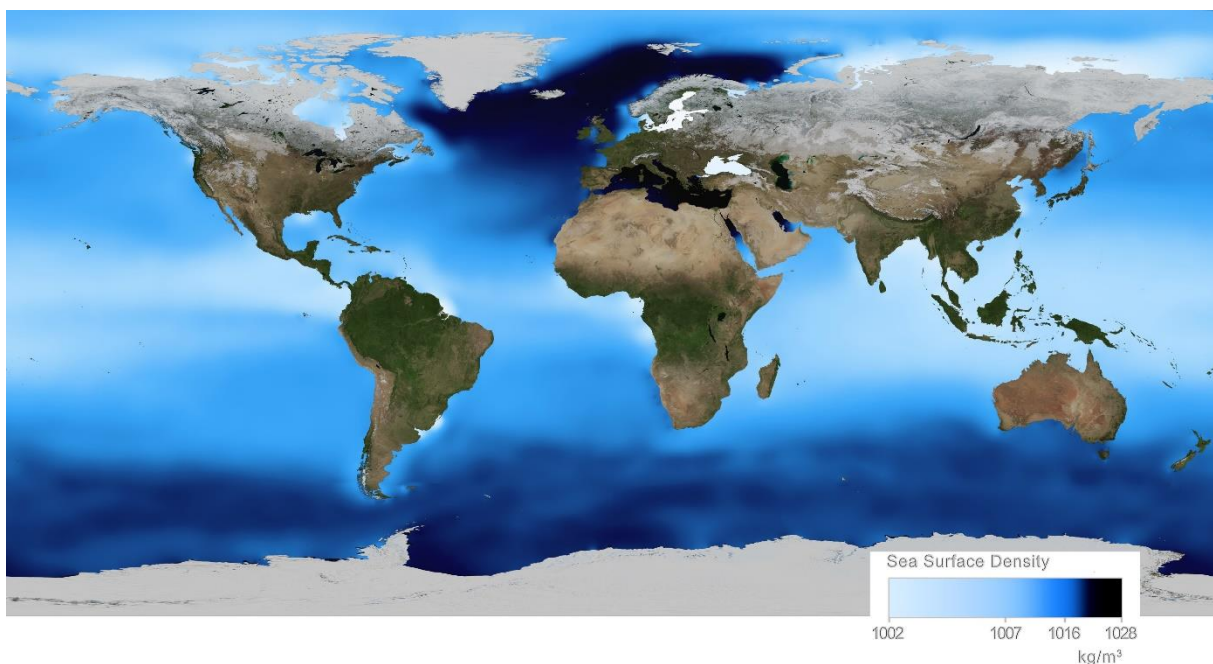


Figure 2.2: Global map of average sea surface density (Kostis, 2009).

On the ocean floor, concentrations vary greatly, but as with floating plastic debris it tends to accumulate close to populated areas and in seabed canyons. Comparison of quantities in different locations is challenging, as expeditions use different sampling techniques causing variation in min/max size of collected debris, and report their data in a range of units (items/km², % w/w in top 5 cm of sediment, kg/m² etc.). As an example, concentrations of plastic debris (>2.5 mm) ranged from 0-1768 kg/m² on the seafloor off the coast of Morocco, and was found to be highly correlated with fishing activities (Loulad et al., 2017). In a report of only MP (38-4000 µm) off the Australian coast, the abundance range was 0.59-12.53 particles/mL sediment and not correlated with other pollutants, indicating different distribution mechanisms (Ling et al., 2017).

Polymer type and shape

Of MP collected on the ocean surface and beach sediments, the most commonly encountered polymer types are PP, PE (both LDPE and HDPE) and a smaller quantity of PS and EPS. (Morét-Ferguson et al., 2010, Frias et al., 2014, Rios and Jones, 2015). Less frequently encountered polymer types are polyurethane (PU) poly(acrylate/styrene), polyesters and synthetic rubbers, which are predominately found in areas of lower seawater density or have experienced a reduction in density due to weathering. A larger proportion of higher-density polymers and fibres are found close to populated areas and point sources, such as predominantly alkyd MP from ship paint resin in a Korean bay with high maritime activity (Song et al., 2015)

In contrast, MP found in deep sea sediments in the North Atlantic, Mediterranean and Indian Ocean at 300 – 3500 m depth, are of polymer types that are denser than SW and mostly fibrous. These included both polyester and acrylate polymers, but also rayon, polyacetates and polyamides, which are semi-synthetic polymers (Woodall et al., 2014). The authors estimate 4,000,000,000 MP fibres per km² in the sediment of the Indian ocean. A predominance of fibrous MP was also found along the Australian coast (Ling et al., 2017). As for surface MP, local sources are important to consider: MP collected in the intertidal sediments on the west-coast of India were mainly from nearby ship-breaking activities (Reddy et al., 2006). The main source of MP fibres is from washing synthetic garments (Browne et al., 2011).

The shape of collected MP varies greatly on location. As mentioned above, fibres appear to be the predominant form of MP in seafloor sediments. On the open ocean, the relative abundance of 420-4200 µm MP from 6 different locations is fragments > pellets > fibres > sheets > foam

(Morét-Ferguson et al., 2010). The shapes of MP found in beach sediments is a combination of low-density fragments and fibres: fragments/pellets > fibres > foam > films (Wessel et al., 2016).

2.2.2 Distribution

The main natural processes acting on marine plastic debris, ultimately determining their distribution and fate, is illustrated in Figure 2.3 by Pravettoni (2016). As seen, not only polymer density and transport with ocean currents determines the distribution and fate of marine plastic debris – abiotic and biotic degradation is highly important.

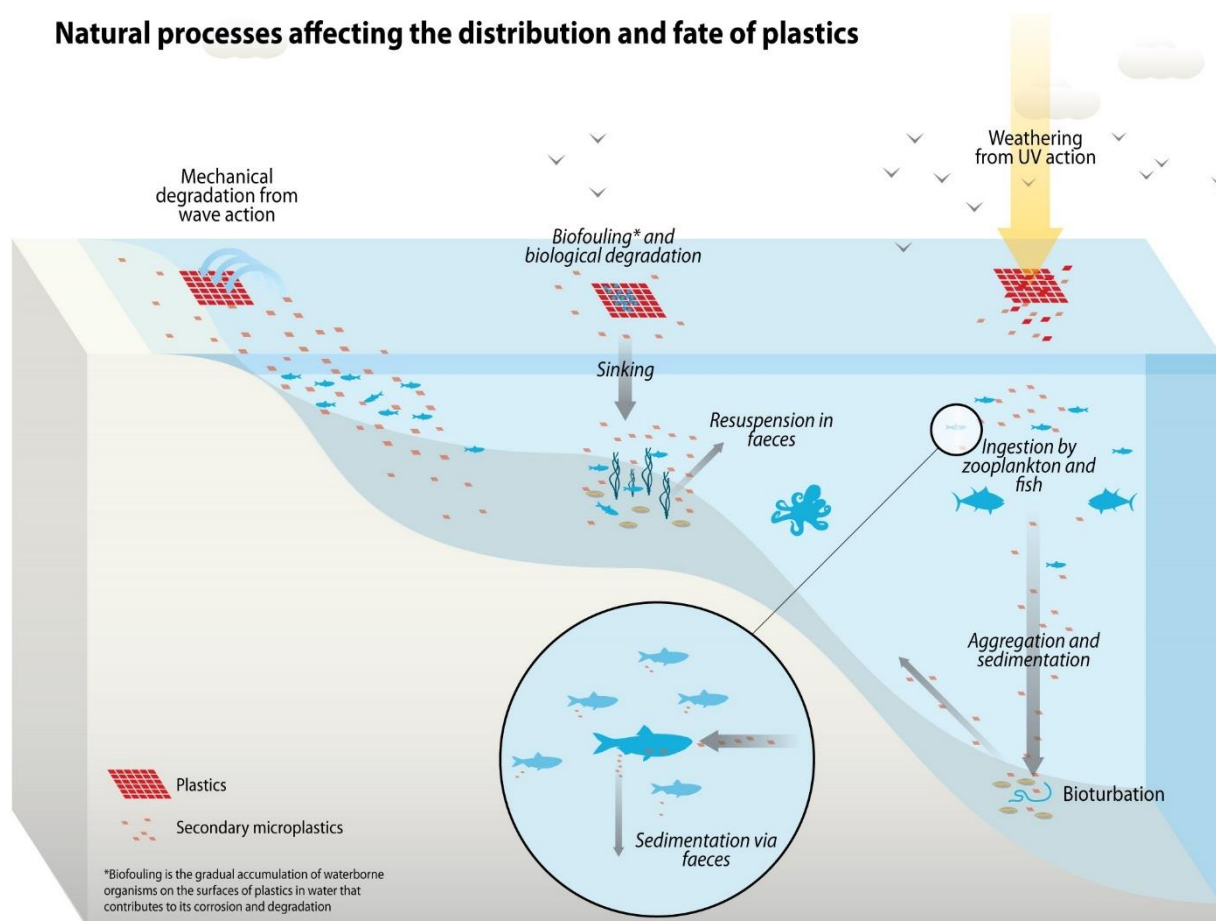


Figure 2.3: Natural processes acting on marine plastic debris (Pravettoni, 2016).

Wave action causes fragmentation, and at shorelines plastic can be trapped in sediments above/below the intertidal zone or transported back to open water/deeper parts of the seafloor. Biological action can slowly degrade the polymer, but the concurrent increase in density due to

biofouling is thought to cause sinking. At some point defouling might occur, causing the particle to rise to higher levels in the water column or surface, depending on size and local water movement. Plastic on the surface is subject to irradiation from the sun, causing i.e. oxidation, chain scission, cross-linking and consequently embrittlement and erosion/fragmentation. Ingestion can trap both MP and larger plastic items in the food web, or if egested transport the MP to deeper water/the seafloor through faecal sedimentation. In addition, climate changes affect marine physical, chemical and biological processes, complicating distribution modelling. The processes are numerous and still to be fully understood – and need to be considered holistically to understand the fate and risk of marine plastic pollution (Gewert et al., 2015, Wang et al., 2016).

2.3 Degradation

Apart from negative environmental impacts, marine plastic debris can provide an energy source for organisms capable of biodegrading polymers. Plastic chemistry is the main factor determining to which extent a polymer is biodegraded; biota show a preference for ester-linkages such as in PU and positively charged particles due to electrostatic attraction (Rocha-Santos and Duarte, 2017). Biodegradation can however expose organisms to higher concentrations of toxic substances incorporated in the polymer (Crompton, 2009). Biofilm formation and biodegradations occurs to some extent on basically all marine plastic debris but is naturally dependent on the local biodiversity. In the open ocean, the biomass concentration on collected MP ranged from 0.2 – 7.5 %, estimated from nitrogen content (Morét-Ferguson et al., 2010). The principal mechanism for the most abundant polymer types is however abiotic degradation, which is the topic of this study and is discussed in the following sections.

2.3.1 Physical degradation

Physical degradation is important as fragmentation to smaller particles increases the surface area, and thus increases the polymer's susceptibility to further thermal, photo- and biodegradation. The different degradations mechanisms are interconnected – e.g. photodegradation causes embrittlement which in turn makes the MP more prone to mechanical degradation.

Mechanical degradation of marine plastic debris occurs as a result of wave action, either through impact with hard surfaces of sediments and rocks, or by grinding if trapped in sediments. If the resulting stress breaks up polymer chains on the surface, embrittlement and erosion of the surface can occur. Sufficient force can result in fragmentation into two or more particles, but this depends on the physical properties of both impacting particles, such as size and shape. (Stevens, 2002).

The chemical changes that can occur upon mechanical stress is polymer chains breaking, forming two radical chain fragments. The progression is dependent on oxygen concentration; in the presence of oxygen the reaction will proceed to peroxide radicals and oxidation as presented in Section 2.3.2. Once initiated, the rate of radical degradation increases exponentially with time, since an increase in the concentration of carbon double bonds and oxygen-containing functional groups increases the rate and spread of reactions (Grassie and Scott, 1988). In the absence of oxygen, radical recombination, double bond formation and further chain scission occurs, but at a rate highly dependent on temperature and concentration of reactive species (Singh and Sharma, 2008). The rate also decreases with time until a limiting molecular weight is reached, which is primarily dependent on the initial stress. Interestingly, the stress (or energy input) required for a given amount of mechanical degradation is less at lower temperatures and for polymers with higher molecular weight (Knight, 1976). Physical impact with e.g. sediment can therefore affect a MP particle without necessarily fragmenting it. Limited literature was found on the importance of mechanical degradation of MP in the marine environment, but the following information has been gathered from physics, environmental data and the few studies on mechanical degradation of plastic:

- 1) Mechanical chain scission predominantly occurs in the middle of polymer chains, depending on homogeneity. Oxidative chain scission occurs either at random locations or at chain-ends in the case of depolymerization reactions (Wagner and Lambert, 2017). Changes in molecular weight could therefore indicate the main degradation mechanism.
- 2) Polymeric materials do not fragment as easily as harder particles owing to their plasticity. At low impact speeds, spherical polymer particles experience permanent flattening of the impact size and meridian tensile cracking, but do not fragment, apart from possible release of NP from the cracking site (Timár et al., 2010). Harder polymers, including those embrittled by weathering, should therefore experience greater fragmentation than softer ones. Shape is however important: non-uniform particles are more susceptible to fragmentation than smooth and spherical ones.

- 3) Particle size matters, but no literature was found on the specific relationship between particle size and fracture energy for polymer particles in the micron-range, a part from a significant increase in strength of polymer particles <500 μm (Gotoh et al., 1997). Fracture energies significantly increase with decreasing particle size until a *limit of breakdown*, below which particles are not fractured at all (only plastically deformed, depending on particle properties), regardless of impact velocity (Masuda et al., 2006).
- 4) Size distributions of mechanically fragmented MP show exponential decay: the number of particles increase exponentially with decreasing size. This has been confirmed by experimental simulation of mechanical abrasion of 1000 μm MP pellets, both by mechanical abrasion alone and in combination with UV exposure (Song et al., 2017). A *limit of breakdown* has not been determined for mechanical abrasion of MP.
- 5) Hydrophobicity and porosity is important, as water absorption increases the rate of both loss of tensile strength, erosion and photodegradation. EPS is a classic example of a polymer that degrades faster in SW than in air; its porosity that allows water absorption which accelerates both photodegradation and erosion as a result of e.g. wave action. For PE the opposite occurred, due to its tightly packed polymer chains (NOAA, 1988).

2.3.2 Photodegradation

Exposure to UV irradiation in the presence of oxygen is believed to be essential for degradation of polymers with a hydrocarbon backbone (Gewert et al., 2015). During exposure to sunlight, polymer debris at land experience heat build-up, which accelerates photooxidation and can enable thermooxidation (NOAA, 1988). Heat build-up does not occur in polymer debris at sea, and oxidation rates is therefore expected to be slower, at least for the most common polymer types. Degradation can therefore be extremely slow in polar compared to tropical regions, both due to increased UV exposure higher sea temperatures – as a general rule, reaction rates double for every 10 °C increase in temperature. Moisture is however important and can enable hydrolysis of polymers containing oxygen. For hydrophilic or already weathered polymers, at equal temperatures the rate of photodegradation in water can exceed that in air (Singh and Sharma, 2008).

Hydrogen radicals are formed by UV irradiation that reach a polymer either recombine or abstract hydrogen atoms from the polymer. Hydrogen radicals have high mobility through the polymer matrix of PS, but not as great through PE, depending on the degree of branching (Yousif and Haddad, 2013). Polymer radicals have limited mobility and are restricted to

hydrogen abstraction or recombination with nearby radicals. Hydrogen abstraction preferentially occurs on a tertiary carbon, which in PE would be on backbone carbon atoms with side-chains, and either in the aromatic ring or on the α -carbon (adjacent to the aromatic ring) in PS. This is either followed by hydrogen abstraction, cross-linking or reaction with oxygen, and continues as a free radical reaction. The general radical reaction is presented in Figure 2.4, showing how crosslinking and chain scission occurs, the latter producing a terminal alkene and an aldehyde/ketone (PE/PS). Other reaction products can also occur from crosslinking of other combinations of radicals, and further radical formation at the newly formed carbonyl and C=C bonds. Other possible oxygen-containing functional groups are ether, peroxide, ester, alcohol and carboxylic acid (Achhammer et al., 1951, Yousif and Haddad, 2013, Gewert et al., 2015).

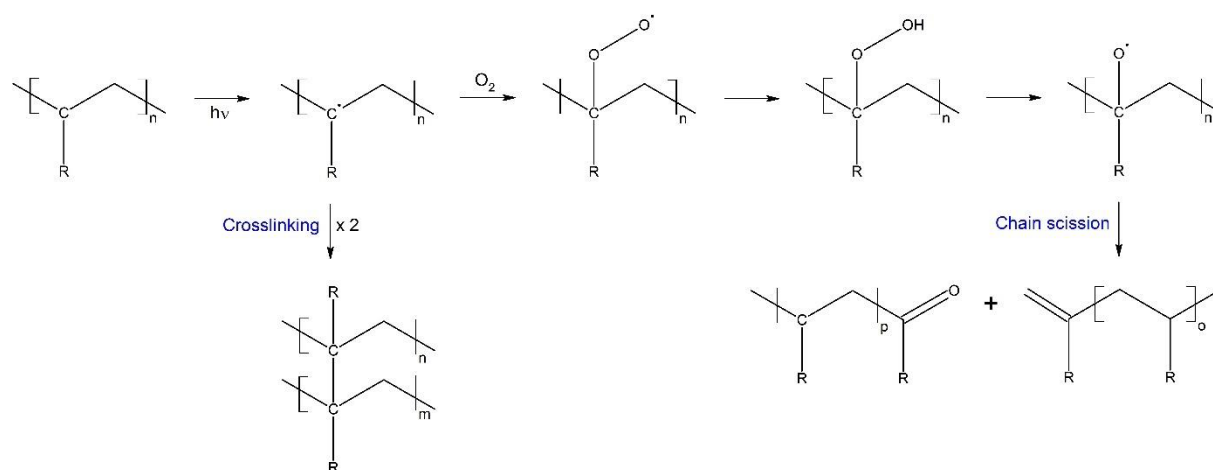


Figure 2.4: Radical mechanism for the photodegradation of hydrocarbon polymers. For polyethylene $R = H$ for and polystyrene $R = \text{benzene}$.

What oxidation products are formed depend primarily on polymer type, temperature and oxygen availability. Significant PE absorption occurs <200 nm, but in the range of sunlight (>250 nm) the maximum occurs around 330-360 nm (Xingzhou, 1997). PE is not readily photooxidized as it does not contain chromophores, and radical reactions are therefore believed to start at polymer defects or on additives (Grassie and Scott, 1988). Plain chain scission, resulting in terminal double bonds can occur for PE in the absence of oxygen (Stuart, 2004). Exposure of PE to UV light in water led to formation of carboxylic acid end groups (Gewert, 2017). Weathered PE collected from beaches had increased surface area, ketone groups and a

negative charge in seawater pH which discourages biofilm formation (Fotopoulou and Karapanagioti, 2012).

PS absorbs strongly <280 nm, and the maximum within the solar irradiation range occurs at 254 nm. Above 300 nm, it is the terminal chain groups of PS that absorb (Yousif and Haddad, 2013). Photodegradation of PS involves mainly chain scission, but the main location is unclear: some sources report random chain scission while others report chain scission on polymer ends causing depolymerization. Yellowing is believed to be due to the formation of conjugated double bonds, and in the absence of oxygen, cross-linking is the dominant reaction mechanism (Ellis and Smith, 2008, Gewert et al., 2015). Guaita et al. (1985) determined a chain scission/crosslinking ratio of 5 by molecular weight distribution (MWD) analysis, regardless of UV exposure time (4 weeks). In air, a range of oxidation products are formed upon UV irradiation, including carboxylic acids, ketones and aldehydes (Rabek, 1990), but the main products formed in seawater are unknown. The photodegradation rate of PS is close to logarithmic/first order (Shyichuk and White, 2000).

Since photooxidation is highly correlated to oxygen permeability, the greatest changes occur on the surface and rapidly decrease with depth - particularly for PE which has lower oxygen permeability than PS. For the same reason, oxidation is limited to amorphous regions (Stevens, 2002). Chain scission on the surface leads to loss of small polymer fragments (NP), which is why surface roughening can be observed (Gewert et al., 2015). The number of formed fragments has been found to vary depending on polymer type, but the resulting size distribution is as for mechanical abrasion, exponential increase in number with decreasing size both in the μm - and nm -range (Lambert and Wagner, 2016b, Lambert and Wagner, 2016a). Chain scission leads to a decrease in MW, which in theory will increase with decreasing particle size, as the penetration depth will eventually comprise the whole particle. Cross-linking will cause embrittlement, making the polymer more susceptible to fragmentation upon physical impact. Co-occurring mechanical stress and UV exposure increases degradation (scission + crosslinking) at the surface (Guaita et al., 1985), which could cause accelerated degradation in the intertidal zone on a sunny day. Oxidised polymers also have the potential to “trap” water molecules due to hydrogen bonding with oxygen-containing functional groups (Cholli et al., 1984). Increased water content will change the density and thus possibly affecting the fate of MP, e.g. by speeding up sinking rate of low density MP. In addition, hydrophilic functional groups (especially esters) enable hydrolysis reactions to occur, which can cause disintegration of highly oxidised polymers (Singh and Sharma, 2008).

2.3.3 Release of associated substances

As mentioned above, oxidation can result in loss of polymer fragments, which can be small molecules consisting of only one or several polymer units (*mers*): monomers and oligomers, respectively. These are also present in pristine polymers, not significantly in PE but PS is known to contain residual unreacted monomer, dimers and trimers. These, as well as residues from the manufacturing process (solvents, catalysts, lubricants) and additives (examples in Table 2.2) can leach out to environmental compartments. As many additive types increase the polymer's resistance to degradation, the degradation rates, and thus leaching, is largely dependent on the type and quantity of additives. On the other hand, leaching might accelerate degradation of both the polymer and the leached substance, causing a lower net environmental harm. (Teuten et al., 2009, Choi et al., 2005, Bilitewski et al., 2012).

Leaching occurs to a greater extent from weathered polymers due to increased surface area, permeability and water uptake - the exception being if cross-linking is the dominant mechanism and fragmentation does not occur. Salinity has not been correlated with the leaching of polymer additives, but water turbulence and UV irradiation showed a positive relationship for most substances (Suhrhoff and Scholz-Böttcher, 2016). Weathering can in many cases cause degradation of additives, particularly UV exposure; Suhrhoff and Scholz-Böttcher (2016) detected relatively few additives after UV exposure, but found new substances that likely were additive degradation products. Additive degradation can be for the better or worse, depending on if the degradation products have less or greater potential toxicity than the parent compound.

Apart from leaching of polymer additives/residues to the ocean, leaching can also occur inside organisms after ingestion. In addition, plastic debris can accumulate hydrophobic substances from the environment and act as vectors for e.g. persistent organic pollutants (POPs). Polymer monomers, oligomers, additives, manufacturing residues and adsorbed substances from the environment will collectively be referred to as *polymer-associated substances*. The toxicity of consequences of leaching to the ocean is regarded as negligible in comparison to leaching after ingestion, which might neither be a major contribution to pollutant concentrations in the marine food web. Potential adverse environmental effects still need to be determined, as environmentally relevant concentrations are rarely useful in laboratory experiments. Effects might be restricted to long-term exposure and to confined areas with elevated concentrations of plastic debris and environmental pollutants (Hermabessiere et al., 2017, Kwon et al., 2017).

2.4 Analysis of microplastics

2.4.1 Chemical characteristics

Chemical properties of polymers that are of interest include the composition and structure of the bulk polymer, additives, residues from the production, surface chemistry and charge. Nuclear magnetic resonance (NMR) is an excellent technique yielding structural and quantitative information, such as the polymer functional groups, percentages of copolymers and tacticity (the orientation of functional groups). For the assessment of polymer degradation, particularly of aromatic and conjugated polymers, UV spectroscopy is a valuable technique. Chromatographic techniques are generally limited to pyrolysis gas chromatography (Pyr-GC) due to the high MW of most polymers (Clavier, 2008). High MW is also an issue in traditional mass spectrometry (MS) techniques, but the development of matrix-assisted laser desorption/ionization time-of-flight (MALDI-TOF) MS has allowed analysis of intact PE and PS chains up to 4500 and >10,000 Da, respectively (Wallace and Blair, 2007, Wyzgoski et al., 2007). Thermal analysis methods, such as differential scanning calorimetry (DSC) allows determination of e.g. crystallinity and percentage of copolymers and plasticizers (Clavier, 2008). The zeta potential surface charge can be determined by electrokinetic measurements, e.g. by dynamic light scattering (DLS) (Stamm, 2008). In addition, polymer degradation can be measured chemically by measuring the CO₂ loss from a closed degradation system (Crompton, 2009). The chemical analysis methods used in this project, infrared spectroscopy, Pyr-GC coupled to MS (Pyr-GC/MS) and energy dispersive X-ray spectroscopy (EDS) are discussed in more detail below.

Infrared spectroscopy

Infrared spectroscopy is an analysis technique which records the amount of infrared (IR) light absorbed (or transmitted) by a sample, at a range of different wavelengths. The acquisition of a spectrum is obtained by a mathematical algorithm called *Fourier transform*, which converts the raw data into a spectrum by decomposing the output signals into wavelengths, thereby the name Fourier transform infrared spectroscopy (FTIR). Spectra are commonly presented with absorbance (or transmittance) on the y-axis, and wavenumber, $\tilde{\nu}$, on the x-axis. Transmittance is an intensity ratio; the intensity of IR light passed through a sample, divided by the initial intensity. It is thus a unitless measure, and usually presented as a percentage. The wavenumber

is usually reported in reciprocal centimetres (cm^{-1}), and is related to the wavelength (λ), frequency (ν_s) and speed of light (c) according to Equation 1:

$$(1) \quad \tilde{\nu} = \frac{1}{\lambda} = \frac{\nu_s}{c}$$

The most common bond vibrations occur in the mid-infrared range; at wavelengths between 2.5 and 25 μm , or 4000–400 cm^{-1} . A sample will absorb IR light at wavelengths that matches its molecular vibrations, causing a change in the vibrational amplitude, but only if the vibrations involve a change in dipole moment. The wavelength of a specific molecular vibration is determined by the masses of the two atoms involved and their bond strength, but is influenced by factors like hydrogen bonding, inductive- and resonance effects. Two factors determine the degree of absorbance at a specific wavelength: (1) the change in dipole moment and (2) the number of bonds/molecules that has a vibrational mode at that wavelength (Rees, 2010). Taking polystyrene and one of its oxidation intermediates (Figure 2.5) as an example:

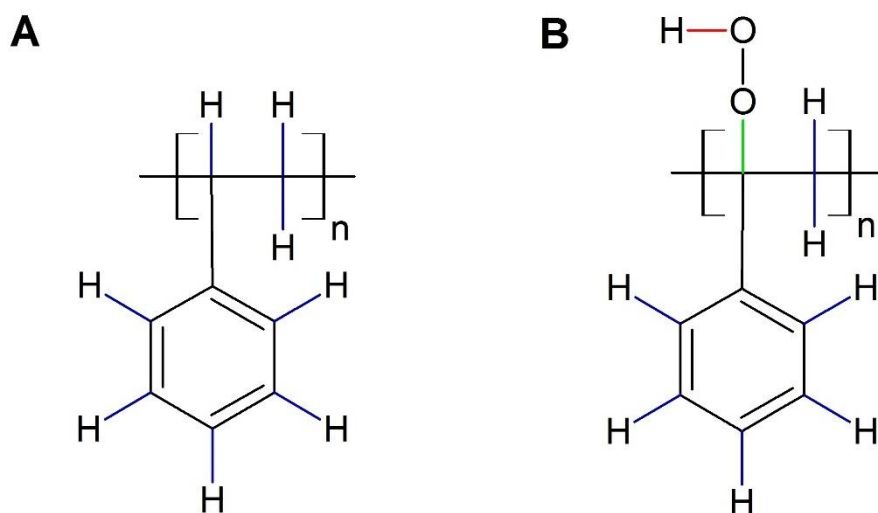


Figure 2.5: The structure of (A) polystyrene and (B) an oxidation intermediate, polystyrene hydroperoxide.

The vibrations of C-H bonds (blue) do not involve a large change in dipole moment, but they are numerous and occur in the mid-infrared range. Two C-H vibration “bands” will therefore be visible in an FTIR spectrum, as aliphatic and aromatic C-H vibrations have different frequencies. Vibrations of the O-H (red) and C-O (green) bonds cause a greater change in dipole moment than those of C-H bonds, and therefore result in greater IR absorbance bands. Vibrations of symmetric bonds like C-C and O-O have negligible changes in dipole moment,

and are therefore not observed. Different vibrational modes also result in more IR bands – e.g. symmetric and asymmetric stretching, rocking, scissoring, wagging and twisting. Furthermore, phenomena like overtones, combination vibrations and resonance give rise to additional IR bands (Pavia et al., 2014). FTIR spectroscopy does therefore not only yield information about functional groups, but also about the molecular environment of certain functional groups – and is thus of assistance in the deduction of molecular structure, possible additives/impurities and changes over time.

There are several different FTIR sampling techniques, but the most common and also most suitable for MP analysis is attenuated total reflectance (ATR) (Milosevic, 2012). An ATR sampling accessory consists of a crystal (e.g. ZnSe) on which the sample is placed, either in liquid or solid (film or powder) form, and clamped down with a compression tip. An IR beam is directed to the sample, and the changes in the IR beam due to internal reflection in the sample is recorded. As it is a reflection technique that only penetrates the top 2 μm of solid samples/films, it gives information about the surface chemistry, which is important to remember when analysing MP with diameters $>4 \mu\text{m}$. For the analysis of larger polymer samples micro-FTIR can be used; a coupling of microscopy and FTIR which allows spatial analysis and mapping of e.g. oxidation sites (Renner et al., 2017, Stuart, 2004).

In addition to polymer identification, FTIR is useful for qualitative and quantitative degradation analysis. The density of PE can be estimated from the absorbance ratio of the $-\text{CH}_3$ and $-\text{CH}_2-$ bands ($1378 \text{ cm}^{-1}/1369 \text{ cm}^{-1}$) – a larger ratio indicating a higher degree of branching and thus a lower density. Formation of double bonds from chain scission can be detected by vinyl C-H bending at 990 and 910 cm^{-1} and C=C stretching in the $1680\text{-}1630 \text{ cm}^{-1}$ region. Numerous oxidation products can also be detected by the appearance of O-H, C=O and C-O stretching bands, centered around 3500 , 1700 and 1100 cm^{-1} , respectively. The specific location of absorption bands is dependent on the local chemical environment which affects the dipole moment of the vibration. Certain additives can also be detected by FTIR, but is often problematic due to common and/or overlapping bands with the polymer itself (Renner et al., 2017, Koenig and Rapra Technology, 2001)

Pyrolysis gas chromatography – mass spectrometry

A recently applied analysis method for MP is pyrolysis gas chromatography – mass spectrometry (Pyr-GC/MS), in which the sample is pyrolyzed and the pyrolysis products

separated by GC and analysed by MS (Rocha-Santos and Duarte, 2017). The main advantage of Pyr-GC/MS is that it does not require sample isolation, polymers and any residual matrix can be placed directly into the pyrolysis unit and still yield qualitative and semi-quantitative data. (Fischer and Scholz-Böttcher, 2017). Apart from determining the type of polymer, Pyr-GC/MS allows detection of polymer-associated substances, which can be detected during the pyrolysis of the polymer itself at e.g. 700 °C or by thermal desorption at e.g. 300 °C. Lower temperatures enables desorption of small and (semi)volatile substances while the bulk polymer remains intact. Thermal desorption can be done either step-wise (at fixed temperatures) or by a temperature ramp (Wang et al., 2017). Filament-type pyrolysis units are commonly used in multi-step pyrolysis of polymers when the aim is to look for traces of monomers/oligomers, additives and solvent residues (Blazsó, 1997). When identifying polymers and additives against reference spectra in e.g. NIST, a 80 % match is generally satisfactory (Dehaut et al., 2016).

Pyrolysis of PS occurs through free radical depolymerization, creating a pyrogram (pyrolysis chromatogram) dominated by the styrene monomer, dimer and trimer, along with oligomer isomers. If quantification is performed it should be based on the combined peak areas of both the monomer and several oligomers, as gas phase (de)polymerization can vary. In MP trace analysis styrene alone is not a good indicator of PS as it also appears in pyrograms of natural polymers such as wool and chitin (Blazsó, 1997, Kusch, 2017)

Pyrolysis of PE generates homologue series of n-alkadienes, n-alkenes and n-alkanes, eluting in triplets in the given order, with the n-alkene having the highest abundance. N-alkanes and n-alkenes are also formed during pyrolysis of different types of environmental samples such as fatty acids from organisms, but mainly with carbon numbers in the lower range. In trace analysis it therefore recommended to base identification upon homologues $>C_{18}$ or ensure proper sample digestion and clean-up. Pyrolysis of LDPE, which has greater branching than HDPE, will result in a greater number of pyrolysis products eluting between the triplet homologue series, allowing estimation of the degree of branching. Aged PE can also be differentiated from virgin PE as exposure to light, heat and mechanical stress can lead to chain scissoring. Thus, traces of peaks from the triplet homologue series can be detected at a lower pyrolysis temperature in aged PE, e.g. at 300°C instead of 700°C (Yang et al., 2013, Kusch, 2017).

A range of polymer additives and manufacturing residues can be detected by Pyr-GC/MS, both by thermal desorption and at pyrolysis temperatures. High-MW additives that do not desorb at e.g. 300 °C will however fragment at higher temperatures, requiring elucidation of their pyrolysis pattern. (Kusch, 2013, Herrera et al., 2003). Additive identification is challenging as

there are thousands of different additives, many of which have similar structures and produce similar mass spectra and/or pyrolysis products. An example is the similar mass spectra of different phthalate esters, which require systematic evaluation of lower-intensity ion for correct identification (Wang, 2000).

Energy-dispersive X-ray spectroscopy

Energy-dispersive X-ray spectroscopy (EDS) is used for elemental analysis and to estimate their relative abundance. EDS is based on the principle that elements all have unique electromagnetic emission spectra, consisting of a set of peaks. Electron microscopes are often equipped for energy-dispersive X-ray spectroscopy, as the two techniques both require focusing an electron beam onto a sample. Samples analysed by EDS ideally have smooth, flat surfaces, as irregular surfaces increase scattering causing fewer X-rays reach the detector. Also, some elements have overlapping X-ray emission peaks, so interpretation must be done with these error sources in mind (Newbury and Ritchie, 2015).

2.4.2 Size

A variety of methods for determining particle size and size distribution is available, and the choice mainly depends on expected size range, density and desired accuracy. Sizing methods for solid or suspended particles in the μm -range include (but are not limited to) sedimentation (e.g. X-ray gravitational), laser diffraction, sieving, electrical sensing zone (e.g. Coulter Counter), flow cytometry and microscopy (Merkus, 2009, Jillavenkatesa et al., 2001). Sieving is a high-throughput and cost-effective method often used on particles in the upper-micron range, but issues such as clogging and potential physical damage make it problematic for MP weathering studies (Crawford and Quinn, 2017).

Microscopic methods and subsequent image processing allows sizing of particles in both the nano- and micro-range depending on the instrument, but is time-consuming and can result in significant errors due to i.a. overlapping particles, contamination, resolution and image processing procedure (BS3406, 1993). Electron microscopy is however an excellent technique allowing both information about size, morphology, and about elemental composition if coupled to EDS as described in section 2.4.1 (Girão et al., 2017). Transmission electron microscopy (TEM) has also been used to detect and determine the size of nanoplastics (3-500 nm) fragments from experimental photodegradation of marine MP (Gigault et al., 2016). If the shape of the

particles is of interest, microscopy methods are the most informative (Gotoh et al., 1997). In cases of unsuccessful separation of MP from matrices, Nile Red staining and subsequent fluorescent microscopy has successfully been utilized to document both presence and size (Shim et al., 2016).

Recently applied techniques for size distribution measurement in MP degradation experiments include nanoparticle tracking analysis (NTS) (Lambert and Wagner, 2016b) and dynamic light scattering (DLS) (Gigault et al., 2016, Hernandez et al., 2017). As both techniques are carried out on suspensions they allow *in situ* measurements. Particles analysed by NTS, DLS and Coulter Counter are either not imaging at all or captured in motion, resulting in low resolution. For this reason, rigorous control of contamination and the presence of other particles in the relevant size range is necessary to avoid misinterpretation (Hernandez et al., 2017).

When size distributions are created from microscopy images, it is important to minimize touching particles and to exclude particles on the edges. The size dimension recommended by particle size distribution standards is the *area equivalent area diameter* (x_A) (BS3406, 1993, ISO16232-7, 2007). Using x_A , which is the diameter of a sphere with the same area as the projected particle, induces less error than dimensions such as Feret's diameter. If the shape of the particle is of interest, the *shape descriptor* (ϕ) can also be included, which is an optional output in size analysis using e.g. ImageJ. (Merkus, 2009, Gotoh et al., 1997). When computing size distributions, a sample size of 800 is required to obtain an acceptable statistical accuracy. The optimal number of bins for histogram presentation depends on the sample size and distribution, but the expected standard error of any bin is kept <2 % if the fraction of particles in the largest bin does not exceed 50 % for sample sizes >625 (Gotoh et al., 1997).

2.4.3 Morphology

Morphology such as overall shape and surface characteristics can be investigated using optical microscopy (micro- and macroplastic) and electron microscopy (micro- and nanoplastic). Scanning electron microscopy (SEM) is a commonly used instrument for MP imaging, and offers a very high resolution compared to optical microscopy: 0.4 versus 200 nm. Non-conductive specimens are generally coated with a thin layer of conductive material such as gold or platinum; Hernandez et al. (2017) coated micro- and nanoplastics with Pt prior to SEM imaging.. Coating does however prevent elemental analysis of the same specimen by EDS (Girão et al., 2017). To avoid or minimize the surface charge build-up that occurs on polymers

due to the high-voltage electron beam under high vacuum in SEM, either the vacuum or the voltage must be lowered, as successfully done by Fries et al. (2013) and Gaillard et al. (2004), respectively. An alternative to SEM is TEM, which offers a higher resolution (down to 0.5 Å) and produces a 2D-image of the whole depth of the sample from the transmitted electrons. TEM has been successfully used to image nanoplastics with a resolution of <2 μm and yielded information about the shape of particles and clusters, but does not offer the 3D details of SEM such as particle- and surface morphology (Gigault et al., 2016).

Since weathering might result in fragmentation and porosity changes, surface area measurements are informative. This can be done with a Brunauer-Emmett-Teller (BET) instrument, utilizing adsorption of nitrogen gas on the analyte's surface area. The advantage of BET measurements is that it measures the specific surface area, which, unlike calculation methods, include surface associated with the particles' texture and porosity (Naderi, 2015).

2.4.4 Experimental considerations

Polymer properties

As PE and PS MP are hydrophobic polymers in powder form, interaction with laboratory equipment must be considered, which can lead to significant loss during e.g. decanting. Equipment such as pipettes are therefore not practical, and aggregation of the MP particles can occur. Weathering can however alter the polymer such that its behaviour during e.g. extraction changes. No literature was found on the behaviour of MP in the presence of inorganic materials such as sediment, but were believed to be insignificant as both PE, PS and quartz is negatively charged in seawater (Sondi and Pravdic, 1998, Fotopoulou and Karapanagioti, 2012).

Density separation

The most encountered method in previous studies is density separation with an saturated aqueous NaCl solution, which works on MP with a density below 1.2 g/mL (Thompson et al., 2004). Density separation can similarly be done with NaI to separate polymers with densities up to 1.6 g/mL (Fischer and Scholz-Böttcher, 2017). Another method is elutriation, in which an upward stream of gas or liquid is applied to a suspension to separate lighter particles from heavier ones. Claessens et al. (2013) achieved recoveries ≥ 98 % with their method specially developed for separating MP from silt, which involved elutriation with tap water and aeration,

followed by NaI density separation by vortexing. A special device developed for separating MP from silt could also be purchased; the *MicroPlastic Sediment Separator* (MPSS) from Hydro-Bios, developed by Imhof et al. (2012). Devices for collecting and separating MP based on electrostatic charging have also been developed (Ward, 2013).

Contamination

As microplastic is found everywhere, such as in air and cosmetics, contamination control is essential. Both personal products (cosmetics, clothes) and laboratory equipment (gloves, weighing pods) composed of synthetic polymers should be avoided as far as possible. In addition, the exposure of MP samples to air should be minimized by e.g. covering containers with aluminium foil as done by (Fischer and Scholz-Böttcher, 2017). Biological contamination is also possible and should be minimized by proper laboratory equipment cleaning procedures (Rocha-Santos and Duarte, 2017).

3 Experimental

3.1 Equipment and materials

The materials and used in the weathering experiments are listed in Table 3.1 (MP materials) and Table 3.2. Additional information about the MP materials can be found in Table A.1 (Appendix A). The choice of MP materials was based on density and environmental abundance. Marine MP exposed to sunlight and ending up in the intertidal zone would have density lower than or close to the density of SW. Three of the most common types of polymers meet this density requirement and has been reported on the ocean surface and in the intertidal zone/beaches: PE, PP and PS. Of these, PE and PS were chosen: two structurally dissimilar polymers with different degradation pathways. Two different sizes were included: one in a size range relevant for zooplankton uptake, ~10 μm (Cole et al., 2013) and a larger size for evaluation of size dependency.

Table 3.1: Details of the microplastic materials used in the weathering experiments.

MP material	Supplier^a	Polymer type	Form	Diameter (μm)	Density (g/cm^3)
PE-10	Cospheric	Polyethylene microspheres	Solid	3-16	0.96
PS-10	PolySciences	Polystyrene microspheres	Aqueous (2.5 % w/v)	10 (nominal)	1.05
PE-100	PLASTOX (Total)	Polyethylene, milled	Solid	75 (median)	0.923
PS-100	PLASTOX (Trinseo)	Polystyrene, milled	Solid	94 (median)	1.05

^aAdditional information from the suppliers can be found in Table A.1 in the Appendix.

The mass of MP needed for all the analyses was estimated by weighing the sample containers before and after each test analysis: approximately 5 mg. From filtration testing, the expected recovery was >50 %, so a sample size of 10 mg would be the absolute minimum. Based on these numbers and the mass available, it was decided to use 15 mg of PE-10 and PS-10 in each sample. A sample size of 100 mg was used of PE-100 and PS-100, giving comparable surface

areas (SA): 6840, 8580, 8380 and 6060 mm²/sample for PE-10, PS-10, PE-100 and PS-100 respectively. A summary of surface area estimations based on information from the suppliers is presented in Table 3.3.

Table 3.2: Materials used in the weathering experiments and extraction procedure.

Material	Source	Details
Seawater	On tap at SINTEF	Source: Trondheimsfjorden, 90 m depth (63°26'N, 10°26'E) Salinity: 33.5 ± 0.2 ‰ Filtered (sand filter, 50 µm)
NaCl	Baker Analyzed®	Purity: Min. 99.0 %
Sand	SINTEF	Source: Hansbakkfjæra (+63°25'N, +10°32'E) Quartz sand collected by Sørensen et al. (2014)
Silt	Sigma-Aldrich	SKU: CLNSED2 – Cleaned Sediment #2 Grade: Certified reference material

Table 3.3: Microplastic surface area estimations based on supplier information. d = diameter, V = volume, SA = surface area and ρ = density.

MP material	Mean (1 particle)			SA/V ratio	ρ (g/cm ³)	Spheres/mg	SA/mg (mm ² /mg)
	d (µm)	V (µm ³)	SA (µm ²)				
PE-10	9.50 ^a	4.49×10 ²	2.84×10 ²	0.632	0.96	2.34×10 ^{6b}	684
PS-10	10.0	5.24×10 ²	3.14×10 ²	0.600	1.05	1.82×10 ^{6b}	858
PE-100	75.4	2.24×10 ⁵	1.79×10 ⁴	0.0796	0.923	4.69×10 ^{3c}	83.8
PS-100	94.3	4.39×10 ⁵	2.80×10 ²	0.0636	1.05	2.17×10 ^{3c}	60.6

^a Mean of supplied diameter range (3-16 µm)

^c Estimated from V and ρ

^b Estimated from supplier information

3.2 Contamination control

All equipment used in the weathering experiments was cleaned and sterilized in the following order: Machine wash, burning at >400 °C overnight (glass/ceramic only) and autoclaving at

120 °C for 20 minutes. Burning was done to remove possible organic residues and sterilization was performed to avoid possible bacterial/algal growth.

As MP is ubiquitous, the following measures were taken to avoid contamination:

Personal

- No latex gloves, hands washed thoroughly with soap and water
- Only MP-free cosmetics, no hair products or nail polish
- Natural fibre clothing and cotton laboratory coat

Laboratory

- Avoided plastic equipment as far as possible
- Rinsed all equipment and glassware with the solvent to be used
- Kept fume-hood clean, cleaned with ethanol
- Minimized air exposure by covering containers with glass stoppers or aluminium foil, including loose aluminium foil covering filter apparatus during filtration
- Procedural blanks

3.3 Weathering experiments

Seawater used in the weathering experiments was filtered using the *Nalgene Rapid-Flow™ Sterile Disposable Bottle Top Filters* into autoclaved 1 L glass Pyrex bottles, using 1 disposable filtration unit for 2 L SW. PE-10, PE-100 and PS-100 was weighed out using a balance scale with 4 decimal places, and an error of ± 0.3 mg. As PS-10 was in a 2.5 % w/v aqueous suspension, 15 mg MP equalled 600 μL which was added using a micropipette. Sand and silt were weighed using a balance scale with 2 decimal places, and SW measured out in a 100 mL measuring cylinder.

The dispersibility of the MP materials in seawater was as follows: PE-10 and PE-100 floated and stuck to the sides of the container. PS-10 dispersed well and slowly settled to the bottom. PS-100 both dispersed, formed aggregates at the surface and stuck to the sides of the container. The small MP particles were more dispersible when agitated and stayed in suspension for a longer time before they sank/resurfaced. To uphold the environmental relevance, it was decided to not improve the dispersibility by e.g. using a dispersant or ultrasonicate the MP-seawater suspensions. Previous research show that sonication significantly alters the surface and porosity of MP (Urgert, 2015, Bergmann et al., 2015).

3.3.1 Photodegradation

The photodegradation studies were conducted using an Atlas Suntest CPS+ system fitted with a xenon lamp (1500 W) and a daylight filter to simulate daylight. The instrument was used at maximum irradiance: “accelerated daylight simulation” (765 W/m^2). Owing to the limited instrumental space, only the smallest MP materials were included in the photodegradation experiment due to their higher surface area to volume ratio (SA/V).

For each MP material (PE-10 and PS-10), five samples were prepared for different lengths of exposure: 0, 10, 20, 40 and 80 days. A blank sample (t_0) containing only seawater was included to assess contamination and extraction efficiency. In addition, control samples were prepared for each MP type, and collected at t_{40} . Control samples (t_{40}) were wrapped in aluminium foil to avoid light exposure, but otherwise treated like the other samples. A detailed list of the samples can be found in Table A.2 in Appendix C. 15 mg/600 μL of sample was prepared with 30 mL filtered SW in a 40 mL quartz test tube with a ground glass stopper, and shaken for 30 s. This volume of SW was sufficient to “wash back” and inhibit MP from sticking to the inner top surface of the quartz tube with the motion of the rocking table.

As the rocking table could not be placed inside the Suntest instrument, the bottom mirror tray of the test chamber was removed and fastened with tape on the rocking incubator. Samples and controls were placed horizontally in random order on the mirror tray and secured with two strips of clear Scotch MagicTM tape. The rocking incubator was placed on two metal boxes underneath the test chamber of the Suntest instrument (Figure 3.1). The rocking incubator speed was set to maximum (45 rpm). The experiment was carried out in a temperature-controlled room.

The Suntest CPS+ instrument settings are listed in Table 3.4, and the spectral power distribution is shown in Figure 3.2. The maximum irradiance of 765 W/m^2 is slightly lower than the solar irradiance at sea level and on a day with clear sky, which is $\sim 1000 \text{ W/m}^2$ (Vignola et al., 2016). Calculations (see Appendix B) demonstrate that the experimental irradiance is 7.7 times higher than the average irradiance in Trondheim (annual, 24-hour days) (Olseth and Skartveit, 1986). The instrument modification (to an open system) was not accounted for in the theoretical values above, which likely reduced the sample irradiation to $<765 \text{ W/m}^2$. The black standard temperature (BST) sensor, whose purpose is to estimate and control the temperature obtained by the samples, was set to the lowest setting since the samples were unlikely to reach high temperature in an open system. The BST sensor was taped vertically on the back wall of the exposure chamber for the first 7 days, and then moved to a horizontal position on the right-hand side wall due to instrument error messages. A traceable dual thermometer was used to monitor

the temperature on the sample tray and in the room, which ranged from 11.6 - 49.2 and 8.3 - 15.2 °C, respectively. The temperature on the sample tray reached 49.2 °C despite the open system, but was generally in the 30 - 35 °C range except right after restarts.



Figure 3.1: Experimental set-up of the photodegradation experiment: Rocking incubator with samples under the Atlas Suntest CPS+ instrument. The test chamber is located behind the yellow door.

Table 3.4: Atlas Suntest CPS+ instrument settings for the photodegradation experiment.

Parameter	Setting	Available range/options
Irradiance control	300 – 400 nm	320 nm or 300-800 nm/lux
Irradiance (300 – 400 nm control region)	65 W/m ²	30 – 65 W/m ²
Irradiance (250 – 800 nm)	-	250 – 765 W/m ²
Black standard temperature	35 °C	35 – 100 °C
Chamber temperature	50 °C	-
Filter system	Daylight (reduced IR)	Window glass filter
Print interval	720 minutes	

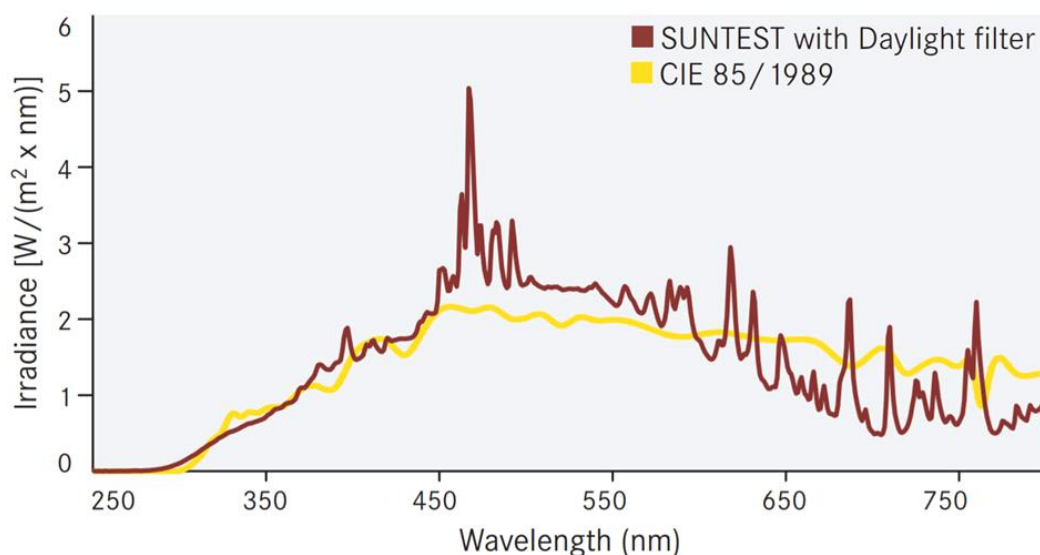


Figure 3.2: Spectral power distribution of Atlas Suntest CPS+ with xenon lamp and daylight filter compared to solar irradiance (CIE 85/1989).

Samples were removed after 10 (t_{10}), 20 (t_{20}), 40 (t_{40}) and 80 (t_{80}) days, which corresponds to 2.5, 5, 10 and 20 average months in Trondheim. The instrument run was interrupted several times due to error messages regarding e.g. the placement of the BST sensor. It was restarted as soon as the issue had been resolved, and the total runtime accumulated at each sampling point was still 10, 20, 40 and 80 days, respectively.

After exposure, each sample was vacuum filtered using a DURAN glass filtration apparatus with a Millipore HA filter (0.45 μm retention, 45 mm diameter), using 15 mL DI water to rinse the quartz tube and 15 mL to wash down the sides of the filtration apparatus. The filter was vacuum dried for 5 min, transferred to a glass petri dish and dried in a fan oven at 35 °C for 2 hours with the lid 2 cm open. The MP was carefully scraped into a glass vial and weighed. All samples were stored in the dark at room temperature.

3.3.2 Mechanical degradation

The two different sediments used in the weathering studies will be referred to as silt and sand according to their particle size, and collectively referred to as sediment (undefined size). The intention of this experiment was to use an environmentally relevant MP:sediment ratio. In the literature, the concentration of MP in sediments is mainly reported as number of pieces per area or mass of soil, and conversion to mass of MP per unit weight of soil is difficult due to the variation in particle sizes (Van Cauwenberghe et al., 2015). An overview of published literature

reporting MP concentrations in sand/silt by is presented in Table 3.5. The majority of MP found in these studies are in the upper micron and millimetre-range. For example, only 0.2 % of the MP found by Carson et al. (2011) was below 250 μm . An underestimation of the fraction of MP in the lower micron-range (and NP) is possible, as these studies did not involve validation of the density separation methods. Techniques for separating and quantifying MP in the lower-micron and nano-range is still under development. A portion of the MP particles could have settled during density separation, e.g. because of interaction/heteroaggregation with the sediment or high density due to polymer type or biofouling. It was decided to use 5 g silt/sand in this study, resulting in 0.3 and 2 % w/w small and large MP, respectively; these concentrations are within the range reported in environmental samples.

Table 3.5: Reported microplastic concentrations in sediments by weight.

Size range (μm)	Concentration (% w/w)	Details	Reference
<250 – >4000	0.12 - 3.3	<ul style="list-style-type: none"> • Beach sand • Mean value in top 5 cm • NaCl density separation PU, nylon, PS, PES and glass wool • Two beaches, Hawaii 	(Carson et al., 2011)
>1.6	0.008143	<ul style="list-style-type: none"> • Intertidal sediment • Mean value in top 5 cm • NaCl density separation and filtration • Ship-breaking yard, India 	(Reddy et al., 2006)
<5000	1 – 6.7 ^a	<ul style="list-style-type: none"> • Intertidal beach sand • Range in top 1 cm • Water density separation • 125 beaches, Canary Islands 	(Baztan et al., 2014)

^a Assuming a sand density of 1.5 kg/L (reported as g/L, sand density and dry/wet unknown)

All four MP materials were subjected to mechanical degradation using both silt and sand sediment types. For each combination of MP and sediment, four samples were prepared for different lengths of exposure: 0, 10, 20, 40 and 80 days. Blank samples (t_{40} and t_{80}) containing only SW and sediment (one with each type of sediment at each time point) were included to assess contamination and extraction efficiency. In addition, a control sample with only MP was

prepared for each type of MP, which was weathered without sediment for 40 days. A detailed list of the samples can be found in Table A.3 in Appendix C.

All samples were prepared in 250 mL conical flasks with glass stoppers. It was desirable to minimize the amount of SW to increase the likelihood of interaction/physical impact between MP and sediment. Testing showed that a volume of 100 mL was enough to avoid a dry spot in the middle of the conical flask during the swirling motion of the shaking incubator. The swirling motion kept the silt in suspension, while the sand was rotating at/near the bottom. The samples were shaken for 30 s prior to placing them into the shaking incubator. The lid was closed, allowing no light inside, and the rotation set to 150 rpm. The temperature (set to 20.0 °C) was in the range 19.7 - 20.7 and 25.9 - 29.6 °C in the first and last 40 days, respectively, as the cooling function of the shaking incubator stopped functioning. Samples were removed after 20 (t_{20}), 40 (t_{40}), two blanks and the four control samples) and 80 (t_{80} and two blanks) days, wrapped in aluminium foil and stored in dark room at room temperature until extraction.

For each sample, the MP material was separated from the sediment by density separation using NaCl, as follows:

1. 25 g NaCl_(s) was added to the sample and shaken for 2x 10 s.
2. Each sample was poured into a density separation setup (see Figure 3.3), consisting of a glass funnel with latex tubing on the end closed by a clamp. The conical flask was rinsed out with 2x 10 mL 1.2 kg/L NaCl_(aq).
3. The sides of the glass funnel were rinsed down with 5 mL of the NaCl solution.
4. The glass funnels were covered with Al foil and let settle.
5. After settling, the bottom clamp was opened, allowing the sediment and half of the solution drain out.

For the samples containing silt the settling time was 1.5 hours and steps 3-5 were repeated trice (4 settling periods). For the sand samples, a single settling period of 2 hours was sufficient.

The remaining solutions were vacuum filtered. A DURAN[®] glass filtration apparatus was used for the small MP materials (PE-10 and PS-10), using 35 mL DI water to rinse out the glass funnel and 15 mL to wash down the sides of the filtration apparatus. For the large MP materials (PE-100 and PS-100) filtration was performed with a Buchner funnel and Whatman GF/F filters (0.7 µm retention, 7 mm diameter), using 50 mL DI water to rinse out the glass funnel and 150 mL to wash the MP on the filter. Filter drying, transfer to vials and storage were as for the photodegradation experiment.

3.4 Sample analysis

3.4.1 Light microscopy

Light microscopy was used to determine particle size distribution and particle morphology of the large MP particles (PE-100 and PS-100). The sediments were also imaged, and classified according to size as silt and sand (ISO13322-1, 2014). Imaging was performed using a Leica M205 C stereomicroscope equipped with a Leica CLS150 LS light source. Glass microscope slides were pre-cleaned with ethanol. Approximately 2 mg of MP material was on a slide, distributed horizontally to reduce overlapping MP particles, and a cover slide placed on top. For each sample, 10 images were taken at 80x magnification to document the MP morphology, and another 10 at 20x magnification for size distribution measurement. The light source was set to maximum, and to maximize the contrast and detail the images were captured in dark-field mode. The display settings were as follows: exposure time: 150 ms, white balance: auto, brightness levels: 75 (minimum) and 150 (maximum).

The light microscopy images were processed using ImageJ software to determine size distribution and possible changes with weathering time. Each image was adjusted in the following way: image type: 8 bit, threshold: 100/255 (min/max), BW and dark background. The *Analyze Particles*-function used to get area of each particle with the following settings: no limits on area or circularity, holes included and particles on the image edges excluded. The achieved optical resolution at 20x magnification was 0.57 pixels/ μm . From the projected area, the area equivalent diameter (x_A) was calculated and used in further analysis. To ensure objective analysis, all samples were treated in the same way, and foreign particles and particle clusters were not manually excluded. Blank microscope slides were analysed to assess the background level of contamination.

3.4.2 Scanning electron microscopy

A Supra 55VP field emission scanning electron microscope (FE-SEM, Carl Zeiss AG) equipped with an energy dispersive X-ray spectroscopy (EDS) detector (from EDAX) was used to image the small MPs (PE-10 and PS-10), and to examine the surface morphology for possible changes with weathering time. Method development work identified the following optimal SEM settings: detector: secondary electron, aperture: 30 μm , accelerating voltage: 1.00 kV, working distance: 5.7 mm, brightness: 50 ± 1 % and contrast: 33 ± 2 %. Three images were captured at four different magnifications (500, 1000, 2000 and 5000x) to get both an overview of each

sample and close-up images showing the surface morphology. To minimize possible errors, samples of the same MP type from the same experiment (e.g. all photodegraded PE-10 samples) were analysed together on the same SEM sample holder.

The sediments were analysed by EDS at 10 kV to confirm their elemental composition. Sediment EDS spectra were also used qualitatively; compared against EDS spectra of MP samples to evaluate if the density separation method successfully separated MP and sediment particles.

3.4.3 Fourier Transform infrared spectroscopy

Changes in MP polymer chemistry were studied using a Bruker ALPHA FTIR spectrometer equipped with an Eco-ATR (attenuated total reflection) sampling module. The ZnSe sampling crystal and clamp was cleaned with 1-propanol and air dried between each sampling. Prior to each sample, a background spectrum was recorded with the ATR clamp open. To allow possible (semi-)quantitative analysis, spectra were collected in absorbance mode (as opposed to transmittance) (Stuart, 2004). Three spectra in the 4000 – 600 cm^{-1} range (32 scans) were recorded of each sample using the same sample material and averaged.

Background subtraction, baseline correction (rubberband correction with 64 baseline points) and vector normalization were performed in the OPUS software. Normalization was necessary as the absorbance is dependent on sample thickness, which cannot be controlled when analysing MP in powder form using an ATR crystal. Two normalization methods were tested: (1) Min-Max and (2) Vector normalization. Vector normalization (mean centering) was chosen as it is more commonly used in quantitative analysis (Lasch, 2012) and resulted in more clustered baselines, giving a better visualisation of differences in both minor and major absorbance bands. Spectral differentiation was tested but not used further as the processing steps above were considered sufficient for the qualitative/semi-quantitative analysis. For the same reason, peak heights (absorbance units) were used instead of peak areas (integrated absorbance units). Vector-normalized spectra were compared directly; using peak ratios was attempted but discarded as the only suitable reference peak for PS gave temporal trends equivalent to those found by direct comparison. The advantage of direct comparison is that unexpected changes will not be overlooked; the peak ratio method is based on the assumption that the reference peak changes minimally (within the set of samples to be compared) and does not overlap with other peaks (Stuart and Ando, 1997).

3.4.4 Pyrolysis-gas chromatography-mass spectrometry

Chemical composition of photodegraded MP (PE-10 and P-10) was analysed using a flash-pyrolysis unit (Pyrola) with a platinum filament (resistive heating) coupled to a TRACE Ultra gas chromatograph with an ITQ 1100 Ion trap quadrupole mass spectrometer (Thermo Fisher Scientific). A 30 m DB-5 capillary column ((5 % phenyl)-methylpolysiloxane, 0.25 mm ID, 0.25 μm film thickness) from Agilent was used; a non-polar column widely utilized to separate polymer pyrolysis products (Fischer and Scholz-Böttcher, 2017, Kusch, 2014). The Pyr-GC/MS settings are listed in Table 3.6. Manual fractionation pyrolysis was carried out by “desorption pyrolysis” at 250 °C followed by a GC/MS run, then at 600 °C on the same sample with a new GC/MS run. The pyrolysis unit temperature was calibrated at regular intervals and when the filament was changed. The parameters tested during the Pyr-GC/MS method development can be found in Table A.5 (Appendix C).

Table 3.6: *Pyrolysis-gas chromatography-mass spectrometry settings*

Unit	Parameter	Setting
Pyrolysis	Chamber temperature	175 °C
	Pyrolysis time	2 s
	Manual fractionation temperatures	250 and 600 °C
GC	Carrier gas	Helium
	Inlet temperature	280 °C
	Injection mode, ratio and flow	Split (1:13), 1.5 mL/min
	Temperature program	40 – 90 °C at 5 °C/min, 90 – 300 °C at 10 °C/min (5 min hold for PE-10)
	Average velocity	25.6 cm/s
MS	GC/MS interface temperature	300 °C
	MS temperature	200 °C
	Ionization technique	Electron ionization (EI)
	EI source voltage and temperature	70 eV, 230 °C
	Scan mode and mass range	Full scan, 41 – 600 m/z

The PS-10 samples were applied to the filament in dry form. A drop of toluene was used to fix the PE-10 to the filament and let to evaporate for 1 min; without fixation it flew off due to its

fluffy and static properties. An aromatic hydrocarbon was recommended by the PE-10 supplier (Cospheric), and toluene did not co-elute with any of the PE desorption or pyrolysis products.

To identify the “minimal residual surfactant” in PS-10 as stated by the Supplier, the PS-10 solvent and three potential surfactants (Tween 20, Tween 80 and sodium dodecyl sulphate) were analysed. The aqueous phase was separated from the MP particles by centrifuging 150 μ L in a GC insert vial for 5 min. One drop of the resulting aqueous phase applied to the filament, let to air dry before analysis.

After each sample analysis, the filament was cleaned using a blow torch, and 2-3 blank Pyr-GC/MS runs conducted due to contamination/carry-over. Blanks with and without toluene were also run to eliminate spatula and solvent contamination. Peak areas were integrated using Xcalibur software (Thermo Fisher Scientific). Identification was achieved using the NIST Mass Spectral Library and by comparison with reference spectra in *SciFinder* and *Pyrolysis-GC/MS Data Book of Synthetic Polymers* (Tsuge et al., 2011).

3.4.5 Coulter Counter

The size distribution of PE-10 and PS-10 was measured using a Beckman Multisizer 4 Coulter Counter equipped with a 100 μ m aperture tube (particle size range: 2-60 μ m). The analysis was carried out using approximately 0.3 mg MP material in 20 mL seawater (0.0015 % w/v) and was successfully performed without dispersant in PS-10. As PE-10 did not disperse sufficiently it was made up in a 0.1 % Tween (polyoxyethylene (20) sorbitan monooleate) solution according to the supplier’s protocol (Cospheric, 2014). Blanks were subtracted from the size distributions: 0.1 % Tween solution and pure seawater for PE-10 and PS-10, respectively.

3.4.6 Data processing

Microsoft Excel was used to sort and prepare data for other software and for basic calculations. IBM SPSS Statistics was used to graphically represent particle size distributions and perform statistical analyses. Pre-processed FTIR spectra were graphically presented using SigmaPlot, while microscopy images and figures were assembled using Adobe Photoshop CS3.

3.5 Method development

3.5.1 Separation of microplastics from sediment

Before conducting a full-scale mechanical degradation experiment, a method to separate MP from the sediment had to be established. As the MP materials all had densities $<1.2 \text{ g/cm}^3$, density separation using NaCl was investigated as an easy, cost-effective and non-toxic approach. A saturated NaCl solution was prepared by mixing 300 g NaCl with 855 g DI water. The resulting volume of a solution of NaCl and water is not additive (Bockris et al., 1998), so the density was determined by weighing 100 mL of the resulting solution in a 100 mL volumetric flask: 1.91 g/cm^3 .

The applicability of density separation using NaCl was initially tested using a 50 mL separating funnel, on a mixture of 50 mg PS-100, 0.50 g clean silt and 25 mL NaCl solution. This set-up was not used further as the silt did not easily flow through the stopcock. Furthermore, not all the silt particles sank to the bottom of the separation funnel, and lowering the density of the NaCl solution to $\sim 1.15 \text{ g/cm}^3$ did not significantly increase sinking of these particles. The silt particles that did not settle in the NaCl solution were presumably organic residue, as they were generally larger and had a different appearance than the settled silt. It was therefore decided to pre-wash the silt to remove the low-density particles by subjecting it to density separation prior to using it in the mechanical degradation experiment.

Test experiment

A small-scale test experiment using a conventional funnel with tubing and a clamp instead of a separation funnel was conducted. The non-cleaned silt was used, as any low-density particles in silt could be manually removed from the filter paper at this quantity. 10 mg MP (PE-100 and PS-100) were added to 10 mL volumetric flasks containing 100 mg silt and 5 mL SW (1:10:500 MP:silt:SW ratio). The flasks were put in a 500 mL beaker with padding to avoid fracturing and subjected to mechanical weathering in the shaking incubator for 7 days at $20 \text{ }^\circ\text{C}$ at a rotation of 150 rpm (horizontal, circular rotation).

The density separation method was developed based on a manual from NOAA (2015): *Laboratory Methods for the Analysis of Microplastics in the Marine Environment: Recommendations for quantifying synthetic particles in waters and silt*. A 7 cm long piece of plastic tubing was attached to the stem of a 10 cm conical glass funnel and closed with a clamp as shown in Figure 3.3.



Figure 3.3: The set-up of the density separation, to separate microplastic particles from soil.

The density separation procedure was as follows:

- (1) 25 mL NaCl solution (1.2 g cm^{-3}) was added to each funnel, the samples added, and the sample flasks rinsed with 2x 10 mL NaCl solution.
- (2) The suspension was left to settle for 2.5 hours.
- (3) Another clamp was attached directly beneath the tip of the glass funnel, right above the settled silt, and the bottom clamp opened. The top clamp was slowly loosened to let ~5 mL of the liquid drain out, washing out the silt below.

The procedure was repeated twice, but with a settling time of 15 min the second and third time. During the first drainage of the test sample, the tip of the glass funnel broke, and all except a few mL of the liquid was spilled. MP was however visible in the conical part of the funnel, so the sample was included in the remaining filtration and drying procedure:

- (4) The liquid remaining in the conical part of the separation funnel was removed by a pipette and vacuum filtered using a 70 mm Büchner funnel with a Whatman GF/F filter. The liquid remaining in the separation funnel was drained and kept in case of unsuccessful density separation.

- (5) The conical part of the separation funnel was rinsed with 50 mL DI water, which was added to the Büchner funnel. The sample was vacuum dried for 10 minutes.
- (6) The filter paper was placed in a petri dish, along with MP scraped from the edges of the Büchner funnel. The petri dishes were placed in a fan oven at 35 °C for 5 hours and stored in a desiccator until the next day.
- (7) The MP was carefully scraped off the filter paper into a pre-weighed vial.

Large pieces that appeared to be fibres from the filter paper were plucked out of the PE-100 test sample. The recoveries were 57.4 and 33.6 % for PE-100 and PS-100, respectively. Light microscopy showed no foreign particles in the PE-100 test sample, but a particle distinctively different from the rest was observed in the PS-100 test sample (Figure 3.4). A few foreign-looking particles were also discovered in later light microscopy images of pristine PS-100; contamination already present or introduced during light microscopy imaging. The density separation was considered successful. In the full-scale experiments, the length of tubing was increased to 15 cm to accommodate 5 g of sand, and the number and length of settling periods adjusted to optimize separation efficiency.

Sediment cleaning

To remove the low-density particles interfering with the density separation, the silt was pre-cleaned by mixing 100 g silt with 400 mL SW in a conical flask. SW was chosen instead of the NaCl solution as the lower density of SW should allow the elimination of more particles. The following steps (1-3) were performed five times:

- (1) The conical flask was refilled with SW, closed with a glass stopper and shaken
- (2) The suspension was let to settle for 3 hours
- (3) Floating debris was removed with a spatula, and the liquid removed with a pipette

The silt was transferred to a petri dish and dried in a fan oven at 105 °C for 1.5 hours. As the silt solidified in the drying process, it was re-ground using a mortar and pestle.

When density separation was tested on the cleaned silt, significant quantities of fine silt particles accumulated at the surface, suggesting that a fine fraction had been produced in the grinding process. To remove low-density debris in a new silt sample, the same cleaning method was used, but with a few modifications. A 500 mL beaker was used for easier access when removing floating debris, and the following steps performed six times: first with the NaCl solution, twice with SW and thrice with DI water.

- (1) The beaker was filled with liquid, the suspension stirred and covered in Aluminium foil
- (2) The suspension was let to settle for 3 hours
- (3) Floating debris was removed with a spatula, most of the liquid removed by decanting and the remaining liquid removed with a Pasteur pipette

Importantly, the silt was placed in a petri dish and dried in a fan oven at 45 °C for 2 hours, then at 35 °C for 1 hour, weighing every hour to keep track of water loss and keep it from drying out completely and forming a solid mass.

The field-collected quartz sand (200 g) was washed using the final washing procedure as described above. However only 5 washes, all with SW, and a 1 hour settling time were used as there was minimal floating/suspended debris. To remove the fine sand fraction, the sand was sieved using a 250 µm stainless steel sieve under running tap water for 5 minutes, then rinsed with 1 L DI water.

Evaluation of density separation efficiency by light microscopy

After the mechanical degradation test experiment, the test samples and a procedural blank sample (only SW, filtered as with MP samples) were examined to look for silt and filter paper residue. Images of pristine PS-100 and PS-100 from the test experiment is shown in Figure 3.4.

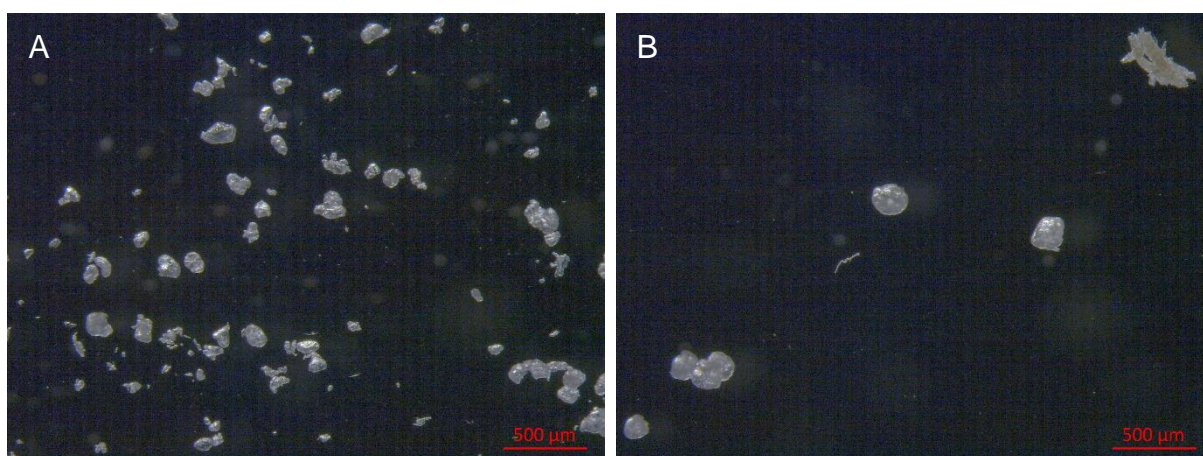


Figure 3.4: Light microscopy images of (A) pristine PS-100 and (B) PS-100 sample from physical degradation test experiment, captured at 2.5x magnification

The particle that is distinctively different from PS-100 (upper right corner of Figure 3.4 B) is likely not silt or a fibre from the filter paper, but contamination. Similar brown-coloured particles were later found in pristine PS-100, indicating pre-existing contamination.

When comparing images of PS-100 before and after density separation, it seems like the smallest particle fraction of PS-100 is absent. To check if the loss had occurred in the density separation step or could be explained by interaction with the silt particles, a recovery test was performed. Pristine PS-100 was recovered according to the mechanical degradation test experiment procedure, excluding the density separation step. Light microscopy images of PS-100 recovery test sample also indicate absence of the smallest particle fraction, so the loss must have occurred during filtration and drying procedure, possibly to the filter paper.

4 Results

4.1 Characterization of pristine microplastic materials

Microscopy images

SEM images of pristine PE-10 and PS-10 at 2000x and 5000x magnification are shown in Figure 4.1 and Figure 4.2, respectively.

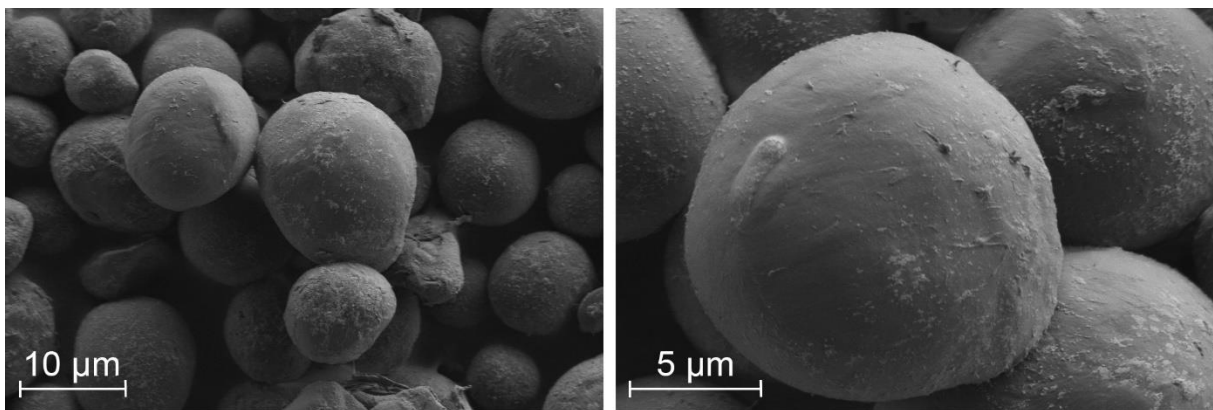


Figure 4.1: SEM images of pristine PE-10 at 2000x (left) and 5000x (right) magnification.

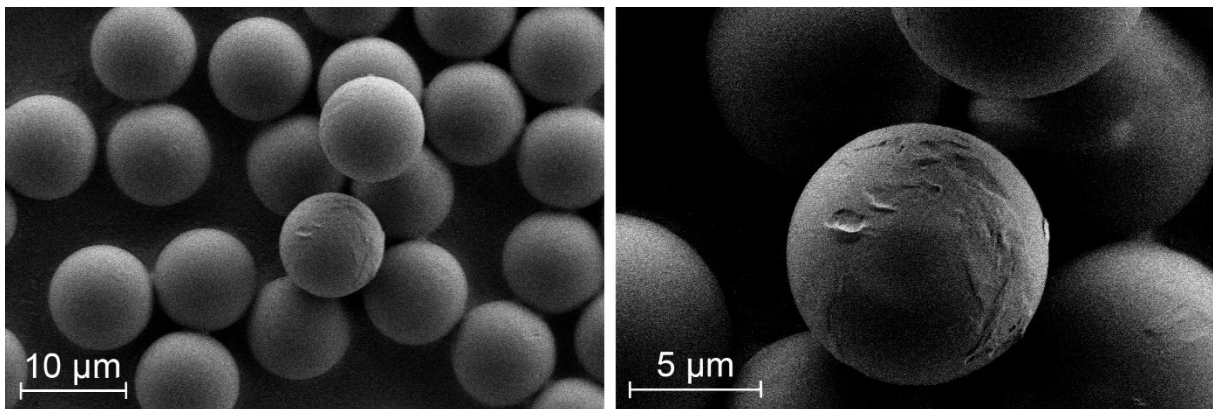


Figure 4.2: SEM images of pristine PS-10 at 2000x (left) and 5000x (right) magnification.

Light microscopy images of PS-100 and PE-100 are shown in Figure 4.3. The shape and morphology of the two MP materials is significantly different: the PS-100 particles are smoother and more spherical than PE-100 that exhibits a large variation in shape. It was manageable to distribute the PS-100 particles on the microscope slide so that the majority of

particles were not touching. For PE-100 this was challenging as there were numerous clusters of tangled particles as seen in Figure 4.3 (C).

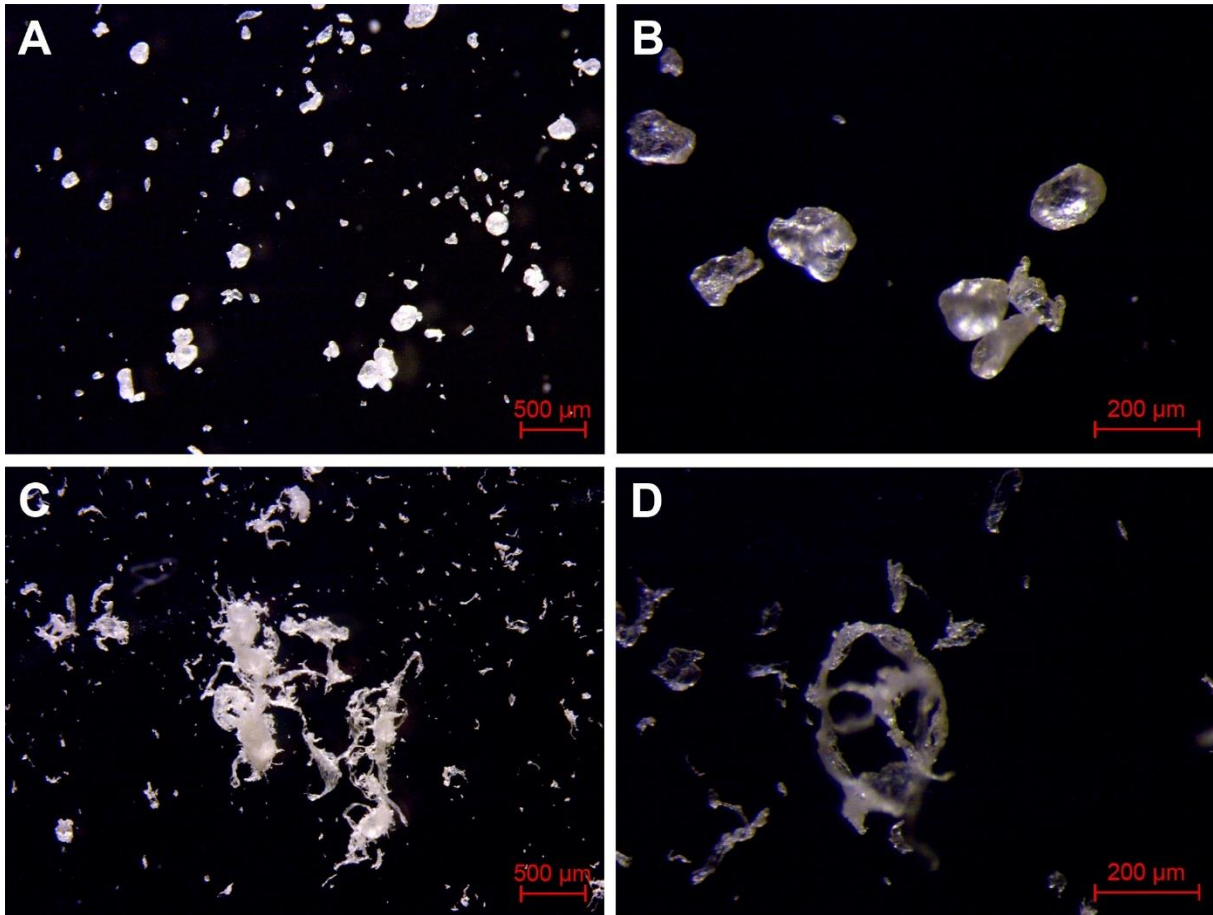


Figure 4.3: Light microscopy images of pristine MP at two different magnifications: PS-100 at (A) 20x and (B) 80x and PE-100 at (C) 20x and (D) 80x magnification.

Size distribution

Coulter Counter size distributions of PE-10 and PS-10 are presented in Figure 4.4 and Figure 4.5, respectively. The PS-10 size distribution is narrow, while the size distribution of PE-10 is logarithmic and broader; in agreement with the supplier's statement of >90 % in the 3-16 μm size range.

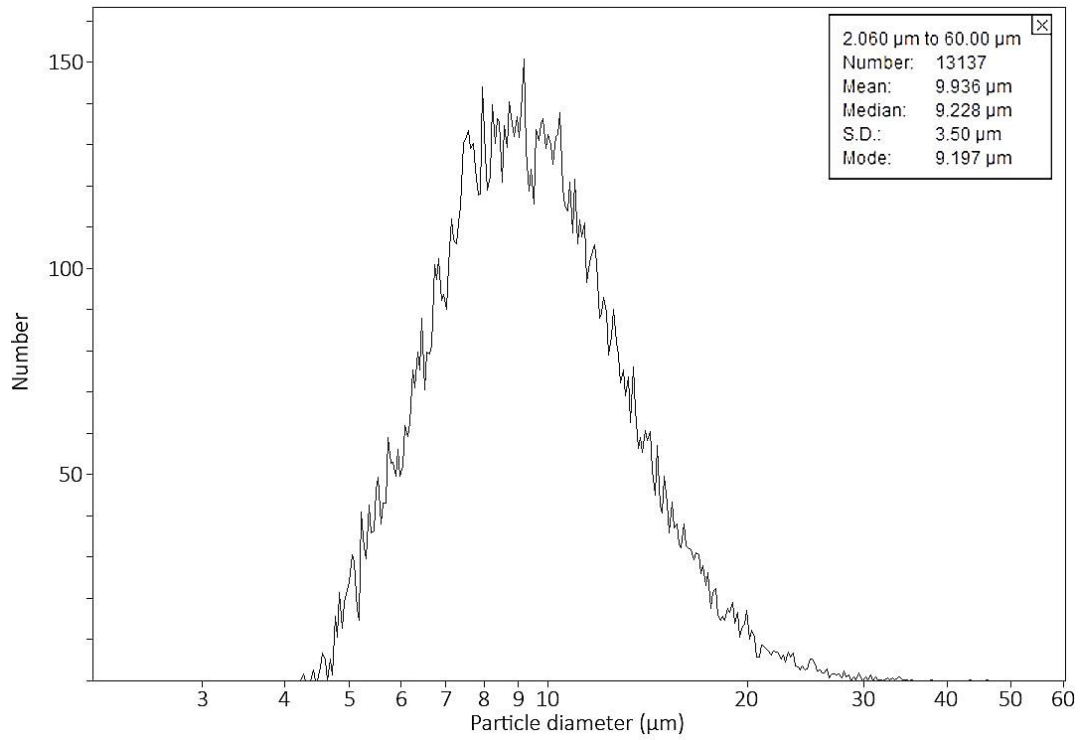


Figure 4.4: Coulter Counter size distribution of pristine PE-10 (logarithmic and number-based).

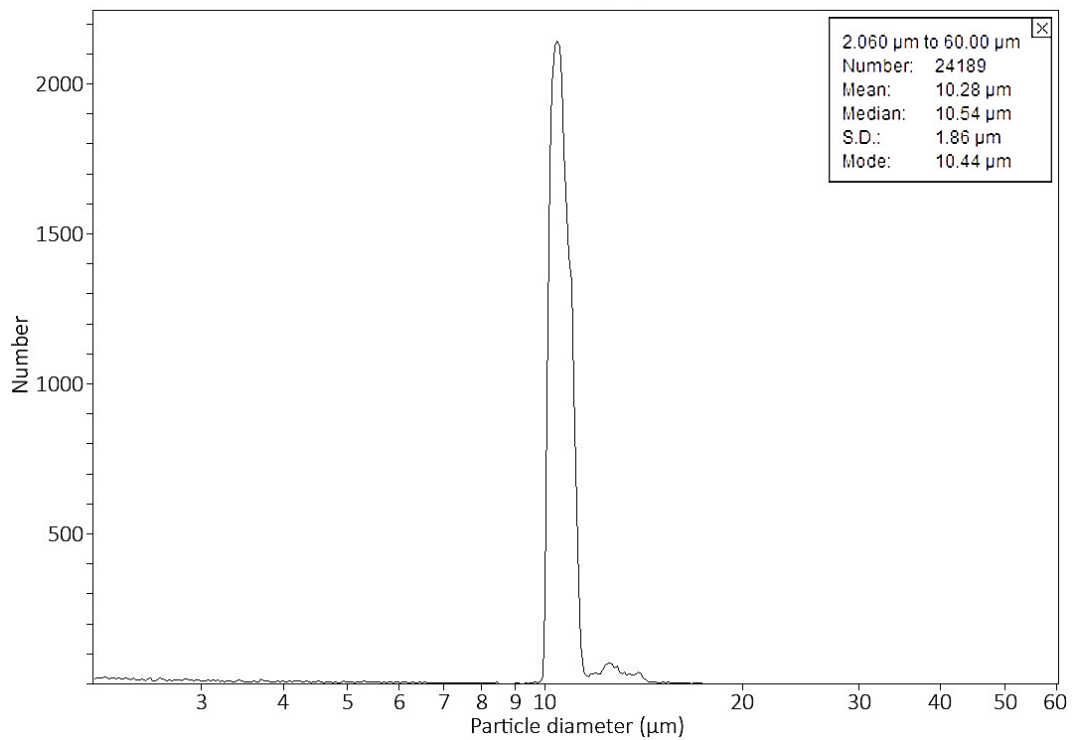


Figure 4.5: Coulter Counter size distribution of pristine PS-10 (logarithmic and number-based).

The size distributions of PE-100 and PS-100 obtained from light microscopy images are presented in Figure 4.6 and Figure 4.7, respectively. Two histograms are shown: (A) all particles and (B) excluding particles with diameters corresponding to <5 pixels as recommended by British Standard BS3406 (1993).

The size distributions appear logarithmic, as it exhibits a near-gaussian shape with a logarithmic x-axis as in the presented histograms. The lower part of the potential gaussian shape is removed when particles <5 pixels are excluded, particularly for PE-100. A Rosin-Rammler distribution is common for particles produced by milling, which is similar to a logarithmic distribution but with a tail on the lower end of the scale (Gotoh et al., 1997). Again, exclusion of particles <5 pixels removes part of the tail in a potential Rosin-Rammler distribution for both types of MP.

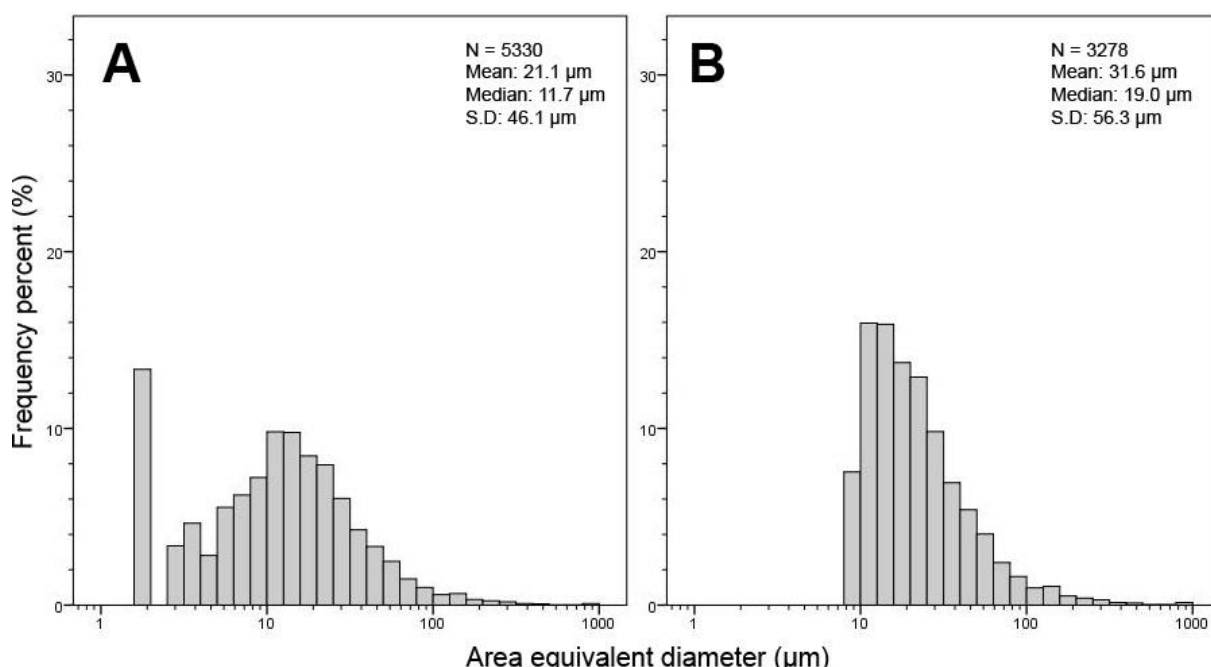


Figure 4.6: Histograms showing the logarithmic size distribution of pristine PE-100, (A) whole size range and (B) excluding particles with diameters <5 pixels, equivalent to 8.77 μm.

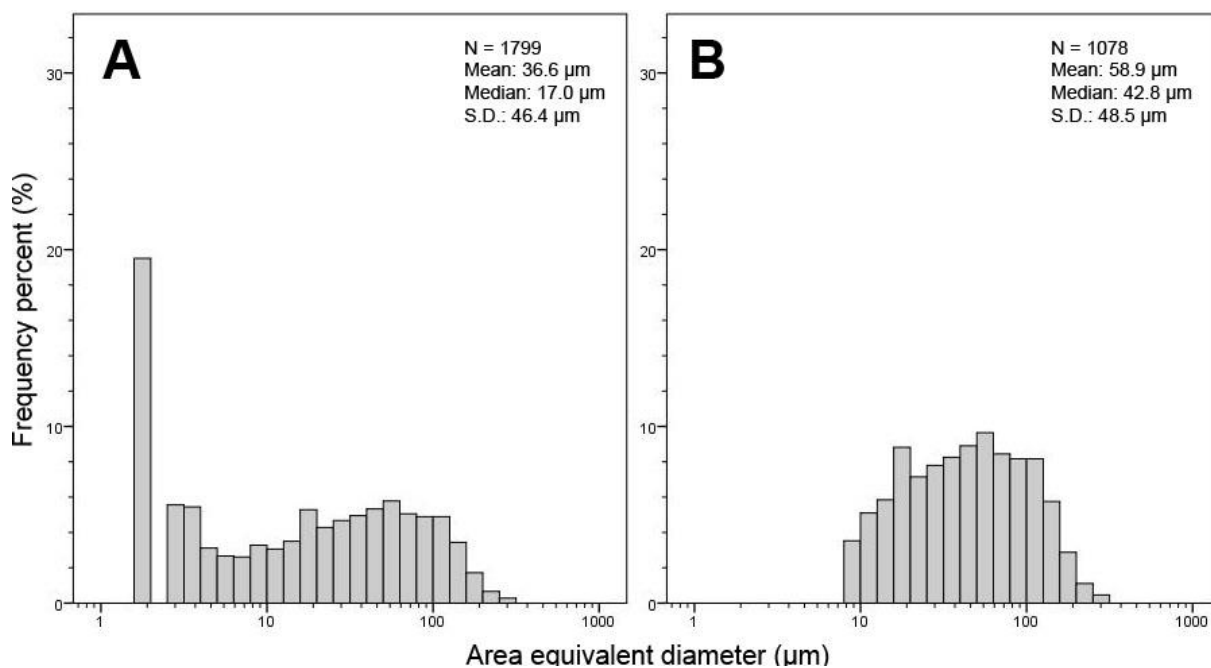


Figure 4.7: Histograms showing the logarithmic size distribution of pristine PS-100, (A) whole size range and (B) excluding particles with diameters < 5 pixels, equivalent to 8.77 μm .

Fourier Transform infrared spectra

The FTIR spectra of pristine PE (PE-10 and PE-100) and PS (PS-10 and PS-100) are presented in Figure 4.8 and Figure 4.9, respectively.

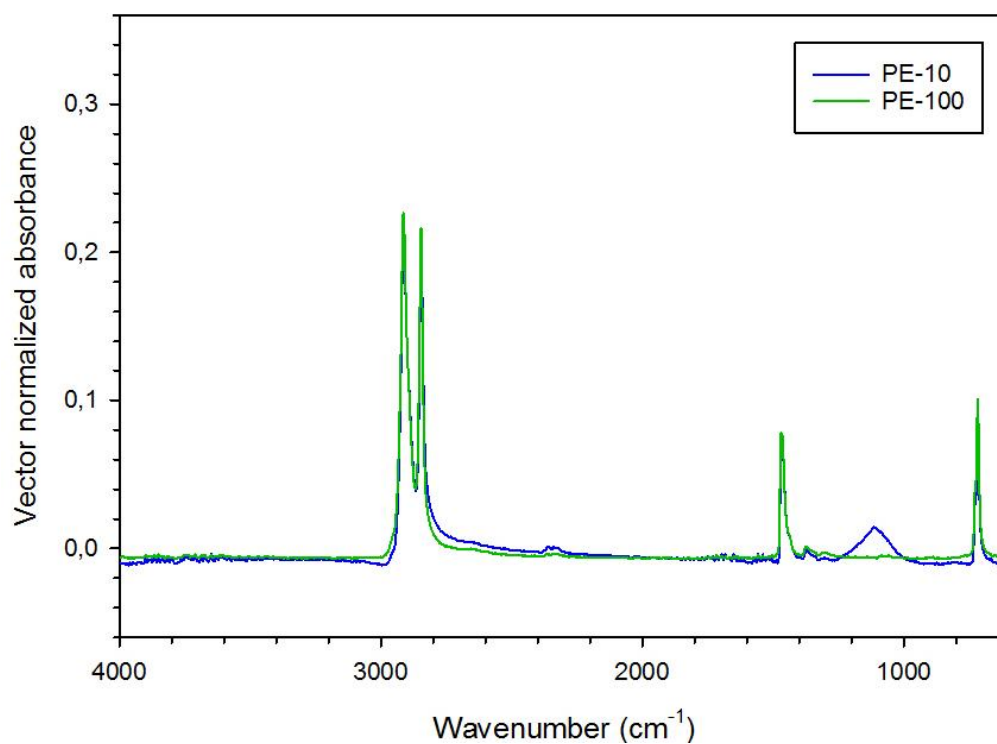


Figure 4.8: ATR-FTIR spectra of pristine PE-10 (blue) and PE-100 (green).

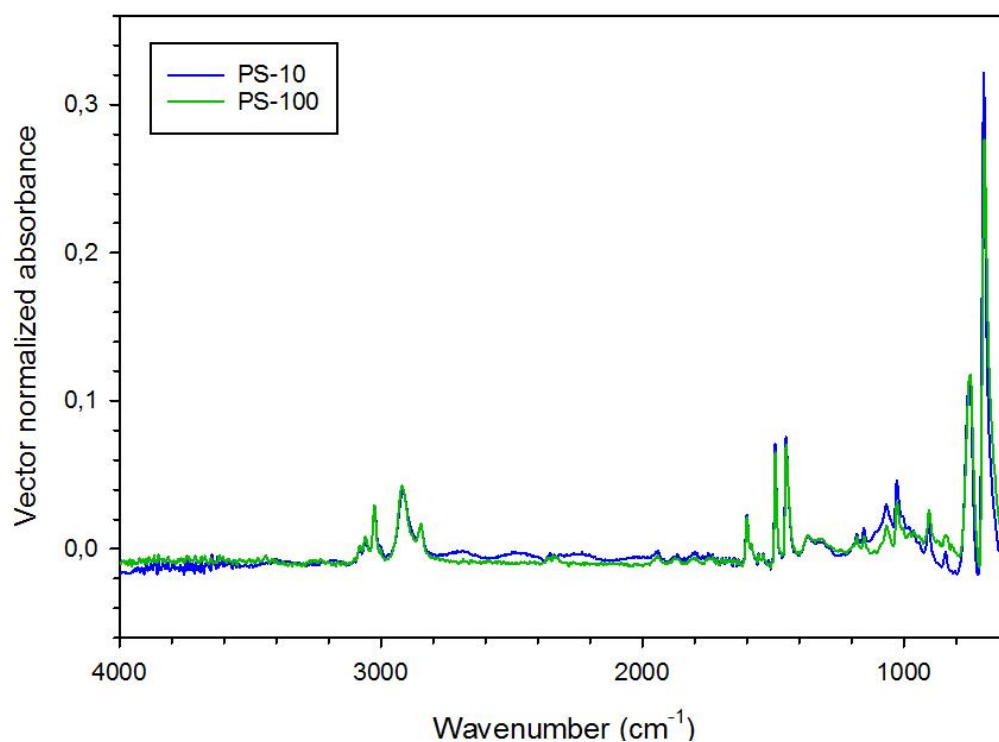


Figure 4.9: ATR-FTIR spectra of pristine PS-10 (blue) and PS-100 (green).

The absorbance bands characteristic of the respective polymers are assigned to molecular vibrations in Table 4.1 (Kuptsov and Zhizhin, 1998, Vasile et al., 2005, Diem, 2015, Nuruzatulifah et al., 2016). For PE-10 and PE-100, the shape and maximum of the C-H wagging band (1377 cm^{-1}) confirms that both are LDPE; in HDPE it would occur at 1366 cm^{-1} (Gulmine et al., 2002). The broad band at 1116 cm^{-1} in PE-10 is not typical for PE, and the supplied product information states that it is 100 % LDPE. The most likely explanation is Si-O-Si asymmetrical stretching from residual silicone oil which is used in the production of polymer microparticles (Dawson and Koppenhagen, 2003).

Both PS-10 and PS-100 can be classified as atactic and amorphous as there is a single band in the $1100\text{-}1050\text{ cm}^{-1}$ region (Luongo, 1971). This is in agreement with the information from the PS-100 supplier (CARAT) which measured a glass transition temperature (T_g) of $95\text{ }^\circ\text{C}$; the T_g of amorphous and crystalline PS is 94 and $100\text{ }^\circ\text{C}$, respectively (Ellis and Smith, 2008). Amorphous polymers can contain crystalline regions, and in PS the presence of bands at 981 cm^{-1} is indicative of crystallinity (Takeda et al., 1959). In this region PS-10 and PS-100 has maxima at 977 and 981 cm^{-1} , respectively, indicating that PS-100 has a higher crystallinity than PS-10. Undetected crystalline regions inside the MP are possible as the penetration depth of ATR-FTIR with a ZnSe crystal is $\leq 2\text{ }\mu\text{m}$ (Renner et al., 2017).

Table 4.1: Infrared absorption bands of functional groups in polyethylene and polystyrene

Polymer	Frequency (cm⁻¹)	Vibration
PE-10	2915/2848	C-H asymmetric/symmetric stretching
	1470, 1464	CH ₃ /CH ₂ bending, doublet
	1377, 1368	CH ₃ /CH ₂ wagging, doublet
	729, 719	CH ₃ /CH ₂ rocking, doublet
PS-10	3059/3024	C-H (aromatic) asymmetric/symmetric stretching
	2917/2848	C-H (aliphatic) asymmetric/symmetric stretching
	1601, 1583	C=C (aromatic) stretching, doublet
	1493/1451	C-H aromatic/aliphatic bending
	1180, 1154, 1068	C-H (aromatic) in-plane bending
	905	C-H (aromatic) out-of-plane bending
	1028, 905, 752, 696	Mono-substituted benzene
	752	C-H (aliphatic) rocking, phenyl ring wagging/twisting
	696	Phenyl ring out-of-plane bending

4.2 Recoveries

A summary of the MP recoveries is listed in Table 4.2, whilst recoveries of individual samples can be found in Table A.6 and Table A.7 in Appendix D. A measurable mass was recovered from one of the four blank samples: 0.2 mg (sand blank t₈₀) which is 0.004 % w/w of the sand initially added. The silt samples had traces of brown-coloured particles.

Table 4.2: Mean MP recoveries and relative standard deviation (RSD).

	MP type	Recovery			
		Mean (mg)	Mean (%)	RSD (%)	
Photodegradation experiment	<i>PE-10</i>	7.7	56	29	
	<i>PS-10</i>	9.6	61	22	
Mechanical weathering experiment	<i>Silt</i>	<i>PE-10</i> ^a	0.2	0	140
		<i>PS-10</i> ^a	0	0	N/A
		<i>PE-100</i>	66	66	4.5
		<i>PS-100</i>	67	67	15
	<i>Sand</i>	<i>PE-10</i>	8.1	54	54
		<i>PS-10</i>	5.9	39	81
		<i>PE-100</i>	83	83	7.3
		<i>PS-100</i>	74	74	11

^a Due to low recoveries of the t_0 and t_{20} samples, the t_{40} and t_{80} samples were not extracted.

4.3 Photodegraded microplastic

4.3.1 Discolouration

Photodegraded PS-10 showed a gradual yellowing over the exposure period (Figure 4.10), while all other MP samples remained white.



Figure 4.10: Image PS-10 photodegraded for (A) 0, (B) 10, (C) 20, (D) 40 and (E) 80 days and (F) control sample (t_{40}) not irradiated but otherwise weathered under the same conditions for 40 days.

4.3.2 Shape and morphology

Figure 5.11 and Figure 5.12 show SEM images of PE-10 and PS-10 from the photodegradation experiment, respectively.

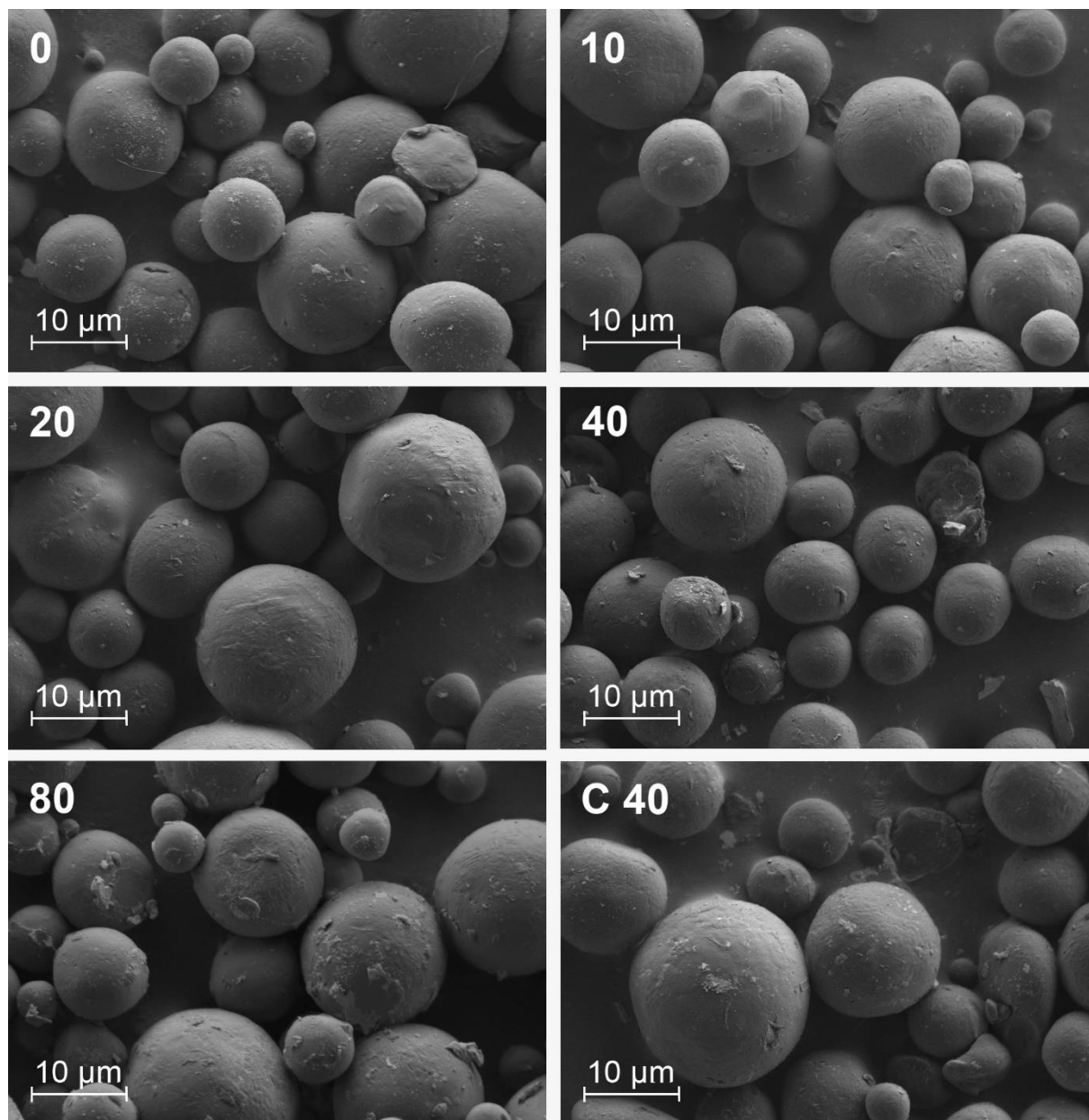


Figure 4.11: SEM images of PE-10 exposed to UV-visible irradiation in seawater for 0-80 days. Control sample (C 40) not irradiated but otherwise weathered under the same conditions for 40 days.

Some embedding of irregularly shaped particles $\leq 1 \mu\text{m}$ is observed in both photodegraded PE-10 and PS-10, which were not present in the SEM images of the pristine materials (Figure 4.1Figure 4.2, respectively). A few similarly shaped particles in the relevant size range were

also found in SEM blank samples (Figure 4.13). While pristine PE-10 (Figure 4.1) contained surface contamination and irregularly shaped “foreign” particles in the same size range as the MP particles, this is mostly absent in the photodegraded PE-10 samples.

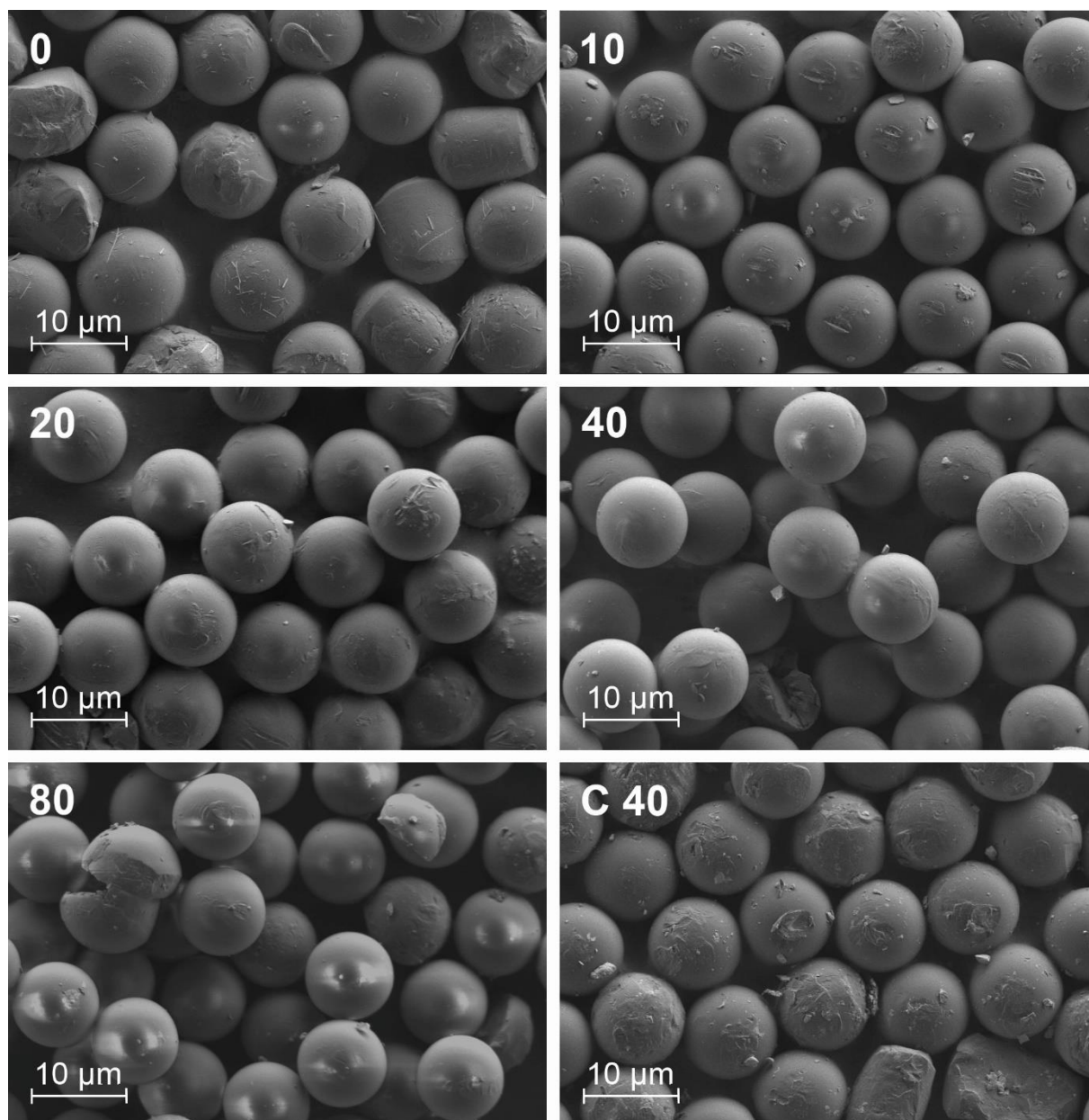


Figure 4.12: SEM images of PS-10 exposed to UV-visible irradiation in seawater for 0-80 days. Control sample (C 40) not irradiated but otherwise weathered under the same conditions for 40 days.

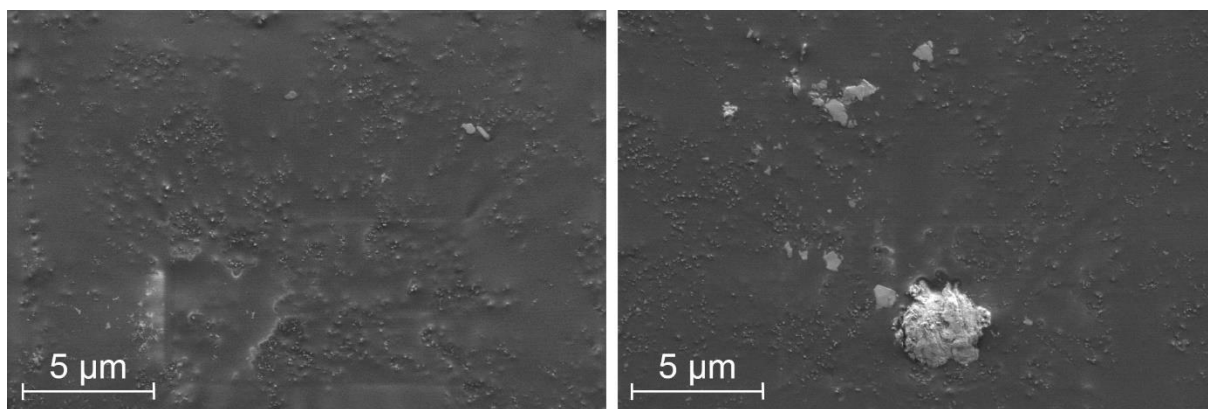


Figure 4.13: SEM images of SEM blank samples (blank carbon adhesive tabs).

SEM images of the surface of photodegraded PE-10 and PS-10 are presented in Figure 4.14 and Figure 4.15, respectively. The particle with the roughest surface from each weathering time point is presented to minimize subjective selection. The surface roughness of PE-10 appears to increase with weathering time, but the change is only observed on some particles. The surface morphology of the control sample (t_{40}) is comparable to the t_{40} and t_{80} samples. For PS-10, a change in surface morphology is observed after 80 days of irradiation.

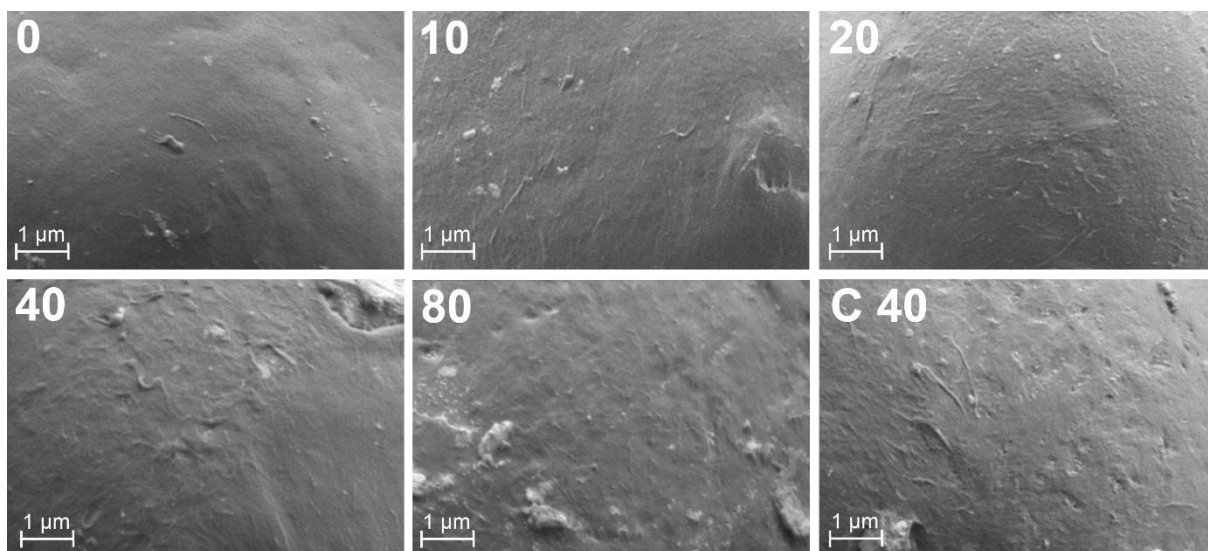


Figure 4.14: SEM images showing the surface morphology of PE-10 exposed to UV-visible irradiation in seawater for 0-80 days, plus control sample (C 40).

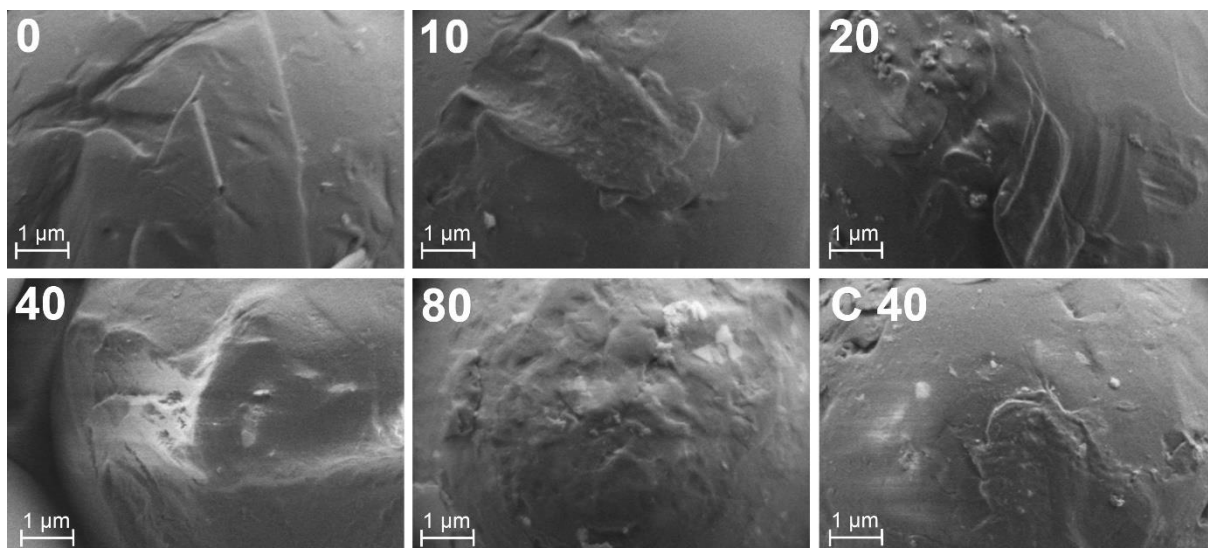


Figure 4.15: SEM images showing the surface morphology of PS-10 exposed to UV-visible irradiation in seawater for 0-80 days, plus control sample (C 40).

The SEM images revealed unknown material on the surface of PE-10 t_{80} . The material is arranged in circular patches with a diameter of 2 μm, some with 2-3 μm long “rods”, as shown in Figure 4.16.

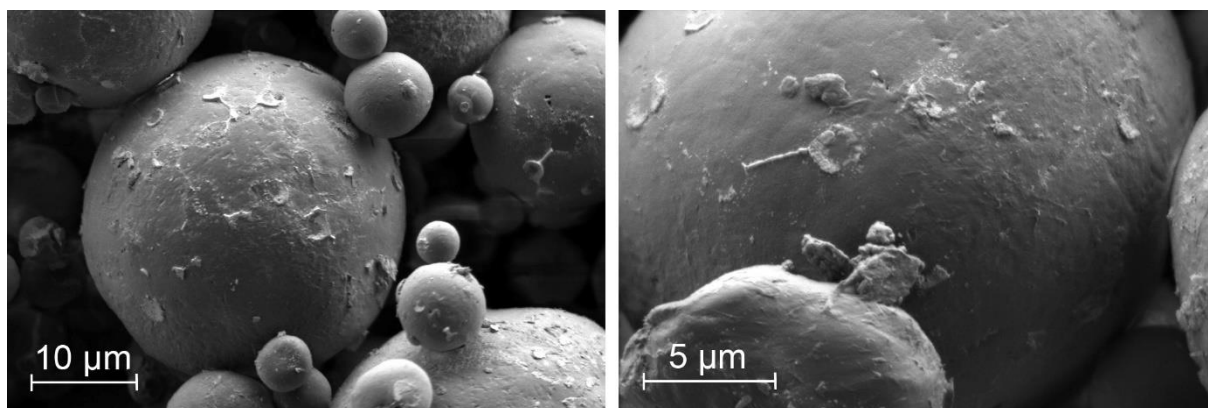


Figure 4.16: SEM images showing the unidentified surface material on PE-10 exposed to UV-visible irradiation in seawater for 80 days.

4.3.3 Chemical characteristics

Fourier Transform infrared spectra

The FTIR spectra of photodegraded PE-10 and PS-10 are shown in Figure 4.17 and Figure 4.18, respectively. Absorbance bands which could be indicative of degradation are presented in Table 4.3 (Brandon et al., 2016, Yousif and Haddad, 2013).

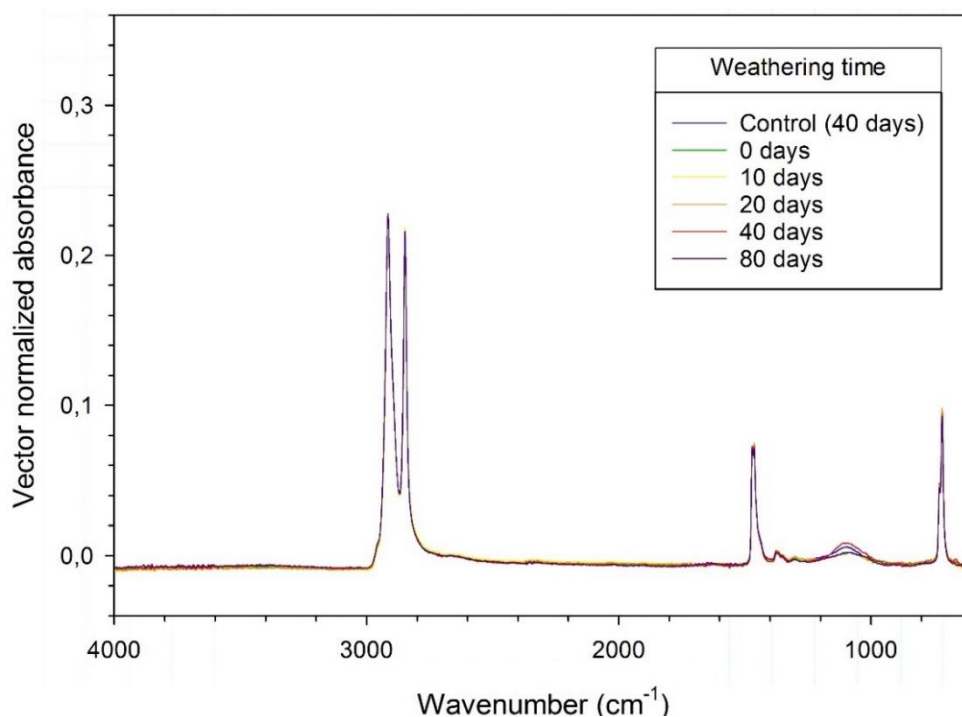


Figure 4.17: ATR-FTIR spectra of PE-10 exposed to UV-Vis radiation for 0-80 days in seawater.

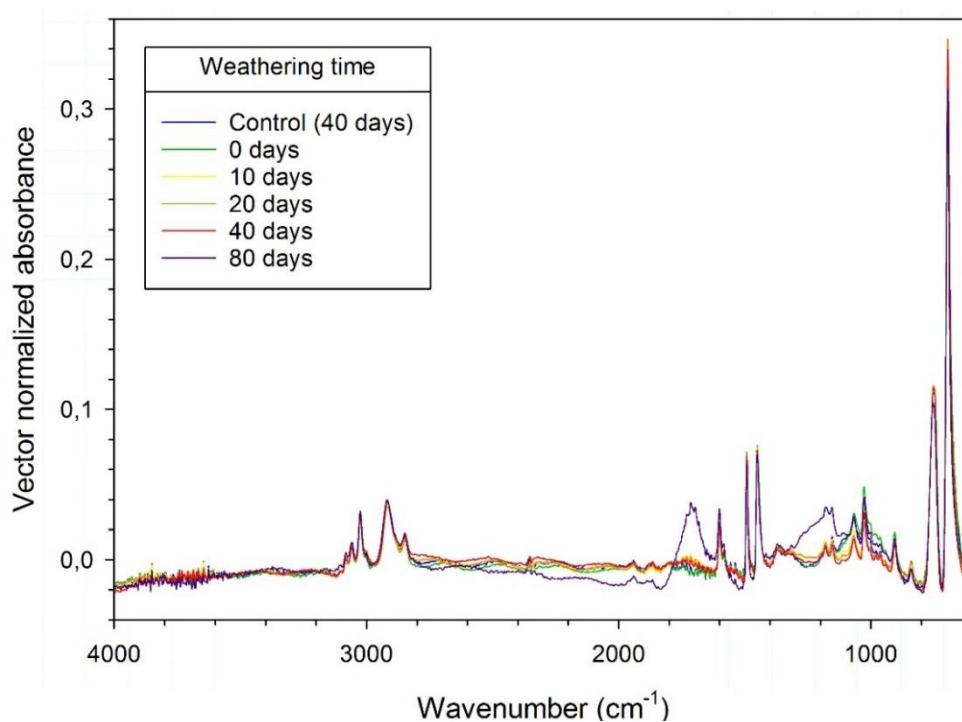


Figure 4.18: ATR-FTIR spectra of PS-10 exposed to UV-Vis radiation for 0-80 days in seawater.

Table 4.3: Infrared absorption bands indicative of degradation in polyethylene and polystyrene.

Polymer	Frequency (cm ⁻¹)		Vibration
	Observed	Reference	
PE-10	1200-1000 ^a	1200-1000	C-O stretch (ether in polymer chain)
PS-10	1714 (1800-1600)	1720-1670	C=O stretch
		1680-1630	C=C stretch
	1350-1100	1350-1000	C-O stretch (aryl-O-R, ether, alkoxy ester, acyl ester)
	842, 623	645-620, 850-810	Para-substituted benzene (crosslinking)

^aAlso present in pristine PE-10, with a greater absorbance

The band in the 1200-1000 cm⁻¹ region in photodegraded PE-10 could be a result of oxidation, but this is however unlikely as it is also present in the FTIR spectrum of pristine PE-10 (Figure 4.8) which is presumably residual silicone oil. Absorbance bands indicative of phthalate additives were not detected in PE-10.

The FTIR spectrum of PS-10 t₈₀ is drastically different from the rest, with broad C=O and C-O stretching bands indicative of oxidation. Increased crystallinity could also be a contributor to the spectral change in the 1350–1100 cm⁻¹ region. Although a slight elevation of the C=O and C-O stretching regions is observed in the t₁₀-t₄₀ samples, it cannot be distinguished from the baseline. None of the spectra show signs of hydroxylation, which would appear as a broad absorption band in the 3600 - 3200 cm⁻¹ region. The possible oxidation products are therefore aldehyde, ketone, ether, ester and peroxide functional groups. The degree of chain scission and cross-linking (and their ratio) could not be estimated from FTIR data due to overlapping peaks and opposite temporal trends. Phthalate additives could not be detected in PS-10 due to overlapping bands.

Pyrolysis gas chromatography – mass spectrometry

Desorption (250 °C) pyrograms of PE-10 and PS-10 are presented in Figure 4.19 and Figure 4.20, respectively. Note the extensive column/septum bleeding (siloxanes) and ghost peaks (contamination/carry-over). Two to three blanks had to be run between each sample to reduce the latter.

Three potential polymer additives were detected in PE-10: phenylglyoxal (A₁), bisphenol AF (A₂) and 1,3,5-triphenylbenzene (A₃). Leaching is possible as A₁ appears to decrease with weathering time, but peak areas cannot be directly compared due to unequal sample sizes (significantly larger t₄₀-sample) and the lack of a reference peak. Table A.8 (Appendix D) shows the details of the labelled peaks in the desorption pyrogram of PS-10. Oxidation is evident at t₈₀ – Figure 4.21 shows the structure of the three most abundant desorbed substances. The potential additives detected in the t₀-sample were not found at t₄₀ or in the control sample (t₄₀), indicating temporal leaching.

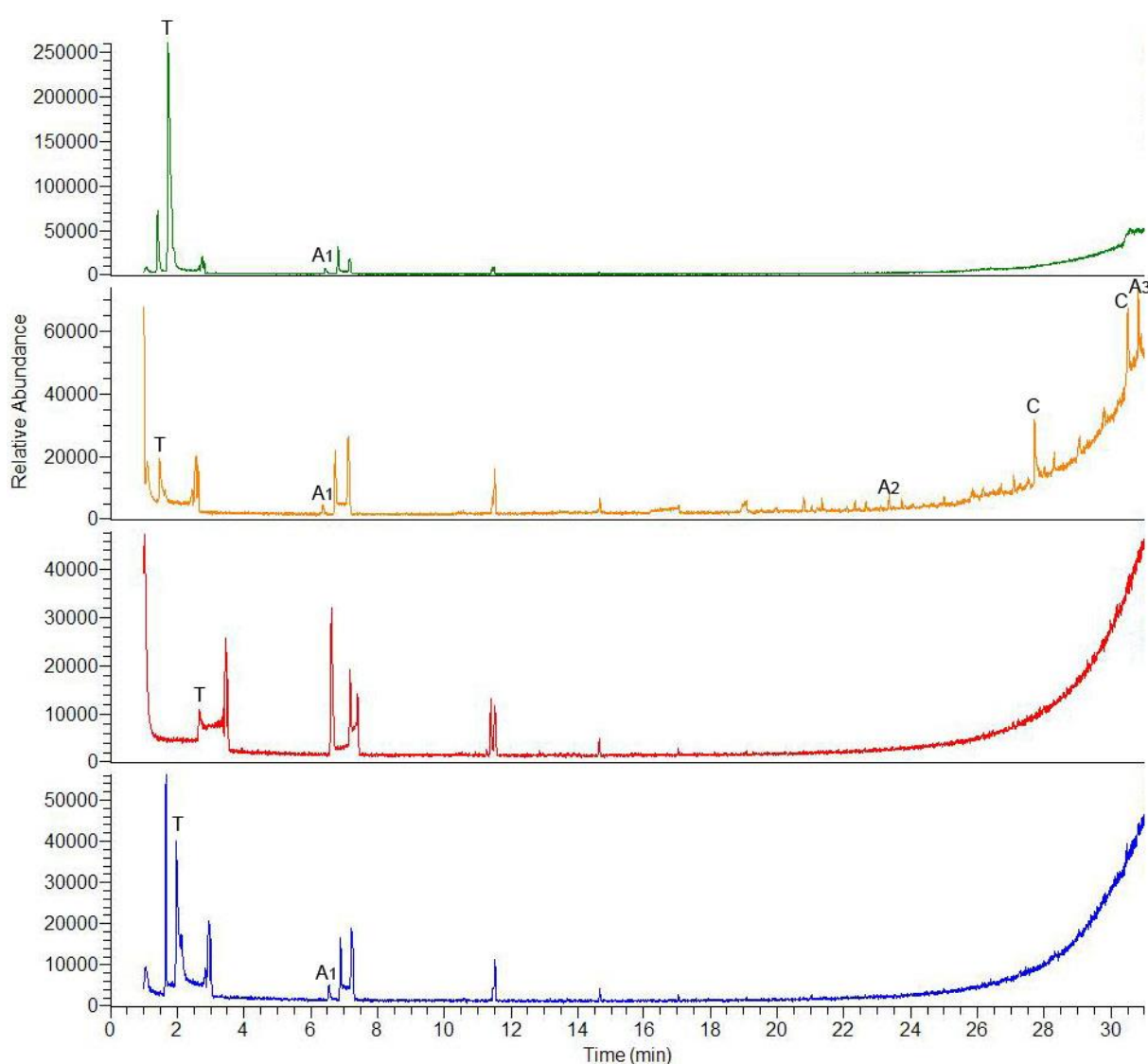


Figure 4.19: Desorption pyrograms (250 °C) of PE-10 photodegraded for 0, 40 and 80 days, plus control sample (C 40). Peak labels: T = toluene, A = possible additive and C = contamination (also found in blanks). Unlabelled peaks are column/septum bleeding or <LOD.

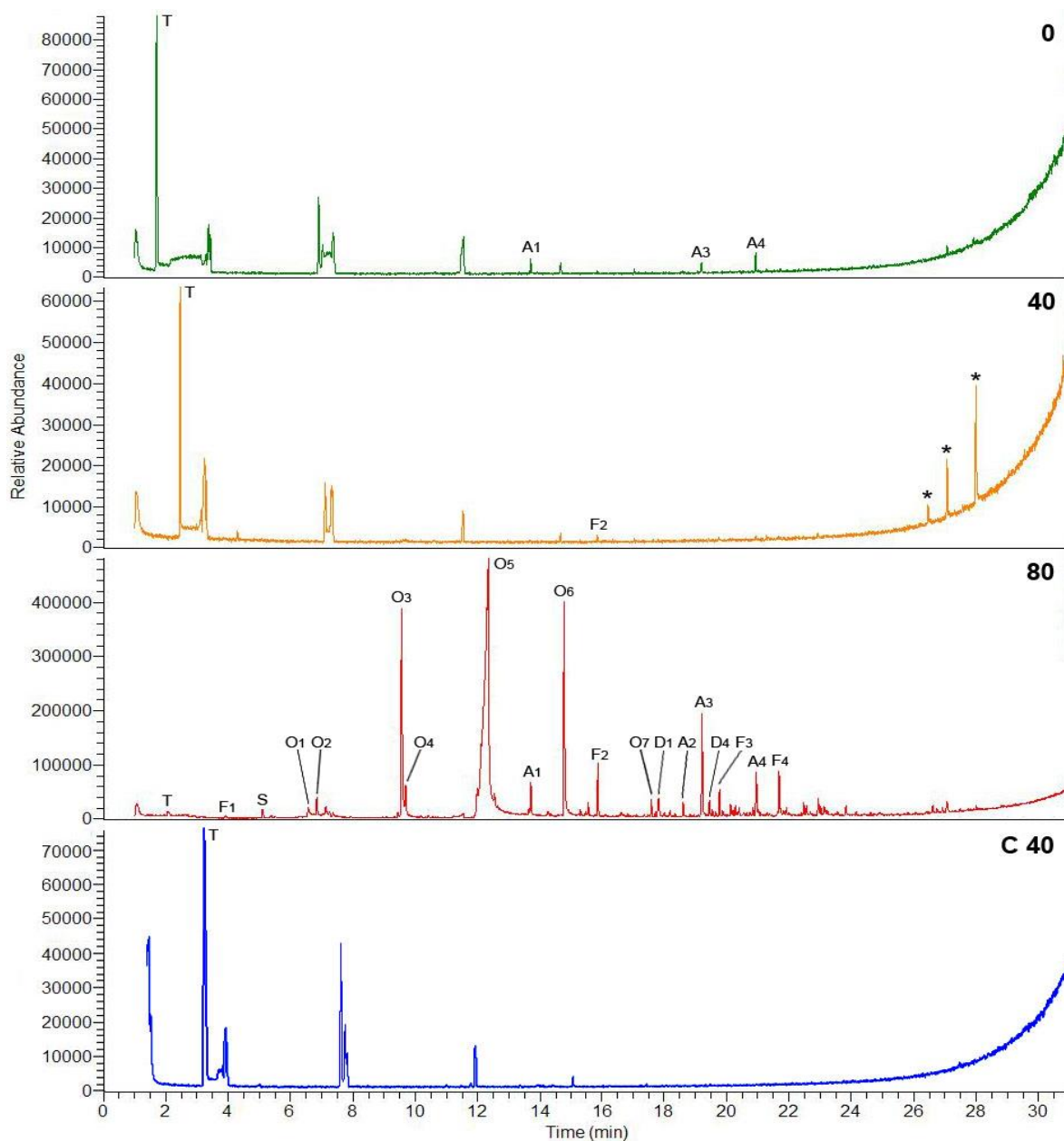


Figure 4.20: Desorption pyrograms (250 °C) of PS-10 photodegraded for 0, 40 and 80 days, plus control sample (C 40). Peak labels: A = additive, F = polymer fragment, * = carry-over, S = styrene monomer, O = oxidized polymer fragment and D = polymer fragment also found in 600 °C pyrogram. Unlabelled peaks in 0, 40 and C 40 are column/septum bleeding.

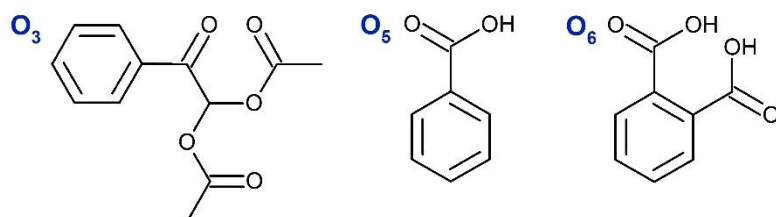


Figure 4.21: Structure of the three most abundant oxidation products desorbed from PS-10 photodegraded for 80 days: 2,2-bis(acetoxy)acetophenone (O₃), benzoic acid (O₅) and 1,2-benzenedicarboxylic acid (O₆).

Pyrolysis (600 °C) pyrograms of PE-10 and PS-10 are presented in Figure 4.22 and Figure 4.23, respectively. The polymer-characteristic pyrolysis products are labelled in the t_0 -pyrograms. The polymer- and degradation-characteristic pyrolysis products of PS are listed in Table A.9 and Table A.10, respectively (Appendix D).

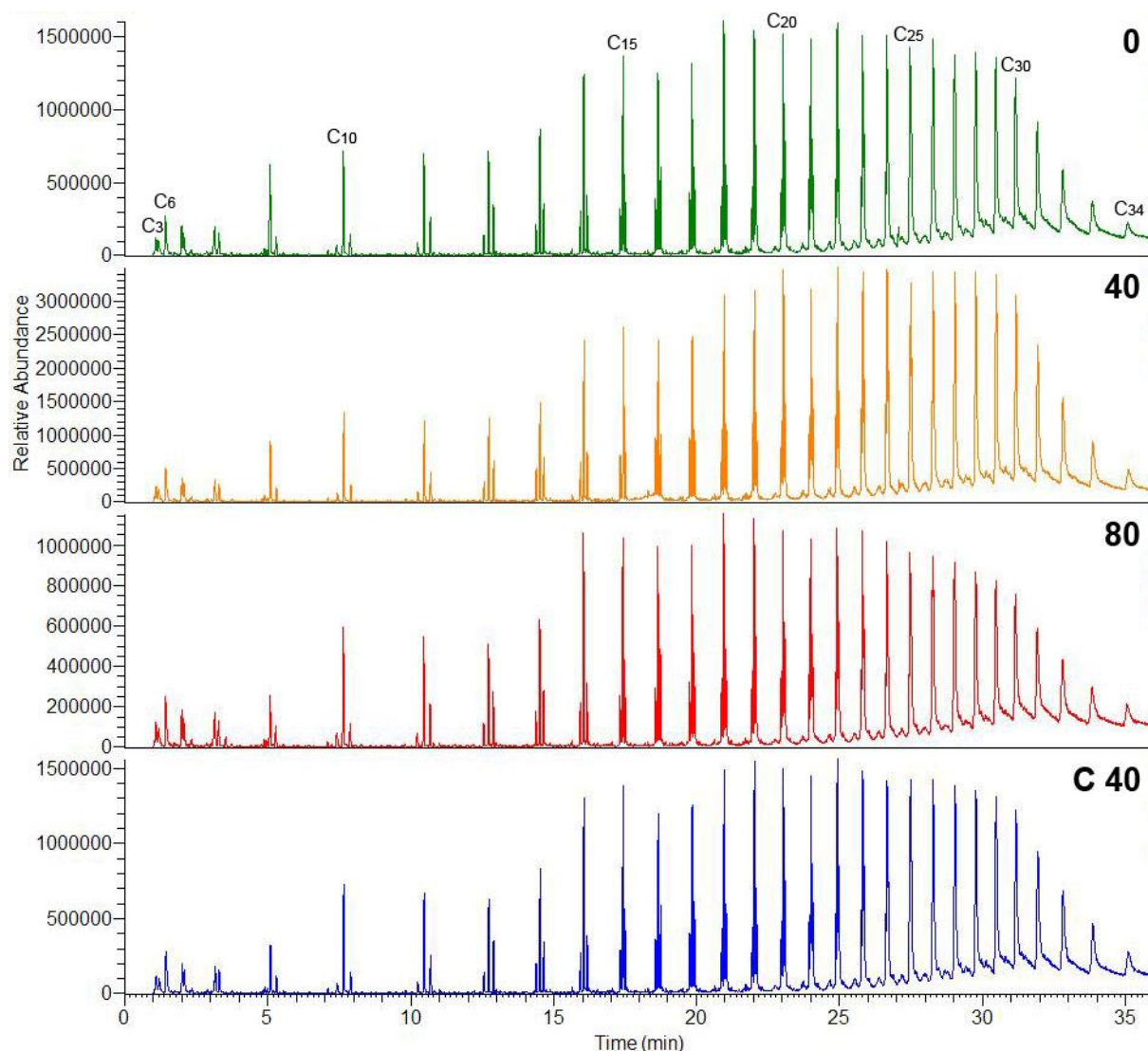


Figure 4.22: Pyrograms (pyrolyzed at 600 °C) of PE-10 photodegraded for 0, 40 and 80 days, plus control sample (C 40). Peak labels: the carbon number of the homologue series triplet (diene, alkene and alkane).

When the pyrograms of PE-10 in Figure 4.22 are overlaid and normalized to C_{18} , it is clear the relative peak heights of the homologues series differ, but not with a clear temporal trend. The peak heights of homologues $>C_{18}$ increase from t_0 to t_{40} , then decrease (to below t_0) at t_{80} , while the opposite occurs for homologues $<C_{18}$. The t_0 and control (t_{40}) sample are comparable.

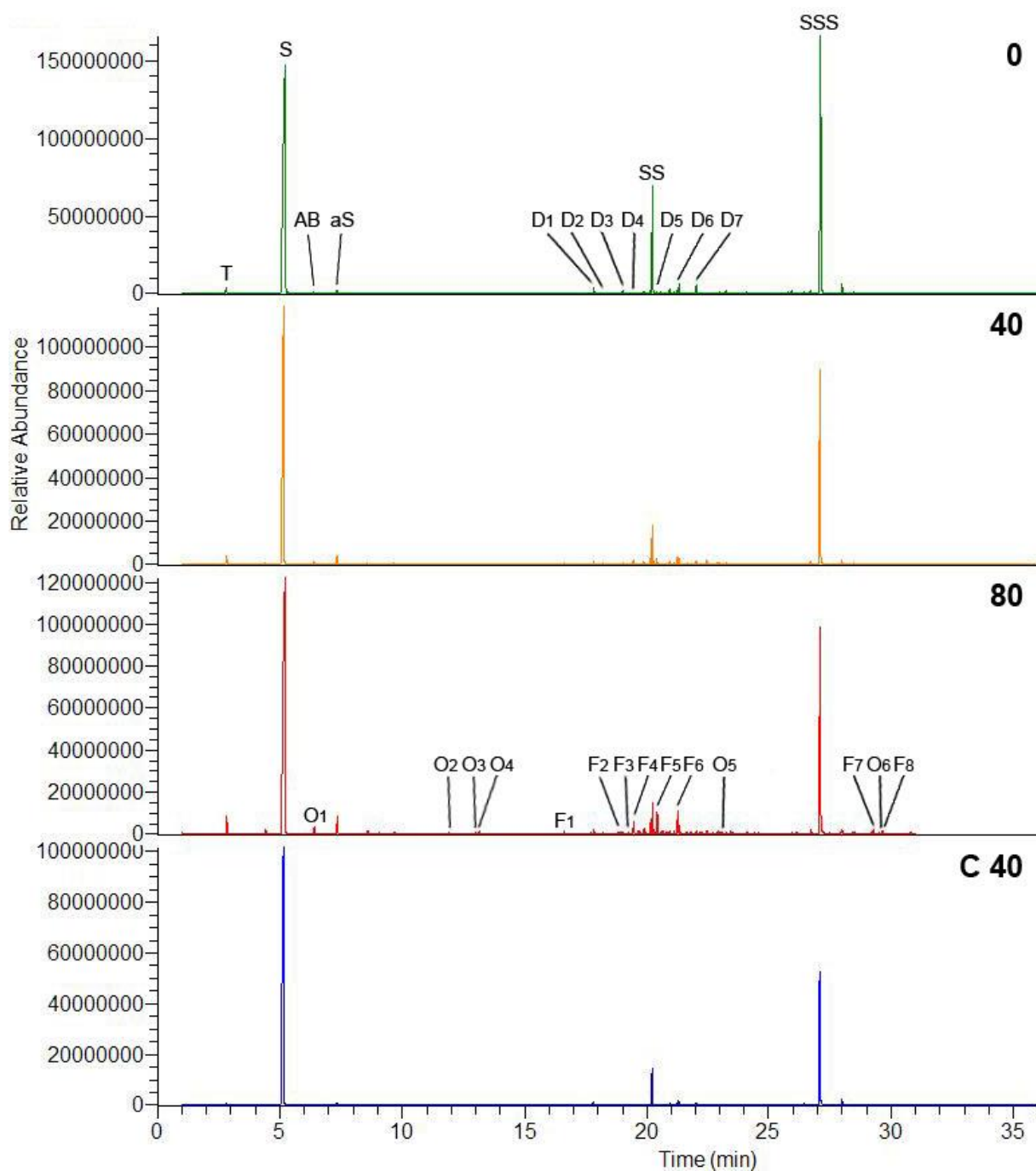


Figure 4.23: Pyrograms (pyrolyzed at 600 °C) of PS-10 photodegraded for 0, 40 and 80 days, plus control sample (C 40). Peak labels: T = toluene, AB = allylbenzene, aS = α -methylstyrene, S/SS/SSS = styrene monomer/dimer/trimer, D = other polymer-characteristic pyrolysis product, O = oxidized polymer fragment and F = polymer fragment.

Several pyrolysis products indicative of degradation/oxidation were detected in PS-10 t_{80} , that either increased in abundance with UV exposure time or were not detected in the other PS-10 samples. These include additional polymer fragments and fragments with carboxylic acid, ether, ester and ketone groups.

To compare the relative amounts of polymer-characteristic pyrolysis products in photodegraded PS-10, the peak areas of the PS-10 pyrolysis products were normalized to the trimer. A clear temporal trend is observed: the relative area of all the pyrolysis products with $MW \leq 208$ Da increase with UV exposure time, except the monomer which slightly decreased from t_{40} to t_{80} . Eluates with $MW > 208$ Da decrease with UV exposure time, except D_5 which showed no temporal trend. Overall, the results indicate that UV exposure affects the polymer such that a larger fraction of low-MW products are formed upon pyrolysis. The control sample had relative peak areas comparable to t_0 or between t_0 and t_{40} , except the monomer and D_1 which had larger relative areas than in the t_0 - t_{80} samples.

4.3.4 Size distribution

As the SEM images show little or no fragmentation, Coulter Counter size distribution measurement of PE-10 and PS-10 was not performed. Although fragmentation of nano-sized particles from the surface of the MP spheres is possible, Coulter Counter measurements would only yield size information down to $0.6 \mu\text{m}$; the lower range of the available equipment.

While no fragmentation was observed in any of the PE-10 samples, some fragmentation occurred in all PS-10 samples, as seen in the SEM images (Figure 5.12). To check for a possible temporal trend, the fraction of fragmented particles in each PS-10 sample was manually counted in the three SEM images captured at 1000x magnification. The mean (\pm SD) particle count was 221 ± 18 , and the results are graphically presented in Figure 5.24. The error bars represent the accuracy of manual microscopy counting (95 % CI), which is calculated from the sample size (% Error = $2/\sqrt{N} * 100$) of both the total count and the number of fragmented particles (Lund et al., 1958). The temporal regression is non-significant ($p = 0,204$, 95 % CI) and the error range is 77-142 %, so the number of fragmented particles cannot be said to increase with weathering time based on microscopy counting.

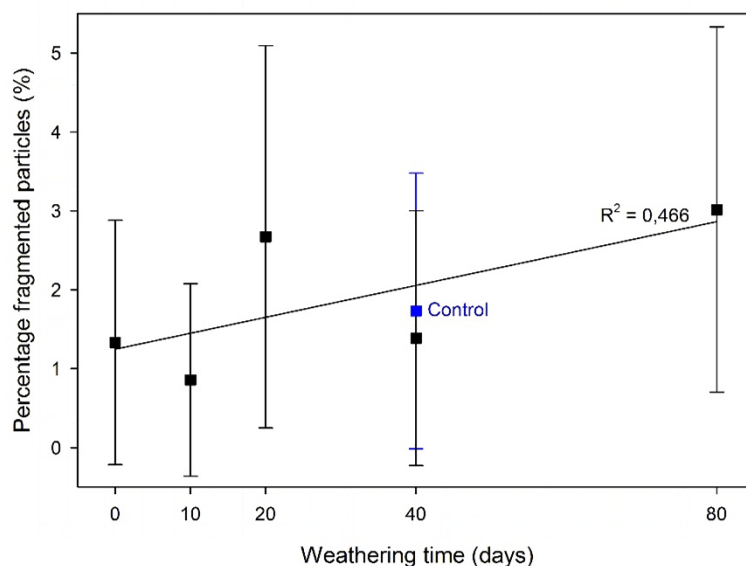


Figure 4.24: Percentage of fragmented particles in PS-10 exposed to UV-Vis irradiation in seawater for 0-80 days. Control sample (t_{40}) not irradiated. Error bars represent accuracy of manual counting.

4.4 Mechanically weathered microplastic

4.4.1 Shape and morphology

PE-10 and PS-10

SEM images of PE-10 and PS-10 mechanically weathered with sand are shown in Figure 4.25 and Figure 5.26, respectively. The images clearly show that the density separation was not successful: the irregularly shaped particles were confirmed to be sand by EDS analysis (see section 4.4.2). Sufficient material for SEM imaging was also found in the sand blank sample (t_{80}), which clearly is residual sand particles (Figure 4.27), confirming the incomplete density separation. A smaller number of extraneous particles are also observed in the MP controls. The largest residual sand particles are one order of magnitude smaller than the pristine sand particles, suggesting that the 150 rpm rotation caused sand particle fragmentation. The smallest observed sand fragments are $<0.1 \mu\text{m}$.

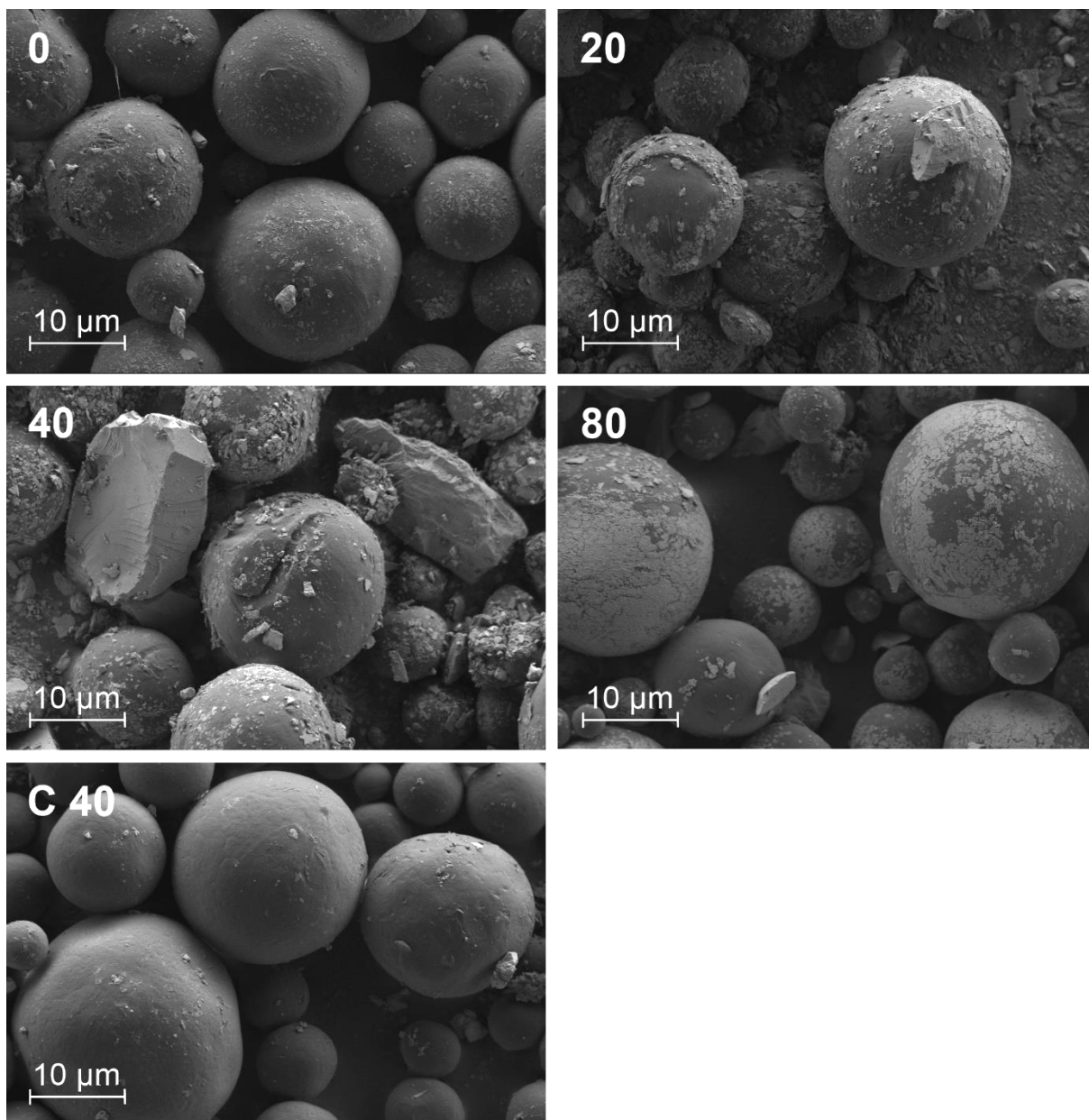


Figure 4.25: SEM images of PE-10 mechanically weathered with sand in seawater for 0-80 days. Control sample (C 40) was weathered under the same conditions for 40 days without sand.

Apart from unassociated sand particles, the MP particles are coated and embedded with the smallest sand fraction ($<0.1\text{-}2\ \mu\text{m}$). The degree of sand embedding and coating of PE-10 appears to first increase then decrease with weathering time. The largest embedded sand particles ($\sim 2\ \mu\text{m}$) appear to be more deeply penetrated in the MP in the t_{20} - t_{80} samples than at t_0 . The t_{20} and t_{40} samples are comparable and contain more extraneous sand particles than the t_0 and t_{80} samples. At t_{80} the sand coating covers a larger portion of the surface area than at t_0 - t_{40} , and the coating particles are smaller (powder-like). The degree of embedding seems to be lower at t_{80} , but upon closer inspection it appears as if the protruding part of many embedded

particles has been weathered away, leaving a more uniform coating surface. The sand coating prevents evaluation of a possible temporal change in surface morphology, but sand embedding clearly causes dents/holes/cracks. The sand-MP interaction and temporal trend is comparable in PS-10 and PE-10, but the extent of sand coating/embedding is slightly greater on PS-10. Also, the transition to a finer particle coating is not as distinct in PS-10 but appears earlier (at t_{40}) and increases from t_{40} to t_{80} .

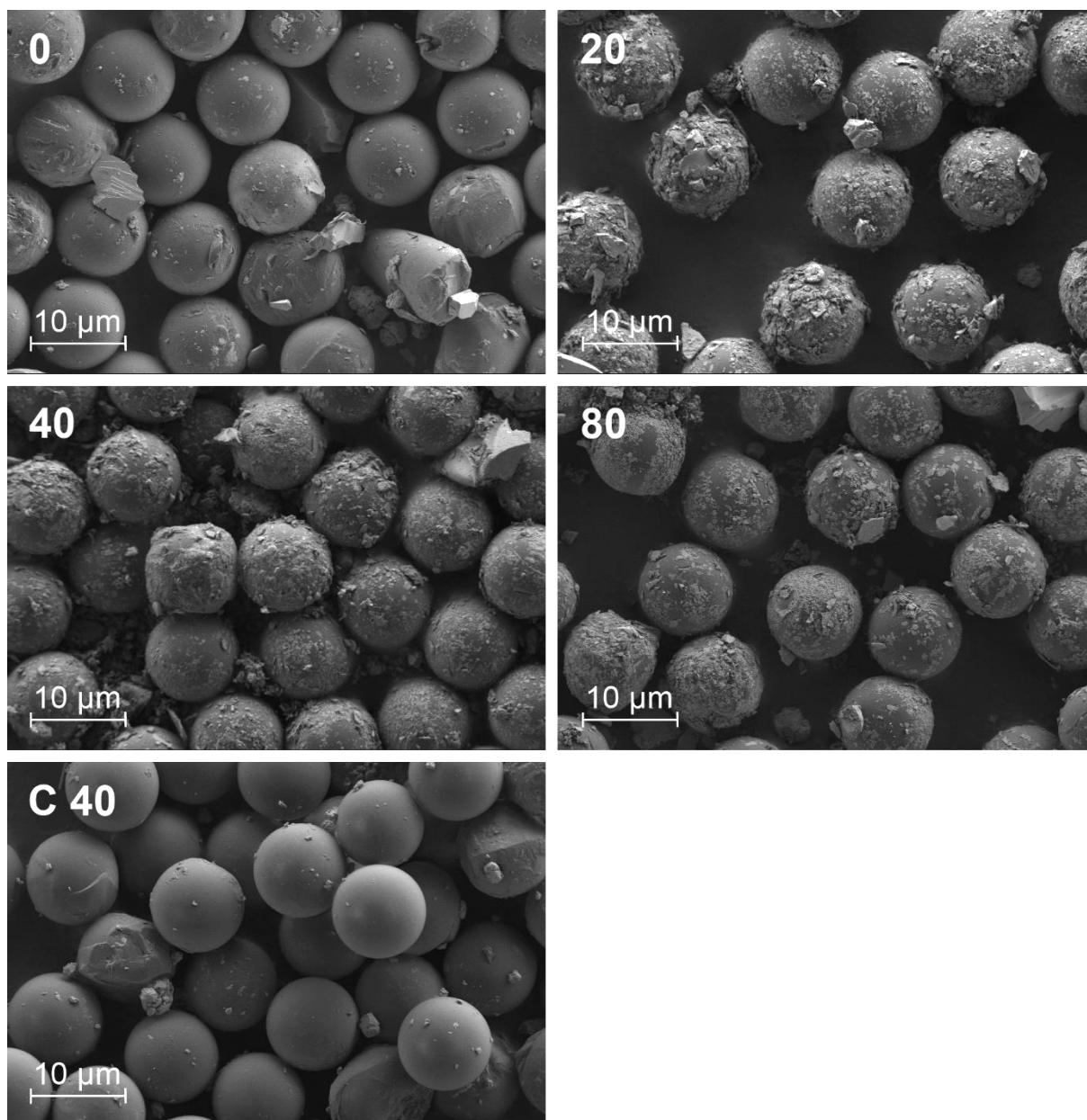


Figure 4.26: SEM images of PS-10 mechanically weathered with sand in seawater for 0-80 days. Control sample (C 40) was weathered under the same conditions for 40 days without sand.

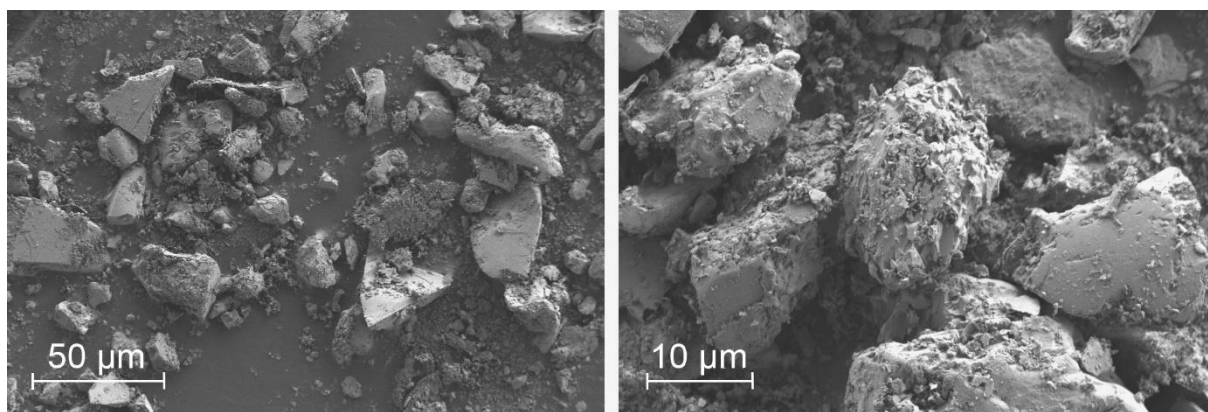


Figure 4.27: SEM images of sand blank sample weathered for 80 days in seawater, at two different magnifications.

PE-100 and PS-100

Light microscopy images of PE-100 and PS-100 weathered with sand are shown in Figure 4.28 and Figure 4.29, respectively. As there is no visual temporal change, only the t_{80} and control samples (t_{40}) are presented, each at two different magnifications. Microscopy images of PE-100 and PS-100 weathered with silt cannot be distinguished from those weathered with sand and are therefore not presented. Note that since the MP particles were manually distributed the number of particles per unit area varies.

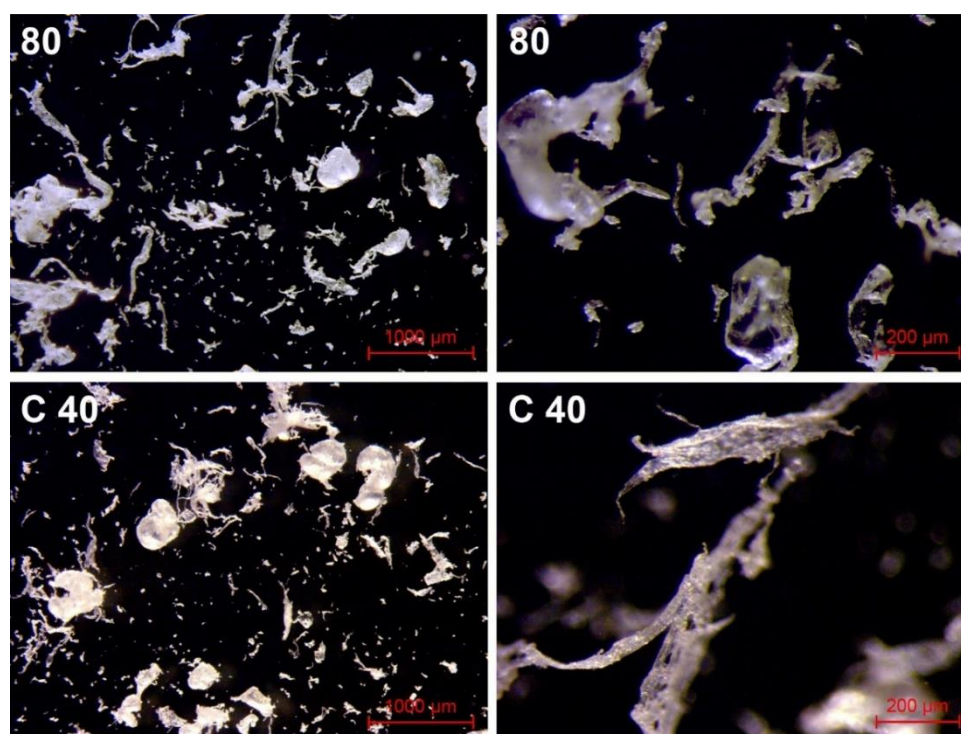


Figure 4.28: Light microscopy images of PE-100 mechanically weathered with sand for 80 days, and control sample (40 days without sand). Magnifications: 20x (LHS) and 80x (RHS).

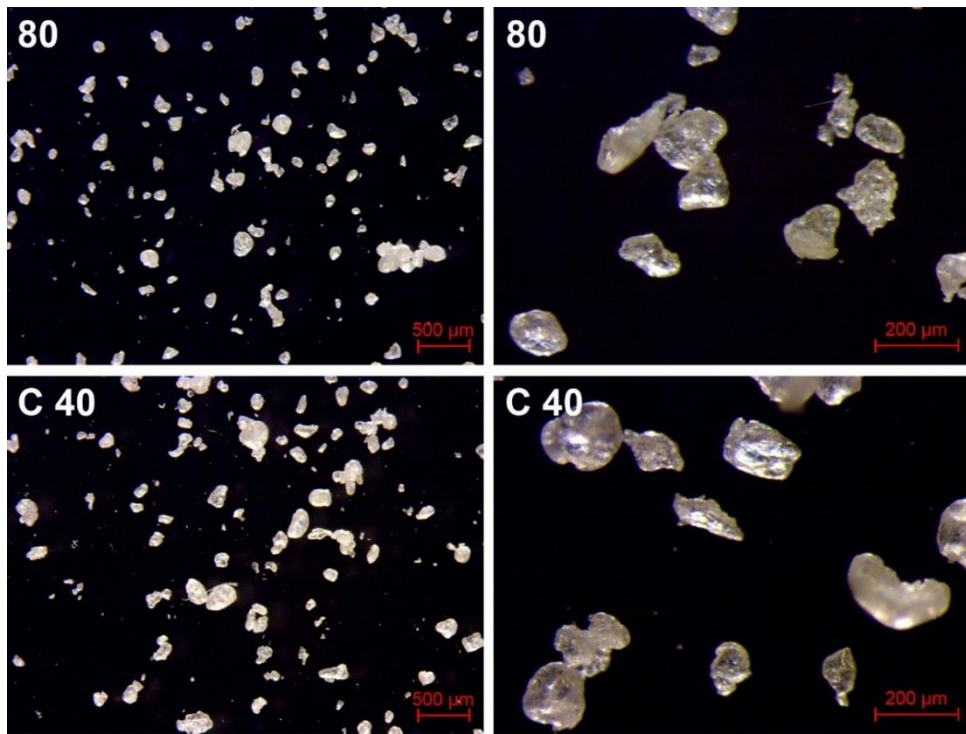


Figure 4.29: Light microscopy images of PS-100 mechanically weathered with sand for 80 days, and control sample (40 days without sand). Magnifications: 20x (LHS) and 80x (RHS).

SEM images of the surface of PE-100 and PS-100 mechanically weathered with sand for 80 days are presented in Figure 4.30. The MP particles have a patchy sand fragment coating as observed on PE-10 and PS-10, and sand particles are accumulating in cracks/gaps.

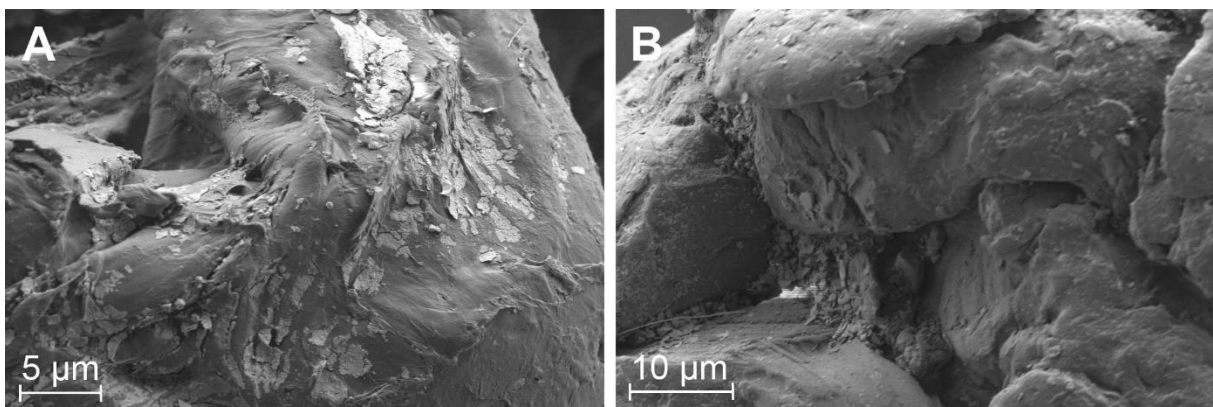


Figure 4.30: SEM images of the surface of (A) PE-100 and (B) PS-100 mechanically weathered with sand in seawater for 80 days.

4.4.2 Chemical characteristics

Fourier Transform infrared spectroscopy

The FTIR spectra of PE-10, PS-10, PE-100 and PS-100 mechanically weathered with sand are presented in Figure 4.31, Figure 4.32, Figure 4.33 and Figure 4.34, respectively. Figure 4.35 and Figure 4.36 show the ATR-FTIR spectra of PE-100 and PS-100 mechanically weathered with silt, respectively.

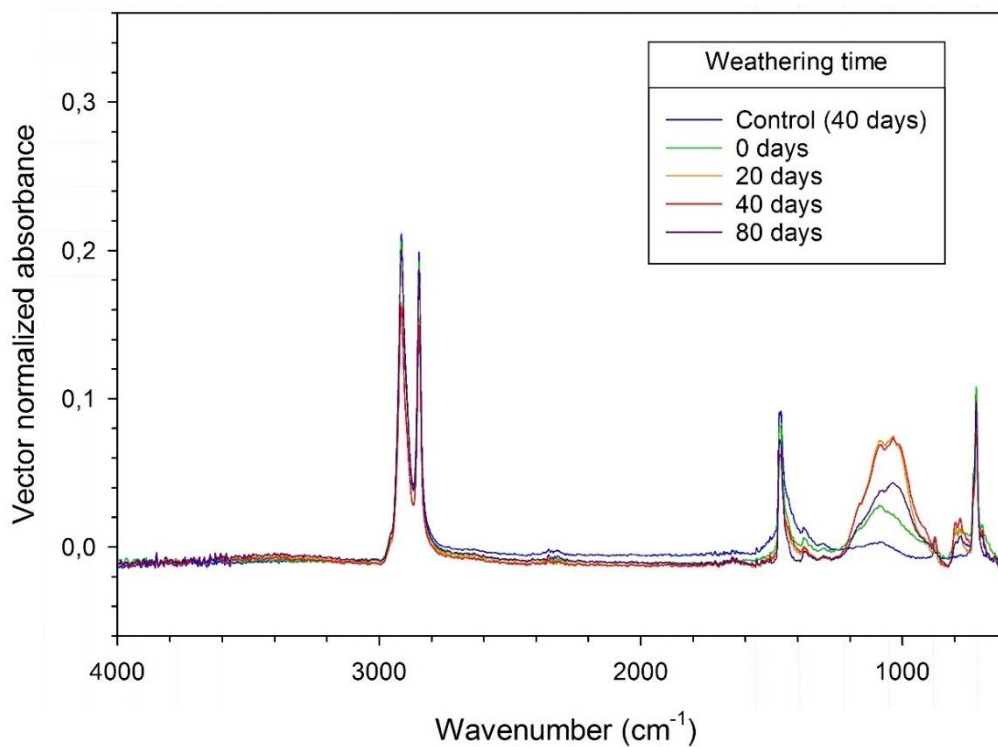


Figure 4.31: ATR-FTIR spectra of PE-10 weathered with sand for 0-80 days in seawater.

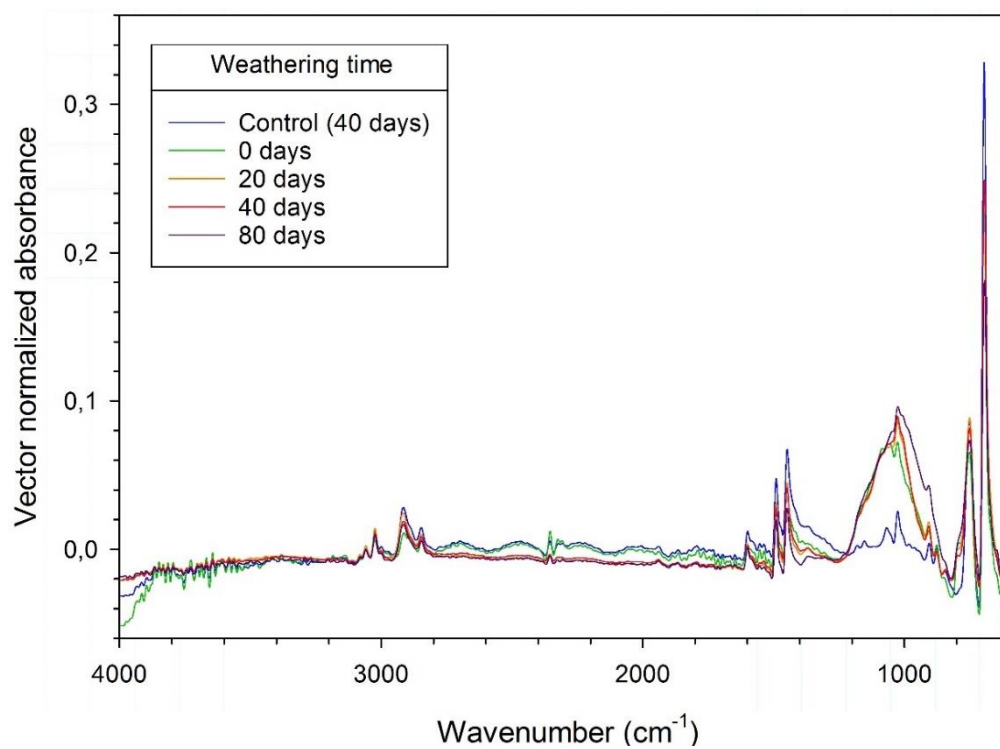


Figure 4.32: ATR-FTIR spectra of PS-10 weathered with sand for 0-80 days in seawater.

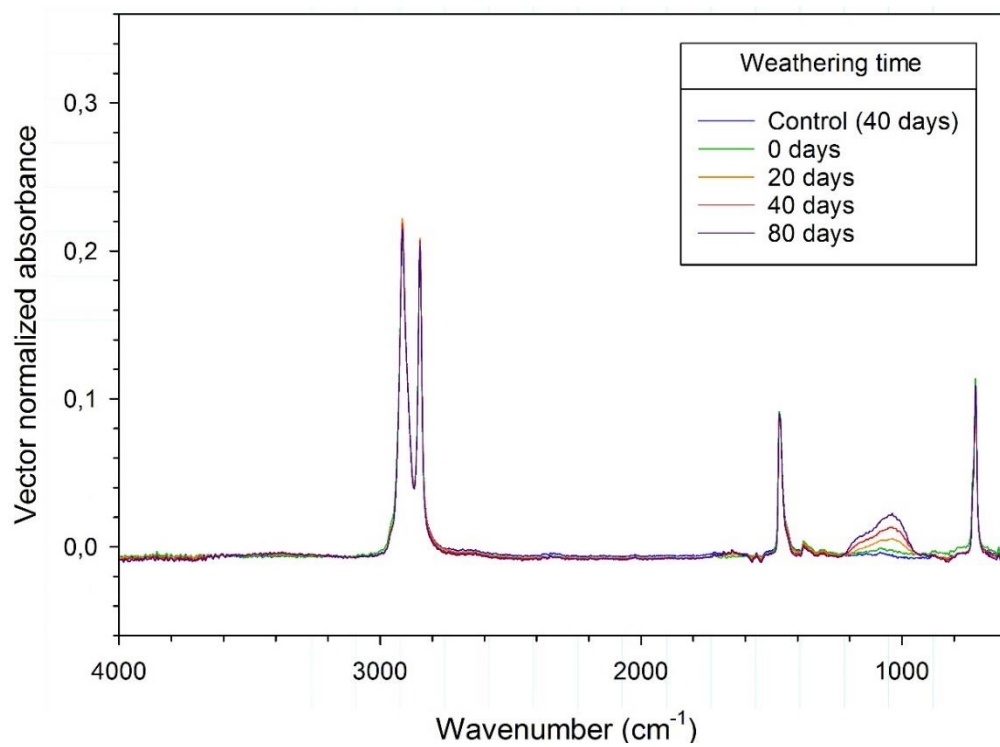


Figure 4.33: ATR-FTIR spectra of PE-100 weathered with sand for 0-80 days in seawater.

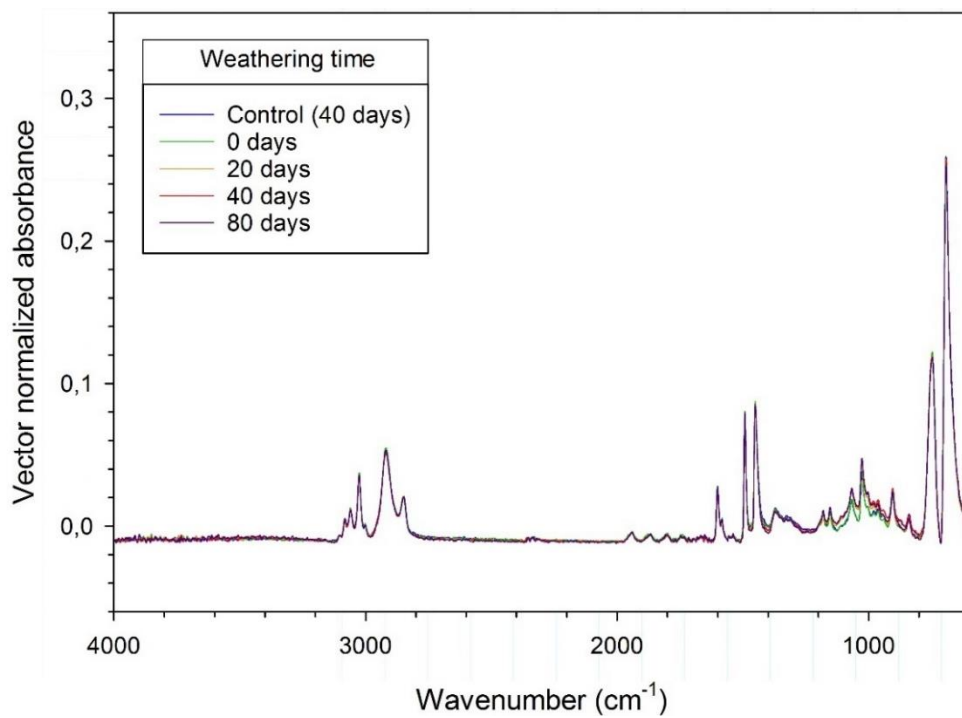


Figure 4.34: ATR-FTIR spectra of PS-100 weathered with sand for 0-80 days in seawater.

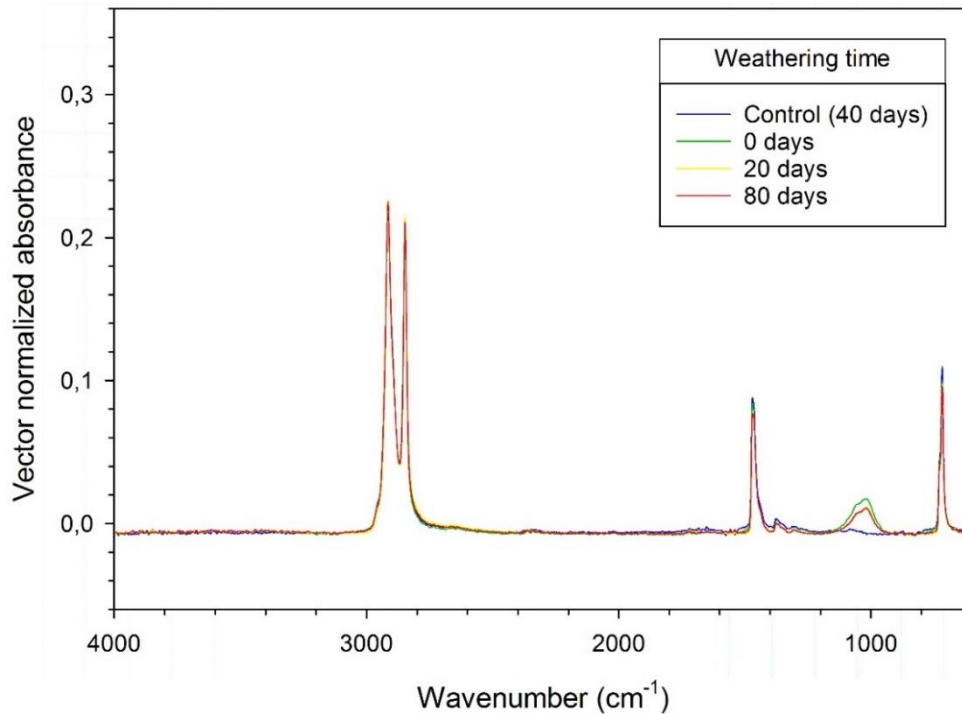


Figure 4.35: ATR-FTIR spectra of PE-100 weathered with silt for 0-80 days in seawater.

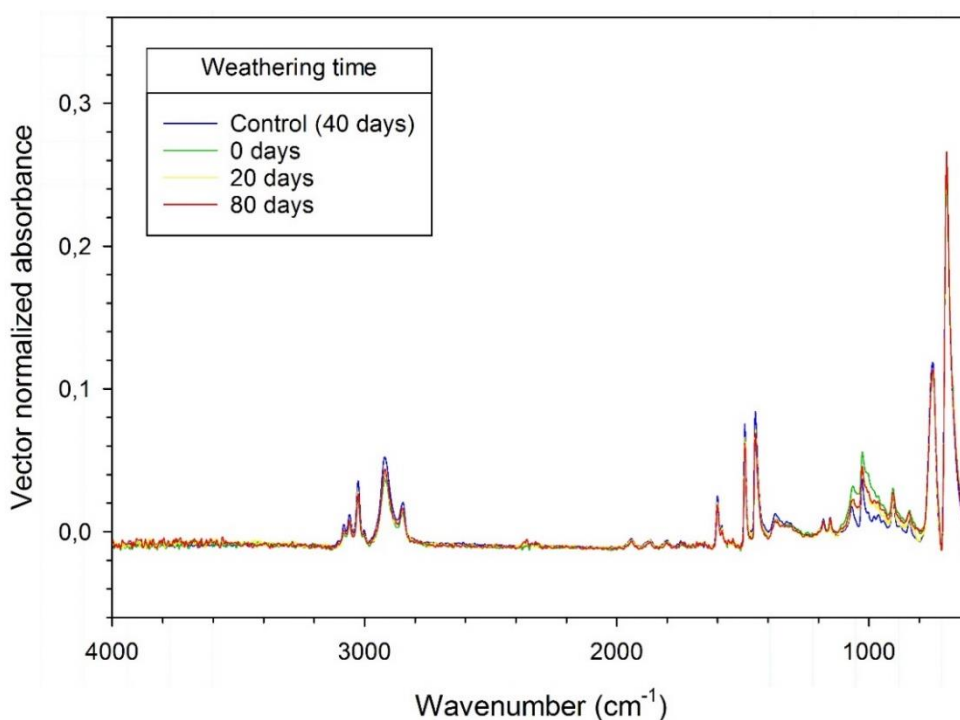


Figure 4.36: ATR-FTIR spectra of PS-100 weathered with silt for 0-80 days in seawater.

A broad band in the 1300-800 cm^{-1} region is present in the majority of mechanically weathered MP samples, but is absent in the controls (blue) to which no sediment was added. The band (centered at $\sim 1030 \text{ cm}^{-1}$) is assigned to a Si-O stretching vibration and is indicative of residual sediment; in agreement with visual observation, microscopy images and absence in controls. None of the ATR-FTIR spectra of the mechanically weathered MP show any signs of polymer degradation. Only PE-100 mechanically weathered with sand showed a temporal increase in crystallinity (decreasing 729/719 cm^{-1} ratio). However, the change is minor (from 0.31 to 0.36 %), with pristine PE-100 and the control sample both having 0.34 % crystallinity.

Overall, the small MP materials (PE-10 and PS-10) contain more residual sediment than the large ones (PE-100 and PS-100), as the absorbance of the Si-O stretch is greater in the small MP materials. This observation is in accordance with the relative sediment content observed in SEM images. The temporal trend of the Si-O stretch in the mechanically weathered MP samples is presented in Table 4.4.

Table 4.4: Temporal trend of Si-O stretch in FTIR spectra of mechanically weathered MP particles.



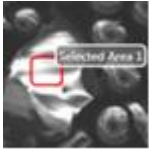

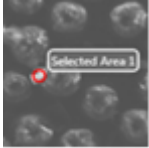



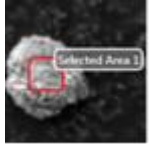
MP material	Sediment type	Temporal trend of Si-O stretch in ATR-FTIR spectra
PE-10	Sand	Increase from t_0 to t_{20}/t_{40} , then decrease
PS-10	Sand	Slight increase (t_{20} and t_{40} equal)
PE-100	Silt	Slight decrease from t_0 to t_{20}/t_{80}
	Sand	Increase
PS-100	Silt	Slight decrease, from t_0 to t_{20}/t_{80}
	Sand	Slight increase, from t_0 to $t_{20}/t_{40}/t_{80}$

Note that the band present in pristine PE-10 (Figure 4.8) assigned to residual silicone oil could overlap with the observed Si-O stretch from residual sand. This appears to be the case in the t_0 sample of PE-10 weathered with sand (Figure 4.31), based on comparison of band shape and maxima. The silicone oil band is greatly reduced in all PE-10 photodegradation samples as well as in the PE-10-sand control (t_{40}), indicating removal during sample preparation- and extraction.

Energy dispersive X-ray spectroscopy

As qualitative distinction between MP and sand particles was necessary, pristine sand, PS-10 and PS-100 (t_0 and t_{40}) were analysed by EDS. Table 4.5 shows a summary of the EDS analysis. Mean errors for C, O and Si weight percentages were 5, 9 and 12 %, respectively, and ranged from 2 - 25 %. A blank EDS spectrum of the background (carbon tabs) was also collected, which gave the following elemental composition: 93 % C and 7 % O – the oxygen stemming from the acrylic adhesive on the tabs. Unambiguous identification of small particles and the MP coating based on EDS spectra was limited by the resolution: (1) EDS spectra collected from small areas/spots in the SEM images could have been (a part) of the background, which could not be discriminated from the MP particles based on elemental composition, and (2) selection of individual particles coating the MP was not possible, so it cannot be ruled out that part of the observed coating could be NP from MP fragmentation.

Table 4.5: Summary of EDS analysis of pristine sand, MP and residual particles in PS-10 and PS-100 mechanically weathered with sand for 0 and 40 days.

Sample	Representative SEM image	Elemental composition (weight %)				Classification
		C	O	Si	Other elements	
Pristine sand		11-18	50-53	25-34	F (1-2), Mg (1), Al (1-2)	Sand
		80-92	2-13	<1	Ca (6), Al (<1)	
PS-10-sand t ₀		0-6	43-52	34-42	Na (0-13), Mg (0-2), Al (0-3), K (0-1), Ca (0-5)	Sand
		79-87	10-15	2-3	Na (1), Al (1-2)	
PS-10-sand t ₄₀		12	44	25	Na (9), Al (10)	Sand and part of polymer
		81-99	1-12	0-13	Al (0-3)	
PS-100-sand t ₀		0-6	43-52	34-42	Ca (0-5), Na (0-13), Mg (0-2), Al (0-3), K (0-1)	Sand
		80-98	2-13	1-6	Fe (0-1), Ni (0-1), Na (0-2), Al (0-3)	
PS-100-sand t ₄₀		6-14	41-54	25-36	Fe (0-3), Na (0-3), Mg (0-1), Al (2-12)	Sand

4.4.3 Size distribution

PE-10 and PS-10

Coulter Counter measurements were not carried out for the same reasons as for the photodegraded MP. Although a slight temporal size increase might have been observed due to sediment coating, qualitative observation was considered sufficient. Residual sand content could have been estimated, but MP fragments and sediment particles could not have been differentiated.

PE-100 and PS-100

Determination of the size distribution of mechanically weathered PE-100 was attempted but discarded due to a significant and varying amount of touching particles (clusters): ISO13322-1 (2014) does not recommend performing size distribution from images with touching particles. Touching particles will induce errors and should be minimized and separating the PE-100 particles was not possible without inducing damage.

Size distribution histograms of PS-100 weathered with sand are presented in Figure 5.37. The histograms clearly show a bimodal logarithmic distribution, plus a large fraction making up the lowest bin (2 μm) in the histogram. To enable direct comparison of the PS-10 samples, the x-axis shows frequency percentage instead of particle number (unequal sample sizes, N).

As one of the aims was to evaluate the change in size distribution with weathering time, it was necessary to examine the atypical size distribution closer. Subtraction of the MB still left a significant portion of the lower log-normal distribution (centered at 10 μm) and only caused a slight reduction (~20 %) of the lowest bin (2 μm). New MB were processed but did not change the outcome. A part of the lower log-normal distribution (centered at 10 μm) still remained after recommended exclusion of particles <5 pixels (BS3406, 1993).

To find out if the bimodal size distribution could be caused by residual sand fragments, microscopy images were captured of pristine sand and the sand blank (t_{80}). The mass recovered from the sand blank (t_{80}) was 0.2 mg, meaning that 0.25 % (w/w) of the mechanically weathered PE-100 and PS-100 samples could be residual sand. Comparison of pristine sand, sand blank (t_{80}), PS-100 weathered with sand (t_{80}) and MB (Figure 5.38) clearly show an overlapping size range confirmed by size distribution histograms (Figure 4.39). To confirm and estimate the size and mass of residual sand, EDS analysis was performed on 69 particles in PS-100 weathered with sand (t_{40}). From the elemental composition, the particles were classified as either polymer,

SiO₂ (sand), CaCO₃ (sand) or unknown. The results and the approximate diameter range of the particles are shown in Table 4.6.

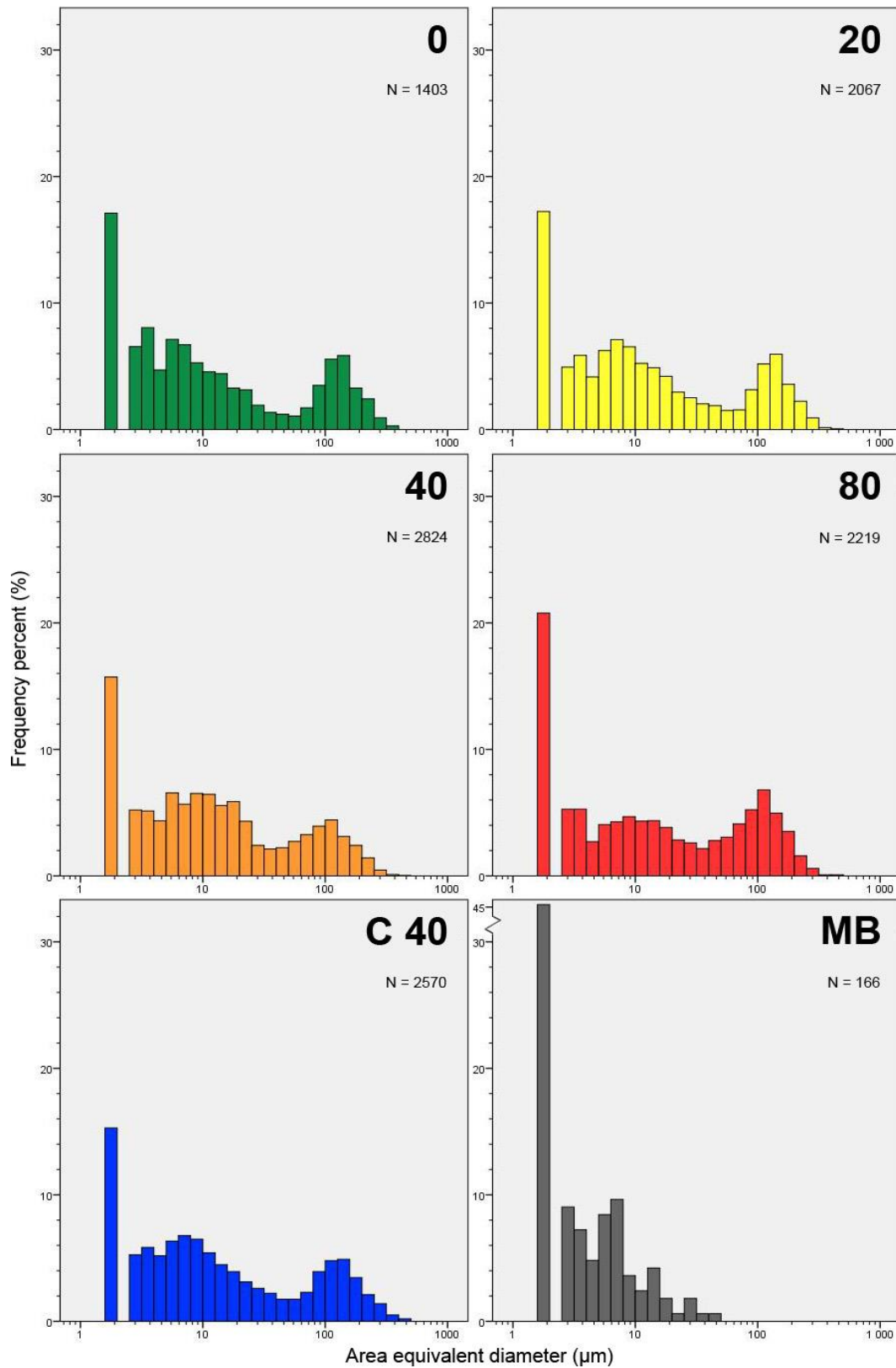


Figure 4.37: Histograms showing the logarithmic size distribution of PS-100 physically weathered with sand for 0-80 days, PS-100 control sample (C 40) and microscopy blank (MB).

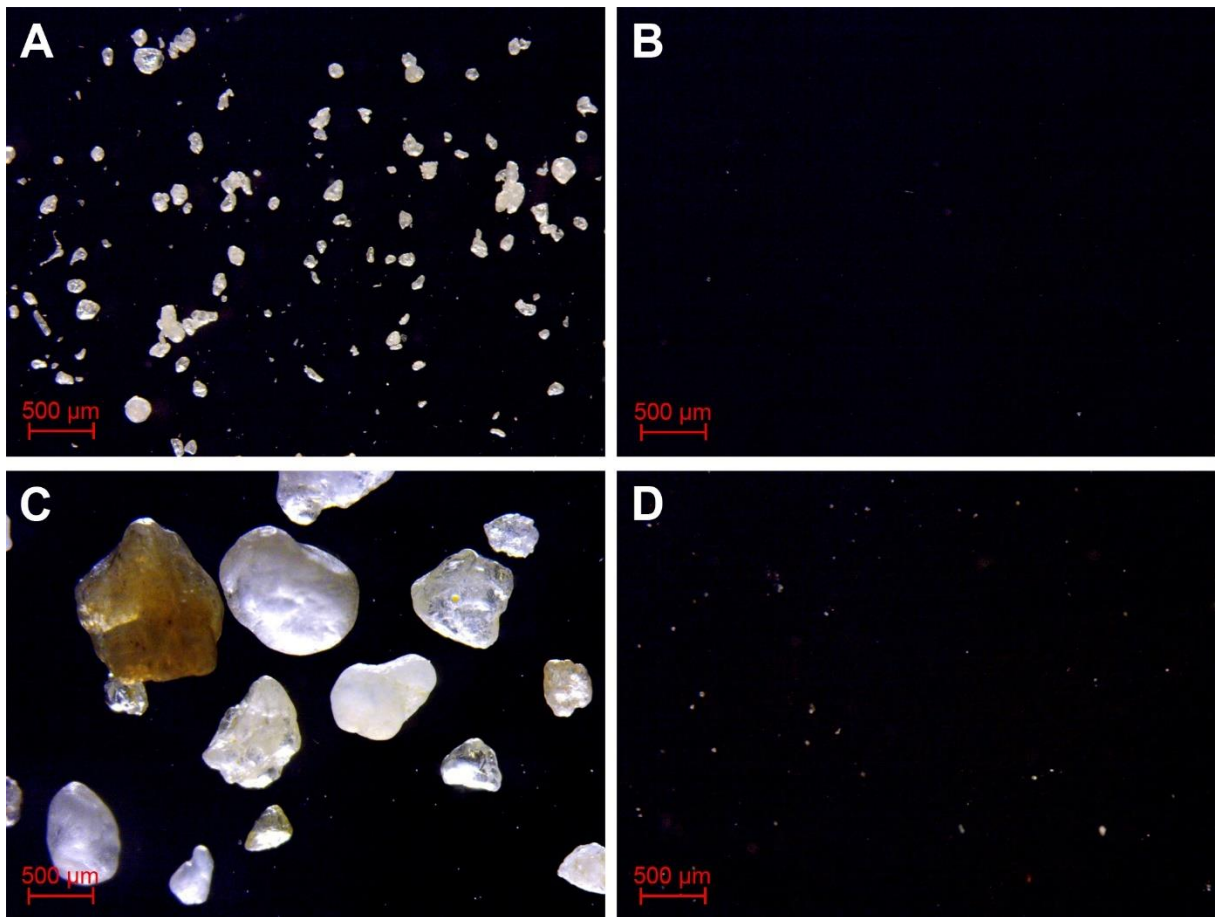


Figure 4.38: Light microscopy images of (A) PS-100 physically weathered with sand for 80 days, (B) microscopy blank, (C) pristine sand and (D) sand blank sample physically weathered for 80 days. Magnification: 20x. Note that the number of particles per unit area varies.

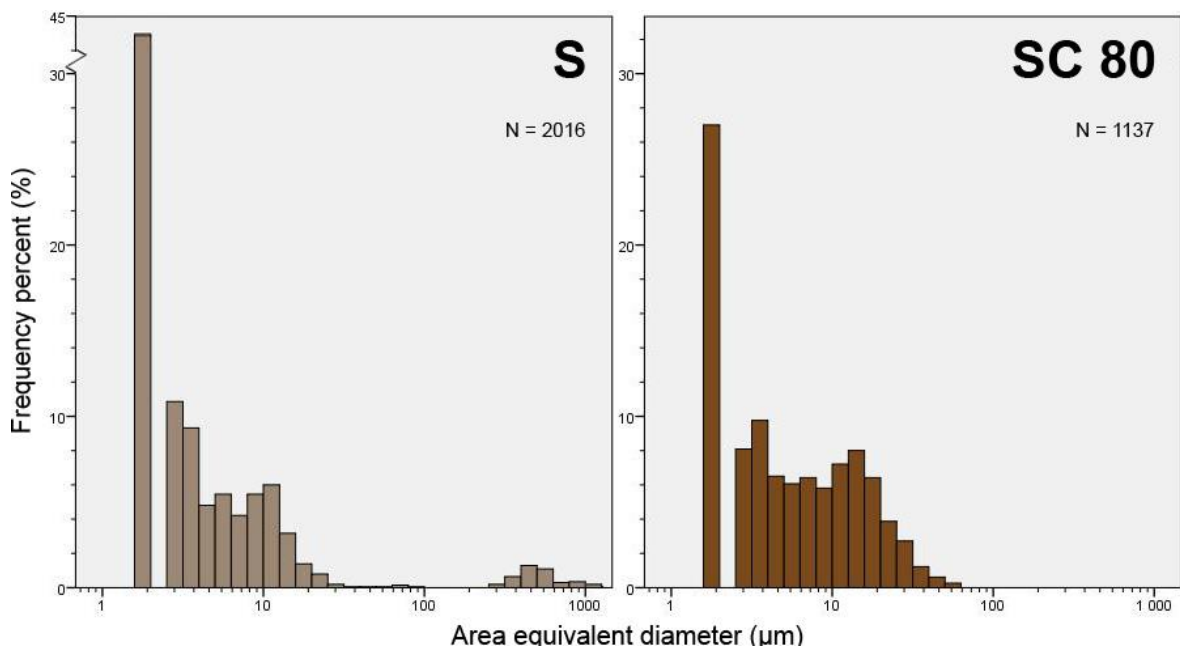


Figure 4.39: Histograms showing the logarithmic size distribution of pristine sand (S) and sand blank sample mechanically weathered for 80 days (SC 80).

Table 4.6: Classification of particles (N=69) in PS-100-sand t40 based on elemental composition from EDS analysis.

	Fraction (%)	Size range (μm)
Polymer	84	0.6 - 185
Unknown	3	2 - 100
SiO₂ (sand)	9	3 – 12
CaCO₃ (sand)	4	3 – 6.5
Total sand	13	3-12

A sand content of 13 % (by number) equals 0.06/0.65 % by mass (weighted/unweighted arithmetic mean). This is within an order of magnitude 0.28 % estimated from the sand blank (t_{80}) recovery. An estimated 0.28 % sand by mass translates to 43 % (by number) of the particles <61 μm in PS-100 weathered with sand t_{40} , so residual sand is likely responsible for half of the particles in the lower log-normal distribution (centered around 10 μm).

Subtracting an estimated sand fragment size distribution from the MP size distributions cannot be justified as it would be based on inappropriate assumptions: (1) equal sand content, which is rejected by ATR-FTIR spectra, and (2) equal sand size distribution, which likely vary due to sand fragmentation with weathering time. Instead, particles $\leq 24.7 \mu\text{m}$ were excluded; the 95th percentile of the sand blank (t_{80}).

Cumulative size distributions of PS-100 mechanically weathered with sand and silt are presented in Figure 4.40 and Figure 4.41, respectively. The size distribution of PS-100 mechanically weathered with silt do not show a bimodal distribution, and no silt was recovered from the silt blank (t_{80}). As the silt-content PS-100 is presumably low or non-existent, only particles <8.77 μm (<5 pixels) are excluded.

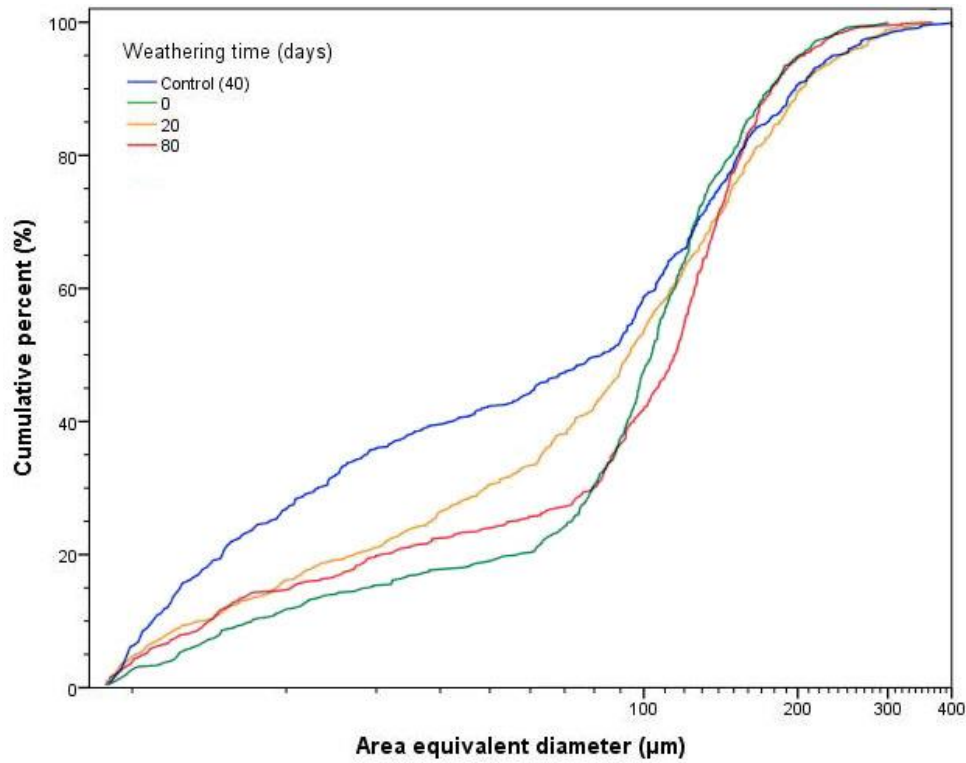


Figure 4.40: Cumulative size distribution of PS-100 mechanically weathered with silt for 0-80 days in seawater and control (t_{40}), above $8.77 \mu\text{m}$ (>5 pixels).

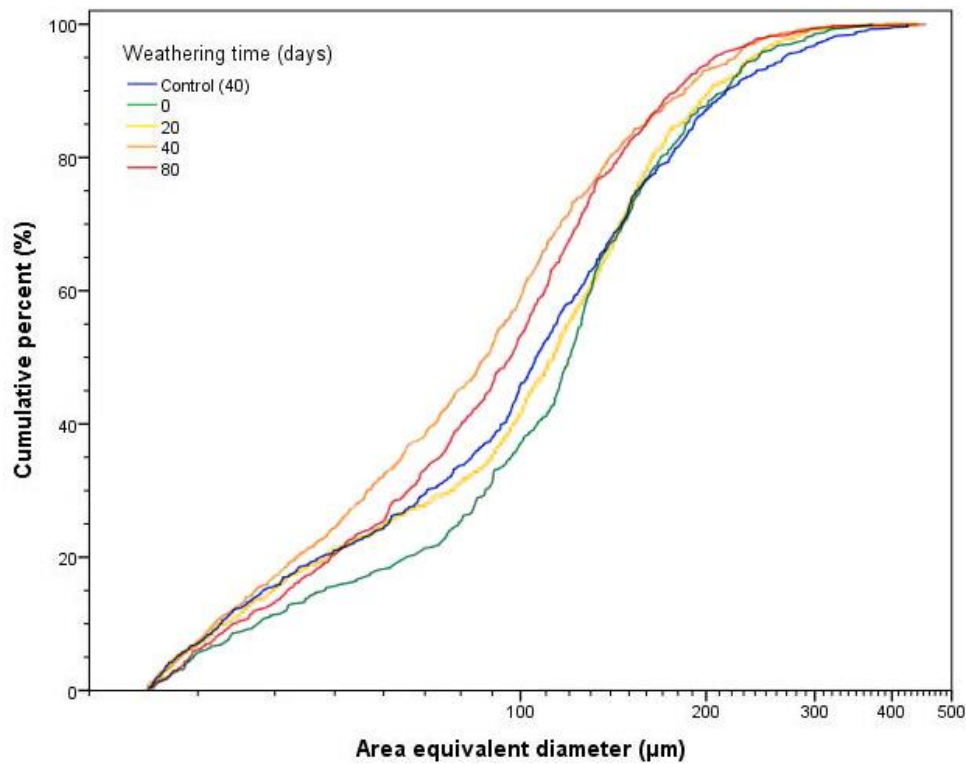


Figure 4.41: Cumulative size distribution of PS-100 mechanically weathered with sand for 0-80 days in seawater and control (t_{40}), from $24.7 \mu\text{m}$ (95th percentile of sand size distribution).

The mean particle sizes in the PS-100 samples mechanically weathered with silt (including control) are statistically significant (Kruskal-Wallis Test, $\chi^2 = 27$, $p = <0.001$). Interestingly, below D50 (50 % cumulative percent), the MP particles in the PS-100 control (t_{40}) is significantly smaller than in those weathered with silt. A size reduction is observed from t_0 to t_{20} , followed by an increase from t_{20} to t_{80} .

The mean size of the PS-100 samples mechanically weathered with sand is also statistically significant (Kruskal-Wallis Test, $\chi^2 = 76$, $p = <0.001$). Linear regression of the mean and median size against weathering time gave $R^2 = 0.64$ and 0.56 , respectively, but neither was statistically significant ($p = 0,20$ and $0,25$, 95 % CI). The MP particles in the weathered samples are clearly smaller than the t_0 sample: the mean sizes are 124 and $99 \mu\text{m}$ in t_0 and t_{40} , respectively, while the control is comparable to the t_{20} -sample. At t_{80} the size distribution is not as shifted to the smaller range as at t_{40} in the region $<140 \mu\text{m}$.

5 Discussion

5.1 Photodegradation

5.1.1 Exposure conditions and extraction procedure

The UV-Vis exposure in the 80-day photodegradation experiment was equivalent to ≤ 616 days in Trondheim. The instrument modification to an open system led to a lower sample irradiance than given by the supplier. The loss of light intensity due to scattering and absorbance is <10 % for the quartz tubes and <0.1 % in 3 cm of SW (Wozniak and Dera, 2007). The combined loss (at each wavelength) due to the open system, quartz tubes, water and suspended particles is unknown. A sample with a reference material could have been included to estimate the light exposure. With accurate exposure data it would have been possible to calculate the solar irradiance over time, or *insolation* ($\text{kWh/m}^2/\text{day}$), required to initiate oxidation in PS.

No signs of biofilm formation were detected by SEM or FTIR, which in the latter would result in broad absorption bands in the $3500 - 3000$ and $1800 - <600 \text{ cm}^{-1}$ region. Biofilms must be considered when analysing MP collected from or exposed to the natural environment, as it can lead to misidentification: FTIR spectra of biofilms closely resemble those of polyamides (Renner et al., 2017). The lack of biological material indicate that the equipment cleaning procedure and seawater filtration was adequate. The lack of O-H bonds in the FTIR spectra of both t_0 and weathered samples also prove that the samples were successfully dried.

5.1.2 Chemical changes

Fourier Transform infrared spectroscopy

No signs of oxidation or chain scission were detected in PE-10 by FTIR. Any changes were either too low to be detected or did not occur – PE is not readily photooxidized as it does not contain chromophores (Grassie and Scott, 1988). Also, photooxidation is highly time- and temperature dependent; lower temperature means longer times before oxidation rates turn exponential (Israeli et al., 1994). The seawater might therefore have been too cold for PE oxidation to occur within 80 days.

Oxidation of photodegraded PS-10 from 40 to 80 days is clear from the FTIR spectrum (Figure 5.1). As the experiment was paused more frequently in the initial 40 days due to sampling and

instrumental errors, the t_{10} - t_{40} samples were most likely maintained at lower temperatures than the t_{80} sample. Thus, the free radicals formed during this period were likely deactivated early in the propagation step, leading to minimal oxidation. The functional groups reported in PS exposed to UV radiation in the presence of air are hydroxyl and carbonyl groups (Achhammer et al., 1951, Reiney et al., 1953). In this study, no distinct hydroxyl group was detected by FTIR, only C=O and C-O bonds, indicating that photooxidation in air and seawater differ. No FTIR spectra of PS photodegraded in (sea)water was found in the literature, only for EPS which had comparable C=O and C-O stretching bands (Andrady and Pegram, 1991). A large range of oxidation functional groups in PS-10 t_{80} were detected by Pyr-GC/MS: ketones (mainly on α -carbon), aldehydes, alcohols, ethers (O directly bonded to aromatic ring), carboxylic acids and esters (multiple, e.g. diacetates). The alcohol and carboxylic acid groups must either be breakdown products or present at very low concentrations and hydrogen-bonded. The slightly elevated baseline in the FTIR spectrum of PS-10-UV t_{80} around 3400 and 2600 cm^{-1} is characteristic for strongly hydrogen-bonded of carboxylic acids (Coates, 2006). The C=O and C-O oxidation bands are broad with several maxima (Figure 5.1), also indicating a mixture of the different functional groups. A possible assignment of the different maxima is shown in Table 5.1 (Rabek, 1990, Coates, 2006, D'Esposito and Koenig, 1979, Grassie and Scott, 1988, Mailhot and Gardette, 1992).

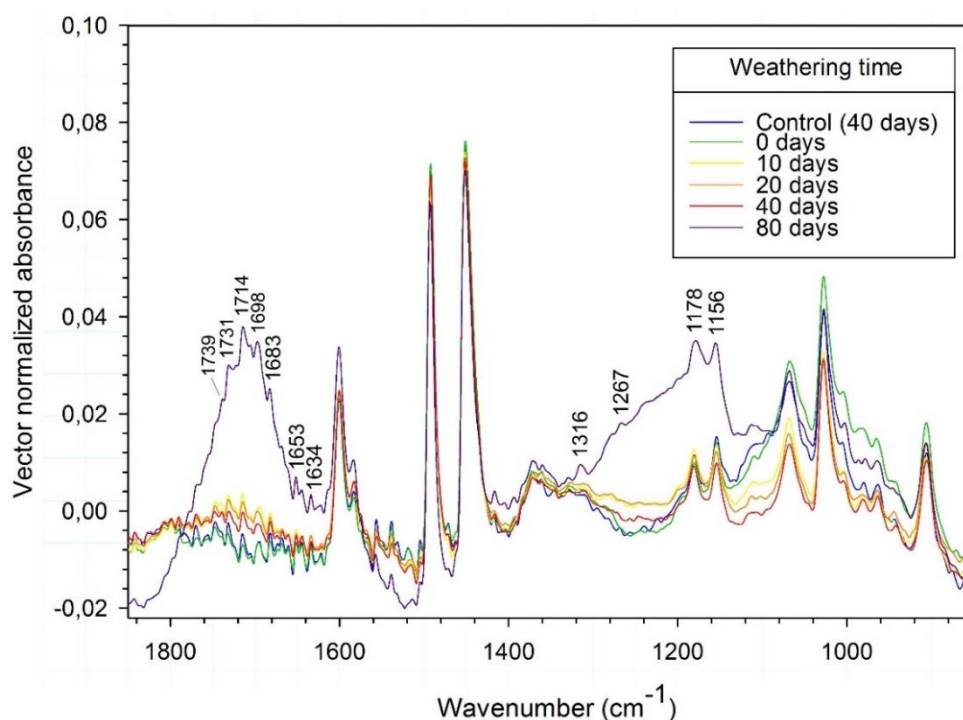
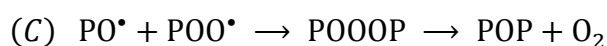
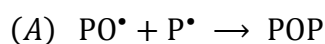


Figure 5.1: ATR-FTIR spectra of PS-10 photodegraded for 0-80 days in seawater, zoomed in to show the 1840 - 840 cm^{-1} region in which the major spectral changes occurred.

Table 5.1: Possible assignment of new FTIR bands observed in PS-10 photodegraded for 80 days.

Frequency (cm ⁻¹)				
<i>Observed</i>	<i>Reference</i>		Vibration	
1820 - 1620	1739	1740	(Rabek, 1990)	Aldehyde (ring-opening)
	1731	1728	(D'Esposito and Koenig, 1979)	Aldehyde
	1714	1713	(Thomas et al., 2014)	Carboxylic acid (H-bonded)
	1698	1670-1700	(Kuptsov and Zhizhin, 1998)	Ketone (alkyl/ β -carbon)
	1683	1685	(Rabek, 1990)	Ketone (α -carbon)
	1653/1634	1660/1632	(Grassie and Scott, 1988)	C=C stretch (alkyl)
1350 - 1100	1316	1350-1150	(Kuptsov and Zhizhin, 1998)	C-O stretch (ester, alkoxy)
	1267	1290-1210		C-O stretch (aryl-O-R)
	1267	1250		C-O stretch (carboxylic acid)
		1250, 1160		C-O stretch (ether)
		1150-1000		C-O stretch (ester, acyl)

The formation of conjugated dienes in the polymer backbone of PS is correlated with yellowing (Ellis and Smith, 2008), in agreement with the observed temporal colour change and increase in aliphatic C=C absorbance (except t_{40}). The formation of ketone groups agrees with the photodegradation mechanism of PS proposed by Yousif et al. (2012) and Gewert et al. (2015) (Figure 2.4). Ring-opening reaction has been reported in photooxidized PS, where the intermediate is a hydroperoxyl-ring on the phenyl ring (Rabek, 1990). Although no studies on ether- or peroxide-linking of photo-irradiated PS were found, the mechanism was found in a list of possible termination steps in the free radical oxidation, as shown in reactions A-C below (Rabek, 1990):



This type of cross-linking mechanism explains the finding of ether and esters by Pyr-GC/MS and a broad C-O stretch by FTIR. Cross-linking is the dominant degradation mechanism in the absence of oxygen (Ellis and Smith, 2008), supporting the results as the oxygen concentration

in surface seawater is <3 % of that in air (0.27 and 9.2 mmol/L, respectively, at average sea level conditions: 1 % water vapour, 17 °C, 1 atm). While hydrogen abstraction is an important radical deactivation mechanism of PS in air (Guaita et al., 1985), the results indicate that it does not occur in to a great extent in seawater. The pyrolysis products indicate that the main radical deactivation mechanism is recombination, forming a variety of adducts: mostly conjugated ketones, aldehydes, ethers and esters. Chain scission and recombination might cancel each other, leading to no observed change in crystallinity; consistent with a previous study (Brandon et al., 2016).

Pyrolysis gas chromatography – mass spectrometry

In agreement with the FTIR spectra, oxidation (in the form of oxygen incorporation) was only observed in PS-10-UV t_{80} . Oxygen-containing functional groups (predominantly carboxylic acids, esters and ketones) dominated the PS-10 desorption pyrogram (250 °C). The abundance of additional polymer fragments exceeded the oxygenated substances in the pyrolysis pyrogram (600 °C). This indicates that oxidation is limited to the surface from which desorption occurs at elevated temperatures.

Determination of additive leaching from photodegraded PE-10 was problematic due to different Pyr-GC/MS sample sizes. For the substances desorbed from PE-10 (Pyr-GC/MS at 250 °C), no information on the use of phenylglyoxal (A_1) could be found. Bisphenol AF (A_2) is a known additive, but could originate from the Pyr-GC/MS instrument as it were detected in some of the blank runs, and it is commonly used as a crosslinker for fluorocarbon elastomers in e.g. seals (Drobny, 2016). 1,3,5-triphenylbenzene (A_3) is a stabilizing and hypercrosslinking agent (Huang and Turner, 2018, Hummel, 2000). The potential additive identified in photodegraded PS-10 is diethyl phthalate (A_2), but it's source is debatable as it was also detected in blank runs, although at lower levels. The three other potential additives detected in PS-10 could not be identified using NIST Mass Spectral Database. There did however appear to be a temporal trend in desorption of substances in PS-10: the potential additives detected in the t_0 -sample were not found at t_{40} or in the control sample (t_{40}), indicating leaching. The oxidation at t_{80} could have led to significant structural change allowing greater Pyr-GC/MS desorption of potential additives that were trapped inside the polymer matrix prior to oxidation. As both PE-10 and PS-10 are high performance microspheres used in research and industry, they likely contain less additives than consumer/industrial plastic materials commonly found in the marine environment.

The pyrolysis (600 °C) products of photodegraded PE-10 show a temporal trend if the t_{40} sample is excluded: the relative peak heights of the homologue $>C_{18}$ decrease with weathering time. The non-temporal trend of the t_{40} sample is likely due to pyrolysis of a larger sample ($>2x$ the signal output). Although leaching of high-MW oligomers is a possibility, chain scission is a more plausible explanation as leaching of PE oligomers was below the LOD in a similar study (Suhrhoff and Scholz-Böttcher, 2016). The proposed temporal trend is however only based on two samples (t_0 and t_{80}) and a control sample (t_{40}) and is therefore questionable.

In pyrograms (600 °C) of photodegraded PS-10, the non-temporal trend of the styrene monomer at t_{80} could be a result of the observed oxidation, e.g. by preferential oxidation of residual monomer, monomer leaching or cross-linking. Unlike PE-10, the temporal reduction in relative amount of high-MW substances (≥ 208 Da) is likely due to greater leaching of high-MW oligomers, instead of chain scission/oxidation. Choi et al. (2005) only detected PS trimer and trimer isomers in PS water extracts and found that the low-MW monomer/oligomers had lower diffusion coefficients than the larger ones. Heat increased diffusion coefficients, which explains why the relative amount of high-MW oligomers (dimer, two dimer isomers and the trimer) in the PS-10 control (t_{40}) is comparable to the t_{40} -sample. The relative amount of PS trimer was indeed lower in the control than in the t_{80} -sample, suggesting that heat plays a greater role than UV-Vis exposure for trimer leaching. The peak areas of the styrene monomer and D_1 were larger in the control sample, which could be explained by e.g. include heat-induced embrittlement and chain scission (thermal degradation). It must be noted that the concentration of residual PS trimer isomers is around 20 times greater than PS monomer.

The results are also in agreement with a recent study that investigated the effect of salinity, UV exposure and water turbulence on the leaching of polymer residues/additives (Suhrhoff and Scholz-Böttcher, 2016). Leachates from PS to seawater were mainly PS oligomers, of which 0.07-0.14 % of the initial concentration (1 % by mass) had leached to SW after 57 days (monomer not quantified due to co-elution). The trimer, pentamer and tetramer leached to a greater extent than the dimer, in agreement with Choi et al. (2005). The PE contained oligomers (C_{12} - C_{32} linear and cyclic), 0.05 % Irgafos® 168 phosphate (antioxidant) and 0.02-0.1 % Citroflex A4® (“green” plasticizer). After 78 days, 0.05 and 4.9 % of Irgafos® 168 phosphate and Citroflex A4® had leached out, respectively, while PE oligomers were below the LOD. Surprisingly, the authors found that UV exposure did not increase leaching, but this could be explained by photodegradation of leachates once in the aqueous phase. Salinity had no impact, but water turbidity (150 rpm) increased average leaching by more than a threefold.

5.1.3 Fragmentation

Despite the lack of detected chemical changes and MP fragmentation, SEM images show a temporal trend in surface roughness of both PE-10 and PS-10, likely due to loss of NP fragments. Progressing surface roughness was however only observed on some PE-10 particles, which could be due to MP aggregation that would shield a large portion of the particles from UV-Vis irradiation. As the surface of the PE-10 control sample (not exposed to UV-Vis radiation) was comparable to the t_{40} and t_{80} samples, factors such as heat and mechanical degradation due to MP motion in SW could be the main determinants for surface morphology changes in PE. Song et al. (2017) exposed dry polymer pellets to UV light of irradiance comparable to this study and found a steady rate of LDPE oxidation despite incorporated UV stabilizers and antioxidants, as well as surface cracking after 180 days. The different results can likely be attributed to different mechanisms of photooxidation in air and SW, mainly due to lower oxygen content in SW, as well as higher temperature (44 °C) in the experiment by Song et al. (2015).

Increasing oxygen content at the surface of PS e.g. due to oxidation is positively correlated with roughness (Muntean et al., 2011). In addition, the proposed mechanism for surface photodegradation is chain scission, resulting in loss of a large number of small polymer fragments (Gewert et al., 2015). This has been confirmed by Lambert and Wagner (2016b), which subjected different polymer pellets/films to UV irradiation in water at 30 °C for 112 days. The number of fragments increased exponentially with decreasing size, with the number of NP fragments 3 orders of magnitude greater than MP. The PS coffee-lid produced the highest number of fragments: 9×10^4 and 6×10^8 particles mL^{-1} in the 2-60 μm and 30-2000 nm size range, respectively. Concurrent with loss of NP fragments, the authors observed “bubbles” on the PS coffee-lid after 14 days, comparable to the temporal trend in surface roughness of both PE-10 and PS-10 in this study (Lambert and Wagner, 2016a). Thus, surface changes can be used as an indicator of NP fragmentation, and PS-10-UV t_{80} likely experienced the greatest NP fragmentation as the surface is significantly rougher than the other PS-10 and PE-16 samples.

5.2 Mechanical degradation

5.2.1 Exposure conditions and extraction procedure

In the mechanical weathering experiment, the circular motion of the shaking incubator did not provide extensive interaction between the sediment and MP particles. This particularly applies

to the sand, which was confined to swirling at the bottom of the conical flasks. A wave-like motion, smaller volume of SW or denser polymer type (e.g. PET) would have caused a greater MP-sediment interaction, which would allow an accelerated experiment simulating weathering in the intertidal zone for years instead of months. Low-density polymer such as PE and PS are however more common on beaches/the intertidal zone than denser polymer types (Frias et al., 2014). The experiment can thus be said to simulate low-impact wave action in the intertidal zone.

Although both types of sediment were cleaned/sieved to remove fine particles that might interfere with the density separation procedure, incomplete density separation was detected both visually and by the various analysis methods. Fragmentation of the sediment particles was not considered and clearly occurred; the sand was sieved to remove particles $<250\ \mu\text{m}$ but SEM images show residual sand particles in the $<0.1\text{-}20\ \mu\text{m}$ size range. The density separation method should have been tested more extensively, i.e. on a full-scale weathered sample. Although a settling time of 1.5 hours should be sufficient for particles with $d \geq 2\ \mu\text{m}$ (Sutherland et al., 2014), using narrow containers decreases the settling velocity (Nakaishi et al., 2012). Small particles were observed sticking to the inclined walls and surface edges (air-glass-liquid interface) of the glass funnel, meaning that friction, adhesion and/or surface tension forces exceeded gravitational forces. It can be concluded that the density separation set-up adapted from NOAA (2015) is suboptimal for density separation of small particles; using a wide container with vertical sides might have resulted in better separation. Recently, several methods have been proven to be more efficient than NaCl density separation at separation MP from sediment. These include density separation using denser solutions such as NaI or ZnBr_2 (Quinn et al., 2017) and custom-made separation systems based on the principle of elutriation (Claessens et al., 2013) and density flotation, both small-scale (Coppock et al., 2017) and large-scale (Imhof et al., 2012). To overcome the issue of residual sediment, Nile Red staining has been used to differentiate MP (PE, PP and expanded PS) from sand (Shim et al., 2016), and also to image weathered MP for size comparison (Song et al., 2017).

5.2.2 Interaction with sediment particles

The evaluation of mechanical degradation in this study was greatly restricted due to incomplete density separation, partly explained by interaction between MP and sediment particles. Inorganic surface coating was unexpected, and has, to the authors knowledge, not yet been

reported in literature concerning marine plastic debris. The reports on MP coating/aggregation in seawater is with organic matter (Van Cauwenberghe et al., 2015), but heteroaggregation with clay has been modelled for freshwater systems (Besseling et al., 2017).

Microplastic recoveries and residual sediment content

The low recoveries of the 10 µm MP particles mechanically weathered with silt indicate heteroaggregation with silt particles – if loss occurred at other stages it would also have occurred for the photodegraded MP (equal sample size and identical filtration procedure). For the successfully recovered samples, the recoveries were generally greater for samples weathered with sand. The FTIR spectra indicate a slight temporal increase in sand content for those mechanically weathered with sand (PE-10, PS-10, PE-100 and PS-100), while the opposite is observed for the MP weathered with silt (PE-100 and PS-100). The results indicate that both heteroaggregation (followed by sedimentation) and coating increases with both decreasing MP and sediment particle size – causing a complete loss of 10 µm MP exposed to silt. The increase in residual sand could be explained by sand fragmentation and thus increased MP-sediment interaction, as non-fragmented sand particles would generally settle during density separation. On the other hand, fragmentation of silt particles could simply result in a thinner layer/coating of sediment interacting with the MP particles, resulting in a decrease in residual silt content. Interestingly, both Ling et al. (2017) and (Strand et al., 2013) found a positive correlation between the concentration of MP and the finest sediment fraction (<63 µm) collected in ocean sediments. These findings agree with the size of residual sediment particles in the mechanically weathered MP samples.

Nature of microplastic-sediment interaction

The coating observed on the MP particles mechanically weathered with sand can be classified as clay (≤ 2 µm), meaning that the sand particles fragmented during the experiment. Quartz clay is negatively charged in seawater, with positively charged edges, while newly created surfaces, e.g. from sediment fragmentation, have a zero net charge, (Sondi and Pravidic, 1998). In seawater, both PE and PS have negative surface charges regardless of surface oxidation (Fotopoulou and Karapanagioti, 2012). Further investigation is therefore needed to determine if the surface coating is purely hydrophobic, or if either material has gained a net positive surface charge allowing electrostatic interaction. A flocculation mechanism similar to

what occurs between oil droplets and clay particles is possible, and it has been argued that PE particles have comparable surface properties to neutral oil droplets (Quesnel et al., 2002, Wells et al., 1995). Another possibility is that either the MP or the smallest sediment fraction retained during density separation gained a positive charge during density separation, as increased salinity causes a decrease in the negative charge (Neihof and Loeb, 1972). Nanomaterial aggregation is known to increase with salinity (Koelmans et al., 2015), which might also be the case for the MP and sediment particles in this study. A salt-free density separation procedure might therefore yield more environmentally relevant MP-sediment interaction results.

5.2.3 Fragmentation

Evaluation of particle fragmentation was restricted due to MP-sediment interaction, and not possible for PE-100 due to particle clustering. In addition, detection of MP fragments in the lower-micron and nano-range was not achievable: the lower size range of the utilized instruments were 3.00 and 8.77 μm , for the Coulter Counter and light microscope (with recommended exclusion of particles $<5 \mu\text{m}$), respectively. While the impact energy between the 10 μm MP and sand particles was not sufficient to cause significant fracturing, part of the observed sediment coating could be MP fragments; differentiation of polymer and inorganic particles $<1 \mu\text{m}$ by EDS was not possible.

Although the cumulative size distributions of mechanically weathered PS-100 indicate fragmentation, it cannot be confidently determined due to potential heteroaggregation and settling of generated fragments with the sediment. Two possible explanations for the observed temporal trends are however as follows:

- 1) Preferential loss of the smallest MP fraction ($<140 \mu\text{m}$) by heteroaggregation with sediment, forming aggregates that settled during density separation.
- 2) Significantly increased brittleness and fragmentation between t_{20}/t_{40} and t_{80} , where individual MP particles break up completely to fragments $<8.77/24.7 \mu\text{m}$ (silt/sand).

Option 1 also explains why the particles below D50 (50 % cumulative percent) are significantly smaller particles in the PS-100 control sample (t_{40}), compared to all PS-100-silt t_0 - t_{80} and PS-100-sand t_0 and t_{40} . While option 2 explains why the mean particle size at t_{80} has increased, physico-chemical changes during the 10-month pause in the middle of the weathering experiment (at t_{40}) could be the reason for the non-temporal trend. During this break, e.g. equilibration of MP-sediment interaction could have resulted in greater loss due to settling of

heteroaggregates during density separation. The non-temporal trends could also be attributed to unrepresentative sampling for microscopy imaging, or variation in residual sediment content and size.

In a degradation study by Song et al. (2017), larger LDPE pellets (3.7 mm) were mechanically weathered with dry sand at lower speed (37 rpm) for 2 months, followed by 0-12 months of UV exposure. The particles did not fragment into large pieces, but lost micron-sized fragments in the 25 - 650 μm size range. An average of 9 and 20 fragments/pellet were produced after 2 months of mechanical weathering and with subsequent UV exposure for 12 months, respectively. The size distribution of the MP fragments showed an exponential increase in the number with decreasing particle size, with 87 % <100 μm . No “missing fraction” (<25 μm) was detected in LDPE subjected to only mechanical weathering, while 9 % were lost after 12 months of UV exposure. The results of this study and the one by Song et al. (2017) indicate that mechanical weathering does not cause extensive fracturing of MP particles, neither in dry form nor in water. Fracturing is however dependent on shape – spherical particles do not fragment as easily as irregularly shaped particles (Masuda et al., 2006), which limits the environmental relevance of both studies. Loss of nano-sized fragments from the surface is however highly probable as the surface changes indicate loss of nano-sized fragments, as already discussed for the photodegraded MP.

5.2.4 Chemical changes

The FTIR spectra of mechanically degraded MPs did not show any signs of oxidation, which is as expected at a temperature <27 °C for 80 days in the absence of UV irradiation. The broad Si-O band could overlap a small C-O stretch in the 1290 - 1160 cm^{-1} region, so slight oxidation cannot be ruled out. Oxidation is however unlikely as no carbonyl or hydroxide bands are present in the FTIR spectra and the weathering experiment did not involve a source of free radicals (such as UV radiation). Although a slight temporal increase in crystallinity was detected in PE-100-sand, the change is minor is possibly caused to the coinciding increase in residual sand. In a similar study it took 36 months for oxidation of PE in still seawater (dark, room temperature) to be detectable by FTIR (Brandon et al., 2016). The authors also detected no change in crystallinity.

5.3 Evaluation of the method

5.3.1 Experimental design

Choice of microplastic materials

Microplastic beads, such as the 10 μm particles utilized in this study, are not nearly as prevalent in the environment as irregularly shaped fragments from larger plastic particles. The rate of degradation is likely higher for irregularly shaped particles, both due to greater surface areas and susceptibility to physical impact. Optimal MP materials for environmental simulation would be collected from the marine environment, either in the required size range, or from larger plastic debris grinded to that size range. Achieving a homogenous MP mixture in the lower micron size range by grinding larger plastic is however challenging, and inhomogeneity would increase experimental errors. Performing weathering studies with more environmentally relevant particle shapes is recommended.

Microplastic handling

Using a spatula to handle MP particles might not be suitable when one of the objectives is to assess changes in particle size, as even careful scraping could damage the particles and result in fragmentation. Indents and streak marks were observed on the 10 μm MP particles imaged by SEM, which could be from impact of the metal spatula used to transfer the MP particles and to remove the recovered MP from the filter papers. Assessment of fragmentation is however justified in this study, as the weathered samples were compared against t_0 and control samples that were prepared and extracted in the same way. Also, no fragmentation was observed after an analogous filtration procedure by Hernandez et al. (2017), who detected both nanoplastics (24–52 nm) and undamaged MP beads (20–200 μm) by X-ray photoelectron spectroscopy. Possible damage caused by scraping could easily be investigated by e.g. SEM. Although pristine MP might be resistant to scraping, sufficiently weathered MP will be more fragile.

5.3.2 Contamination

Despite sample handling precautions to minimize contamination, both light microscopy and SEM images showed traces of extraneous particles. Dust and a small number of fibres were observed in microscopy images of both MP samples and in microscopy blanks (clean microscope slides). In the size distributions histograms of PS-100 and the microscopy blank

(Figure 5.37 and Figure 4.39, respectively), the “particles” making up the lowest bin (2 μm) are likely dust, or alternatively an image processing artefact as 2 μm correspond to 1 pixel. The photodegraded MP has a small number of embedded particles that resemble sediment particles embedding the mechanically weathered sample. Sediment cross-contamination via equipment is however unlikely as equipment used on multiple samples (e.g. spatula) was washed thoroughly and dried between each sample. The particles could be contamination from the SEM laboratory (a few similar particles were observed in SEM blank), from the sample preparation and extraction procedure (e.g. dust, from solvents or glassware) or MP fragments (i.e. NP). In addition, pristine PE-10 had greater surface coating and number of “foreign” particles than the weathered samples, indicating contamination or residue from the manufacturing process that was mostly removed during the suspension and filtration steps. The contamination experienced in this study is generally low and does not significantly interfere with data interpretation, but experiments and analyses should be performed in cleanroom facilities if available.

Filter paper contamination

Fibre-like fragments, and in some cases fibrous clusters, were detected in SEM images of MP samples that were filtered using GF/F filters. The fibre-like cluster found in PS-100 mechanically weathered with sand (t_{40}) is showed in Figure 5.2, along with a SEM image of a Millipore GF/F filter (0.7 μm pore size) captured by Nayar and Chou (2003).

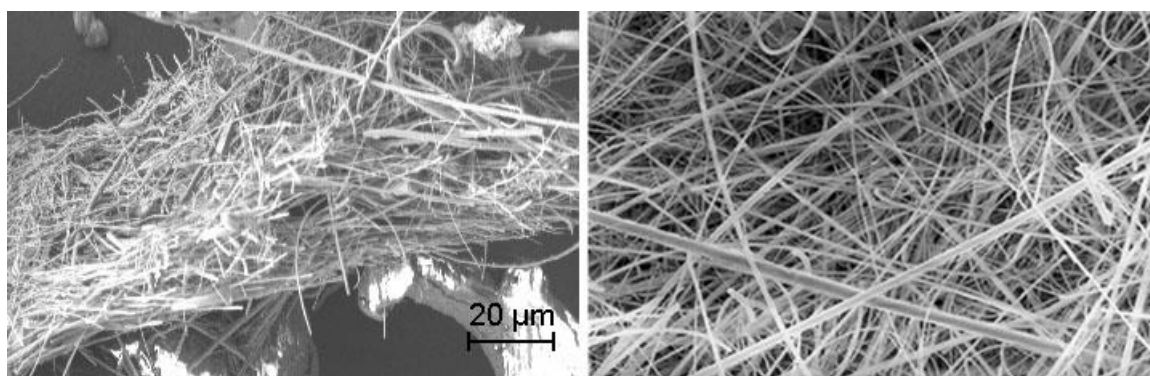


Figure 5.2: SEM image of fibrous cluster found in PS-100-sand t_{40} (left) and of a Millipore GF/F filter (Nayar and Chou, 2003) (right). The images are presented at equal magnifications.

Both visual and chemical analysis by EDS of the fibrous structure strongly suggest that it is a fragment of the GF/F filter. Whatman GF/F filters are composed of binder-free borosilicate

glass microfibers, and the elemental composition of the fibrous cluster is within the wide range of borosilicate glass fibres (Wallenberger and Bingham, 2009). The individual fibre-like fragments were too small to be analysed by EDS, but as they were only observed in samples filtered using GF/F filters, filter paper fibres are a highly probable source. It can be concluded that GF/F filters should not be scraped, not even carefully as done in this study. Filter paper contamination can interfere with both size distribution and chemical analysis; SiO₂ is the main constituent of both GF/F filters and the sediments used in this study. Although not problematic in this study as GF/F fibres cannot be mistaken for MP particles/fragments, other filters such as Millipore HA composed of cellulose acetate fibres are more suitable.

Biological contamination

Unidentified material, in the form of circular patches and rods, were observed on the surface of PE-10 photodegraded for 80 days (Figure 4.16). As the t₈₀ samples were stationary for 10 months before experiment re-start, the circular patches could be crystallization/build-up of material between touching MP spheres, such as NaCl from the seawater. A theory which would also explain the rod-like structures is fungal contamination - the rods being hyphae (a filament segment of mycelia) and the circular patches traces of conidia (spores). Fungal growth is possible in the experimental conditions, and the size of the material is within the lower size range of fungi. Contamination could have occurred during sample handling, but pre-existing contamination is also possible since pristine PE-10 contained traces of silicone oil and irregularly shaped particles/residue that could be from previous fungal growth (Figure 4.1). The t₈₀ photodegradation samples could have reached higher temperatures than the preceding samples, as the SunTest instrument ran continuously for the last 40 days – several interruptions occurred during the first 40 days due to sampling and technical problems. A higher temperature would enable germination, which would explain the finding of possible fungal traces only in PE-10 photodegraded for 80 days. Possible fungal species are *Aspergillus niger* and *Aspergillus fumigatus*, which are common types of mould found in e.g. food, indoor and outdoor environments. Both species have marine strains and grow at temperatures between 12 and >70 °C (24-37 °C optimal range), although with slower growth rates in seawater (Warnock et al., 2013, Suthindhiran and Kannabiran, 2010). Polymer biofilm formation by *A. fumigatus* has been reported, with slower mycelial growth in agitated solutions compared to dry and static conditions (Müller et al., 2011) *A. niger* has been shown to grow on polyester fibres, in which the initial step involved attachment of spherical spores of $d = 2-3 \mu\text{m}$ by an adhesive pad

followed by hyphae growth (Gutiérrez-Correa et al., 2012). The diameter of *A. niger* hyphae is commonly $\sim 1 \mu\text{m}$, but the slightly smaller diameters observed could be due to either loss of the extracellular matrix or caused by the experimental rotation; agitation speeds of 50-200 rpm results in reduced hyphae diameter and a smoother surface (Ibrahim et al., 2015). Considering the appearance and size of the material, growth traces of *A. niger* is the most plausible explanation.

5.3.3 Analysis methods

Determining the size distribution by light microscopy was perhaps the least successful analysis method in this study. The particle size distribution of pristine PE-100 and PS-100 measured in this study is significantly lower than measured by the supplier (Table 5.2). Apart from the potential spatula impact and error caused by irregularly shaped and touching particles, sampling of polydispersed powders can introduce significant errors due size segregation (Gotoh et al., 1997). Using microscopy to determine the size distribution might be acceptable for a single sample, but the resultant errors greatly reduce its applicability to sample comparison. Alternative methods such as laser diffraction are suggested, in addition to methods for tracking the loss/formation of NP like nanoparticle tracing analysis (NTA) (Lambert and Wagner, 2016a).

Table 5.2: Comparison of the particle size distribution determined in this study (light microscopy) with supplier data (Laser diffraction).

		Median (μm)	d_{25} (μm)	d_{75} (μm)	Range (μm)
PE-100	This study ($>8.77 \mu\text{m}$)	19.0	12.8	30.8	8.9 – 930.6
	Supplier	75.4	52.7	115.0	27.2 – 675.3
PS-100	This study ($>8.77 \mu\text{m}$)	42.8	20.9	82.6	8.9 – 313.0
	Supplier	94.3	71.6	123.9	43.8 – 372.5

Imaging by SEM proved to be of great value and is highly recommended, both to assess shape, size (distribution), surface morphology and contamination. Surface changes are correlated to oxidation, and the presence of foreign material can alter physio-chemical properties and toxicity. Undetected microorganisms in particle weathering studies can for example lead to

incorrect theories/conclusions as biodegradation could have played a role. The SEM images captured at various times demonstrate the importance of experience; the surface morphology information from e.g. photodegraded PS-10 (Figure 4.10) is much greater than for pristine PS-10 (Figure 4.2) that was imaged shortly after SEM training.

It must be mentioned that EDS analysis of particles with irregular shapes and topography result in elemental compositions with significant errors. As opposed to ideal flat and polished specimens, the elemental composition can deviate up to 107 % for irregular particles, depending on what location was chosen for EDS analysis. This deviation is due to scattering of the electron beam at irregular/inclined surfaces and altered path length, which result in reduced intensity of the x-ray beam reaching the detector (Newbury and Ritchie, 2015).

The advantages of ATR-FTIR are many, but low reproducibility is an issue when analysing solids and powders due to difficulty obtaining uniform contact between the sample and ATR crystal – poor contact will lead to lower absorbance (Bhargava and Levin, 2008). True qualitative analysis therefore requires calibration, e.g. by the use of an internal standard (peak ratio method) for less complex samples, or spectral processing and multivariate analysis for more complex samples (Larkin, 2011). Simply choosing a reference peak from previous MP weathering work (Yousif and Haddad, 2013) gave unrealistic results, highlighting the importance of considering possible temporal changes in the polymer structure and chemistry. The best options might therefore be simple spectral processing as performed in this study, or multivariate analysis. In addition, evaluation of polymer crystallinity from ATR-FTIR spectra should be done with caution, as the pressure applied to the sample can slightly increase the crystallinity (Noda et al., 1999).

Pyr-GC/MS of weathered polymer samples has a great potential, requiring only 5 - 200 µg material (Kusch, 2017). Interpretation of the results in this study was however restricted due to practical and technical difficulties. Weighing or controlling the mass of MP powder applied on the pyrolysis unit filament was not feasible. The results demonstrate that that pyrogram pattern is affected by sample size (Bart, 2001). The significant carry-over and ghost peaks in the Pyr-GC/MS pyrograms could be explained by decomposition of the polymer sample and deposition at an inadequate interface, e.g. between the injector and column. If the aim is to determine leaching of polymer-associated substances upon photodegradation in water, analysis of MP samples before and after weathering is potentially more useful than analysis of the aqueous phase; UV exposure likely caused degradation of at least some plastic leachates in seawater in a similar study (Suhrhoff and Scholz-Böttcher, 2016). On the other hand, degradation of

leachates will also occur during UV exposure in the natural environment, but likely not as readily as in accelerated experimental studies.

Recommended analysis methods in future degradation studies include surface area measurements by e.g. Brunauer-Emmett-Teller (BET). Increased surface area accelerates degradation, e.g. by increased permeability which allows absorption of water which in turn increases hydrolysis and oxidation rates. Detection of crystallinity changes due to e.g. preferential erosion of amorphous regions could also be valuable – which is more easily detected by differential scanning calorimetry (DSC) than by FTIR. Definite FTIR frequency assignment of the different functional groups formed in photodegraded MP should also be carried out, which would also allow quantitative analysis. Treatment with gaseous NH_3 or SF_4 and subsequent FTIR analysis is one method that allows distinction between different carbonyl functional groups (Stuart, 2004). Also, the ratio of chain scission and crosslinking has not yet been determined for PE and PS microplastic weathered in (sea)water, which can be estimated by molecular weight distribution measurements, e.g. by gel permeation chromatography (Guaita et al., 1985).

5.4 Summary

A summary of the MP characteristics, changes (and possible explanations) detected during the 80 days of experimental photodegradation and mechanical weathering is presented in Table 5.3.

Table 5.3: Summary of characteristics of pristine, photodegraded and mechanically weathered MP*.

MP material and state	Shape and morphology	Chemical characteristics	Size distribution	
PE-10	<i>Pristine</i>	Smooth, clean surface (SEM)	Unknown band at 1116 cm ⁻¹ (FTIR), potential additives (Pyr-GC/MS)	Broad, mean ± SD = 8.00 ± 4.96 μm (CC)
	<i>UV</i>	↑ in surface roughness (SEM)	Possible leaching of >C ₁₈ homologues (Pyr-GC/MS), NC (FTIR)	NC/possible ↓ due to fragmentation (SEM)
	<i>Sand</i>	Sand coating, finer at t ₈₀ (SEM)	Residual sand ↑ (t ₀ -t ₄₀) then ↓ (t ₈₀) (FTIR)	NC/possible ↑ due to sand coating (SEM)
PS-10	<i>Pristine</i>	Smooth surface, slight unknown surface residue (SEM)	Identification (FTIR), potential additives (Pyr-GC/MS)	Narrow, mean ± SD = 10.28 ± 1.86 μm (CC)
	<i>UV</i>	Rougher surface at t ₈₀ (SEM)	Oxidation at t ₈₀ (Pyr-GC/MS and FTIR), leaching of oligomers (Pyr-GC/MS)	NC/possible ↓ due to fragmentation (SEM)
	<i>Sand</i>	Sand coating (SEM)	Residual sand (FTIR)	NC/possible ↑ due to sand coating (SEM)
PE-100	<i>Pristine</i>	Non-uniform shredded particles, clustered (SEM and MIC)	Identification (FTIR)	Broad, mean ± SD = 36.6 ± 56.3 μm, insufficient particle separation (MIC)
	<i>Silt</i>	NC (MIC)	Residual silt (FTIR)	Insufficient particle separation (MIC)
	<i>Sand</i>	NC (MIC), sand coating and in cracks (SEM)	↑ in residual sand (FTIR)	Insufficient particle separation (MIC)
PS-100	<i>Pristine</i>	Uniform, rounded, striations (SEM and MIC)	Identification (FTIR)	Broad, mean ± SD = 58.9 ± 48.5 μm (MIC)
	<i>Silt</i>	NC (MIC)	Residual silt (FTIR)	Possible fragmentation and/or removal of MP <140 μm by heteroaggregation with sediment (MIC)
	<i>Sand</i>	NC (MIC), sand coating and in cracks (SEM)	Residual sand (FTIR)	Possible fragmentation and/or removal of MP <140 μm by heteroaggregation with sediment (MIC)

***Abbreviations:**

UV = photodegraded
Silt = mechanically weathered with silt
Sand = mechanically weathered with sand
NC = no change

CC = Coulter Counter
MIC = light microscopy
↑ = increase
↓ = decrease

5.5 Implications and suggestions for future research

5.5.1 Fate of microplastic in the marine environment

Although PS is regarded as stable polymer that can handle higher temperatures than PE, this study shows that it is less resilient to photodegradation than PE. Measurable oxidation occurred somewhere between t_{40} and t_{80} , which, if assumed to have occurred at t_{60} , is equivalent to ≤ 1.5 years in Trondheim or ≤ 0.5 year in locations at the same latitude as Sahara (Quaschnig, 2016). PS floating on the ocean surface will therefore degrade relatively quickly compared to PE in areas with sufficient sunlight. Oxidation has two major implications: (1) due to preferential weathering and erosion of amorphous regions will increase both the polymer density and strength, which could lead to sinking and decreased degradation rates, and (2) optimal conditions for biofouling, causing increased density and sinking, to depth with insufficient sunlight where defouling and rising occurs. Research indicate that (2) is a more likely scenario for PS than PE: Biofouling increased the sinking velocity of PS pellets by 81 % after 6 weeks in SW, while the minority of PE particles sank only if sufficiently biofouled by blue mussels (David et al., 2017). This means that PE is more likely to reside on or close to the ocean surface, while PS, which also is a denser polymer, can oscillate vertically in the water column through repeated cycles of fouling and defouling. The fouling-defouling cycle causing MP to stay in the top 100 m water column is one of the theories explaining why MP disappears from the surface. A modelling of this theory found a significant size-dependency due to the higher sinking and rising velocity of larger particles. While a 1 mm particle sinks to 75 m depth and resurfaces in one day, a 100 μm particle only sinks to 50 m and resurfaces in 3 days. Smaller particles do not resurface at all; 10 and 1 μm particles oscillate at 10-30 and 16-24 m depth, with oscillation periods of 21 and 180 days, respectively (Kooi et al., 2017). This means that MP and NP can reside in the water column for long periods of time; the biodegradation rates at these depths should be investigated to estimate their lifetimes at sea. Although the number of spherical MP particles are minor compared to irregular fragments, wind can cause spherical particles with $\rho < \rho_{\text{sw}}$ to drift large distances and reside on the ocean surface for up to 10-15 years (Chubarenko et al., 2016).

Research on the interaction between MP and sediment/suspended inorganic matter appears to be focused on freshwater systems. Although the concentration of suspended inorganic matter is generally higher in freshwater systems than in the marine environment, this is not necessarily true in the intertidal zone or in areas close to the ocean floor with high wave action or water movement. This study shows that interaction between MP and sediment could be an important

determinant for the fate of MP in vicinity of sediment, particularly for polymers that are not readily photooxidized and biofouled such as PE. If the mechanism of heteroaggregation with sediment modelled for freshwater can be extrapolated to shoreline seawater, a significant proportion of 10-1000 μm MP and NP (0.1-1 μm) is expected to be efficiently “removed” by aggregation with clay and settling, while 1-10 μm MP remains in the water column (Besseling et al., 2017). The strong relationship between the concentration of MP and both organic content and sediment <63 μm indicate that MP will accumulate in depositional areas (Strand et al., 2013). Although the size distribution of mechanically weathered PS-100 indicate heteroaggregation of MP <140 μm with sediment, the results should be interpreted with caution as heteroaggregation and fragmentation could not be differentiated. Inorganic heteroaggregation and size segregation should therefore be investigated further to determine the mechanism and relationship to properties such as size, concentration and surface charge. It could change the MP exposure and potential effects on organisms, as well as explain a portion of the “lost fraction”. Also, a slight inorganic surface coating of low-density MP could act as a protective layer against photo- and biodegradation.

The main purpose of MP weathering studies is to find out where the MP end up and how long it takes for it to completely break down (mineralize). Mineralization has not found to be different for pristine and photooxidized PE; both exhibited a linear loss of CO_2 which reached 2 % of the polymer mass after 48 days of degradation in SW (Alvarez-Zeferino et al., 2015). The authors did however find significant reduction of tensile strength with weathering time: 9 days of UV radiation (unknown intensity) led to a 20 % decrease in the elongation at break, and 48 days in SW led to a further 10 and 15 % decrease in pristine and photooxidized LDPE, respectively. Although a relatively short experiment, the results of Alvarez-Zeferino et al. (2015) indicate that oxidation does not necessarily accelerate mineralization, but that photooxidation plays a major role in loss in tensile strength. Initial photooxidation will thus increase the polymer’s susceptibility to physical degradation and accelerate fragmentation to MP/NP. Mechanical weathering on the other hand, might be a minor contributor to degradation, causing only slight chemical changes and loss of nano-sized fragments, but should be investigated further in seawater. Song et al. (2017) investigated the effect of UV exposure on mechanically weathered MP, but it might be more environmentally relevant to examine the effect of mechanical weathering on already photodegraded MP. Most plastic debris spend time on the ocean surface before washing up on shorelines (Barnes et al., 2009), and pre-

photodegraded MP would theoretically experience greater fragmentation due to increased porosity/brittleness.

5.5.2 Toxicity

Plastic debris in all size classes has the potential to cause harm, either physically through e.g. internal obstruction, or chemically through exposure of polymer-associated substances and degradation products. Leaching of PE and PS oligomers is not of great concern; the concentration of PS oligomers in coastal sediments is comparable to the level of polycyclic aromatic hydrocarbons, but with <1 % of the toxicity (Hong et al., 2016). As PE is hydrophobic and more resilient to photooxidation than both PS and PP, it likely the main vector for environmental contaminants. Leaching of polymer-associated substances might however be of concern to biota in plastic debris accumulation zones, where concentrations are greater than in open water. As water turbidity increases leaching (Suhrhoff and Scholz-Böttcher, 2016), focusing on areas with high water turbidity might be beneficial, e.g. in coastal accumulation zones close to fishing activities. Chemical exposure through leaching of polymer-associated substances after ingestion is however greater than from water for most organisms. Some species are attracted to MP: zooplankton showed a preference for aged PS beads (15 and 30 µm left in SW for 3 weeks), likely due to biofouling which might camouflage the MP as food items (Vroom et al., 2017). Corals on the other hand preferred pristine MP, which could be attributed to polymer additives acting as phagostimulants (Allen et al., 2017). Yet ingestion-uptake studies indicate that pollutant exposure through MP ingestion is minor compared to uptake from food, at least for species that do not show a preference for MP over food (Hermabessiere et al., 2017). Determining the sources of pollutants entering the bottom of the food web is therefore important. In addition, the main oxidation products for the most commonly encountered plastic types and their leaching and toxicity potential should be assessed. For polymers with hydrocarbon backbones, oxidation must occur for biodegradation and hydrolysis to be possible, but also leads to changes in the polymer's reactivity, potential toxicity and fate.

5.5.3 Nanoplastic, fibres and plastic debris in terrestrial/freshwater ecosystems

As a large number of nano-sized fragments are lost from the surface of MP and larger plastic debris (Lambert and Wagner, 2016b), it is important to find out what happens to the NP. Primary NP added to consumer products such as cosmetics also ends up in the environment

(Hernandez et al., 2017). Despite decreasing sinking velocities with decreasing size (Kowalski et al., 2016), smaller particles experience a greater density increase upon biofouling and heteroaggregation, and modelling indicate that they never resurface (Kooi et al., 2017). The primary fate of nanomaterials in the marine environment is believed to be settling to the deep ocean/ocean floor due to formation of colloids and aggregates (Koelmans et al., 2015), which can plausibly be extrapolated to NP. NP might mineralize faster than larger particles, but has, unlike most MP, the potential to be taken up in the circulatory system of organisms. The extent of NP uptake and potential effects are still unclear (Koelmans et al., 2015), but could be of environmental concern due to polymer-associated substances.

Recent studies indicate that MP fibres are the most prevalent type of MP, both on beaches (Browne et al., 2015) and in the water column (Bagaev et al., 2017). MP fibres have also been found in marine organisms, comprising more than 50 % of the MP found in some organisms and 100 % of deep sea organisms (Desforges et al., 2015, Mathalon and Hill, 2014, Taylor et al., 2016). As the toxicity of PP fibres is 3 orders of magnitude greater than PP spheres (Au et al., 2015), the weathering and fate of MP fibres might be more relevant, at least from a toxicological perspective.

Terrestrial and freshwater ecosystems must not be forgotten – the concentration of plastic debris in soil, lakes, rivers and freshwater sediments in many locations exceed those encountered in the ocean. MP has been shown to enter freshwater and terrestrial food webs; e.g. in freshwater clams (Su et al., 2018) and trophic transfer from soil to earthworms to chickens (Huerta Lwanga et al., 2017). In addition, human exposure MP/NP and polymer-associated substances through food and inhalation, particularly in indoor environments, is a relatively unexplored area (Wright and Kelly, 2017).

Conclusion

Weathering experiments simulating photodegradation on the ocean surface and mechanical degradation of MP in the intertidal zone were successfully carried out on 10 and 100 μm PE and PS. Extraction of photodegraded MP samples was successful, while the NaCl density separation of MP mechanically weathered with sediment (silt and sand) was insufficient, particularly for the 10 μm MP mechanically weathered with silt.

During the 80-day photodegradation experiment, equivalent to ≤ 616 days in Trondheim, 10 μm PE and PS particles did not significantly fragment. A temporal increase in surface roughness was however observed and was particularly distinct in 10 μm PS photodegraded for 80 days. Increased surface roughness is likely due to oxidation and chain scission at the surface, causing loss NP fragments. The implications of nano-fragmentation need to be determined, both in regard to fate of plastic debris in the marine environment and potential toxicity. Photodegraded PE likely experienced a temporal decrease in MW due to chain scission and/or leaching of oligomers $>C_{18}$. PS was significantly oxidized after 80 days, with a range of oxidation products detected, including esters and carboxylic acids, the latter being strongly hydrogen-bonded. This study demonstrates that photodegradation in air and seawater is significantly different, likely attributed to the lower temperature and oxygen availability in seawater. While oxidation of PS increases its susceptibility to physical degradation and affinity to microorganisms, accelerating degradation, PE likely has a longer life-time in the environment. Environmental sampling and experimental studies are however needed to confirm this theory.

The mechanically weathered MP samples contained residual sediment, partly because of insufficient density separation. The sand particles ($>250 \mu\text{m}$) fragmented during the mechanical weathering experiment, forming clay particles that coated the MP and accumulated in gaps. Heteroaggregation is believed to be the cause, which has not yet been reported in literature concerning marine MP. The surface morphology of the mechanically weathered MP was masked by sediment coating, and no change in size was observed for the 10 μm MP particles. A non-temporal size reduction was observed for the mechanically weathered 100 μm MP, which could be explained by settling of MP particles $<140 \mu\text{m}$ in heteroaggregates with sediment during density separation. Heteroaggregation with sediment, particularly in the clay size range, could be an important sedimentation mechanism for marine MP (and NP) exposed to suspended sediment and should be investigated further.

References

- ACHHAMMER, B. G., REINEY, M. J. & REINHART, F. W. 1951. Study of Degradation of Polystyrene, Using Infrared Spectrophotometry. *Journal of Research of the National Bureau of Standards*, 47, 116-125.
- ALLEN, A. S., SEYMOUR, A. C. & RITTSCHOF, D. 2017. Chemoreception drives plastic consumption in a hard coral. *Marine Pollution Bulletin*.
- ALVAREZ-ZEFERINO, J., BELTRÁN-VILLAVICENCIO, M. & VÁZQUEZ-MORILLAS, A. 2015. Degradation of Plastics in Seawater in Laboratory. *Open Journal of Polymer Chemistry*, 5, 55-62.
- ANDRADY, A. L. & PEGRAM, J. E. 1991. Weathering of polystyrene foam on exposure in air and in seawater. *Journal of Applied Polymer Science*, 42, 1589-1596.
- AU, S. Y., BRUCE, T. F., BRIDGES, W. C. & KLAINÉ, S. J. 2015. Responses of *Hyaella azteca* to acute and chronic microplastic exposures. *Environmental Toxicology and Chemistry*, 34, 2564-2572.
- BAGAEV, A., MIZYUK, A., KHATMULLINA, L., ISACHENKO, I. & CHUBARENKO, I. 2017. Anthropogenic fibres in the Baltic Sea water column: Field data, laboratory and numerical testing of their motion. *Science of The Total Environment*, 599, 560-571.
- BARNES, D. K. A., GALGANI, F., THOMPSON, R. C. & BARLAZ, M. 2009. Accumulation and fragmentation of plastic debris in global environments. *Philosophical Transactions of the Royal Society B: Biological Sciences*, 364, 1985-1998.
- BART, J. C. J. 2001. Polymer/additive analysis by flash pyrolysis techniques. *Journal of Analytical and Applied Pyrolysis*, 58-59, 3-28.
- BAZTAN, J., CARRASCO, A., CHOUINARD, O., CLEAUD, M., GABALDON, J. E., HUCK, T., JAFFRÈS, L., JORGENSEN, B., MIGUELEZ, A., PAILLARD, C. & VANDERLINDEN, J.-P. 2014. Protected areas in the Atlantic facing the hazards of micro-plastic pollution: First diagnosis of three islands in the Canary Current. *Marine Pollution Bulletin*, 80, 302-311.
- BERGMANN, M., GUTOW, L. & KLAGES, M. 2015. *Marine Anthropogenic Litter*, Springer International Publishing.
- BESSELING, E., QUIK, J. T. K., SUN, M. & KOELMANS, A. A. 2017. Fate of nano- and microplastic in freshwater systems: A modeling study. *Environmental Pollution*, 220, 540-548.
- BHARGAVA, R. & LEVIN, I. W. 2008. *Spectrochemical Analysis Using Infrared Multichannel Detectors*, Wiley.
- BILITEWSKI, B., DARBRA, R. M. & BARCELO, D. 2012. *Global Risk-Based Management of Chemical Additives I: Production, Usage and Environmental Occurrence*, Springer Berlin Heidelberg.
- BLAZSÓ, M. 1997. Recent trends in analytical and applied pyrolysis of polymers. *Journal of Analytical and Applied Pyrolysis*, 39, 1-25.
- BOCKRIS, J. O. M., BOCKRIS, J. O. M. & REDDY, A. K. N. 1998. *Volume 1: Modern Electrochemistry: Ionics*, Springer US.
- BOLGAR, M., HUBBALL, J., GROEGER, J. & MERONEK, S. 2015. *Handbook for the chemical analysis of plastic and polymer additives*, CRC Press.

- BRANDON, J., GOLDSTEIN, M. & OHMAN, M. D. 2016. Long-term aging and degradation of microplastic particles: Comparing in situ oceanic and experimental weathering patterns. *Marine Pollution Bulletin*, 110, 299-308.
- BROWNE, M. A., CRUMP, P., NIVEN, S. J., TEUTEN, E., TONKIN, A., GALLOWAY, T. & THOMPSON, R. 2011. Accumulation of Microplastic on Shorelines Worldwide: Sources and Sinks. *Environmental Science & Technology*, 45, 9175-9179.
- BROWNE, M. A., DISSANAYAKE, A., GALLOWAY, T. S., LOWE, D. M. & THOMPSON, R. C. 2008. Ingested Microscopic Plastic Translocates to the Circulatory System of the Mussel, *Mytilus edulis* (L.). *Environmental Science & Technology*, 42, 5026-5031.
- BROWNE, M. A., UNDERWOOD, A. J., CHAPMAN, M. G., WILLIAMS, R., THOMPSON, R. C. & VAN FRANKEKER, J. A. 2015. Linking effects of anthropogenic debris to ecological impacts. *Proceedings of the Royal Society B: Biological Sciences*, 282, 20142929.
- BS3406 1993. Part 4; British Standard Methods for Determination of Particle Size Distribution. *Optical Microscope Method*. London: British Standards Institute.
- CARSON, H. S., COLBERT, S. L., KAYLOR, M. J. & MCDERMID, K. J. 2011. Small plastic debris changes water movement and heat transfer through beach sediments. *Marine Pollution Bulletin*, 62, 1708-1713.
- CHAE, Y. & AN, Y.-J. 2017. Effects of micro- and nanoplastics on aquatic ecosystems: Current research trends and perspectives. *Marine Pollution Bulletin*, 124, 624-632.
- CHALMERS, J. M. & MEIER, R. J. 2008. *Molecular Characterization and Analysis of Polymers*, Elsevier Science.
- CHOI, J. O. K., JITSUNARI, F., ASAKAWA, F. & SUN LEE, D. 2005. Migration of styrene monomer, dimers and trimers from polystyrene to food simulants. *Food Additives & Contaminants*, 22, 693-699.
- CHOLLI, A. L., DUMAIS, J. J., ENGEL, A. K. & JELINSKI, L. W. 1984. Aromatic ring flips in a semicrystalline polymer. *Macromolecules*, 17, 2399-2404.
- CHUBARENKO, I., BAGAEV, A., ZOBKOV, M. & ESIUKOVA, E. 2016. On some physical and dynamical properties of microplastic particles in marine environment. *Marine Pollution Bulletin*, 108, 105-112.
- CLAESSENS, M., VAN CAUWENBERGHE, L., VANDEGEHUCHTE, M. B. & JANSSEN, C. R. 2013. New techniques for the detection of microplastics in sediments and field collected organisms. *Marine Pollution Bulletin*, 70, 227-233.
- CLAVIER, R. 2008. *Characterization and Analysis of Polymers*. 1 ed.: Wiley-Interscience.
- COATES, J. 2006. Interpretation of Infrared Spectra, A Practical Approach. *Encyclopedia of Analytical Chemistry*. John Wiley & Sons, Ltd.
- COLE, M., LINDEQUE, P., FILEMAN, E., HALSBAND, C., GOODHEAD, R., MOGER, J. & GALLOWAY, T. S. 2013. Microplastic Ingestion by Zooplankton. *Environmental Science & Technology*, 47, 6646-6655.
- COLLARD, F., GILBERT, B., EPPE, G., PARMENTIER, E. & DAS, K. 2015. Detection of Anthropogenic Particles in Fish Stomachs: An Isolation Method Adapted to Identification by Raman Spectroscopy. *Archives of Environmental Contamination and Toxicology*, 69, 331-339.

- COPPOCK, R. L., COLE, M., LINDEQUE, P. K., QUEIRÓS, A. M. & GALLOWAY, T. S. 2017. A small-scale, portable method for extracting microplastics from marine sediments. *Environmental Pollution*, 230, 829-837.
- COSPHERIC 2014. Preparing Tween Solutions. In: DESANTIS, I. (ed.) *Document Number: SOP-00018, Revision 03*.
- CRAWFORD, C. B. & QUINN, B. 2017. 9 - Microplastic separation techniques. *Microplastic Pollutants*. Elsevier.
- CROMPTON, R. 2009. *Characterization of Polymers*, iSmithers Rapra Publishing.
- CROMPTON, T. R. 2006. *Polymer Additives*, Smithers Rapra Technology.
- D'ESPOSITO, L. & KOENIG, J. L. 1979. A comparison of the thermal and mechanical degradation of glassy polystyrene by Fourier transform infrared spectroscopy. *Polymer Engineering & Science*, 19, 162-165.
- DAVID, K., NICOLE, K. & JOANNA, J. W. 2017. Effects of biofouling on the sinking behavior of microplastics. *Environmental Research Letters*, 12, 124003.
- DAWSON, G. & KOPPENHAGEN, F. 2003. Production of microparticles. Google Patents.
- DEHAUT, A., CASSONE, A.-L., FRÈRE, L., HERMABESSIERE, L., HIMBER, C., RINNERT, E., RIVIÈRE, G., LAMBERT, C., SOUDANT, P., HUVET, A., DUFLOS, G. & PAUL-PONT, I. 2016. Microplastics in seafood: Benchmark protocol for their extraction and characterization. *Environmental Pollution*, 215, 223-233.
- DESFORGES, J.-P. W., GALBRAITH, M. & ROSS, P. S. 2015. Ingestion of Microplastics by Zooplankton in the Northeast Pacific Ocean. *Archives of Environmental Contamination and Toxicology*, 69, 320-330.
- DIEM, M. 2015. *Modern Vibrational Spectroscopy and Micro-Spectroscopy : Theory, Instrumentation and Biomedical Applications*, Chicester, UNKNOWN, John Wiley & Sons, Incorporated.
- DROBNY, J. G. 2016. *Fluoroelastomers Handbook: The Definitive User's Guide*, Elsevier Science.
- ELLIS, B. & SMITH, R. 2008. *Polymers: A Property Database, Second Edition*, CRC Press.
- ERIKSEN, M., LEBRETON, L. C. M., CARSON, H. S., THIEL, M., MOORE, C. J., BORERRO, J. C., GALGANI, F., RYAN, P. G. & REISSER, J. 2014. Plastic Pollution in the World's Oceans: More than 5 Trillion Plastic Pieces Weighing over 250,000 Tons Afloat at Sea. *PLoS One*, 9.
- EU 2017. Communication: Strategy on Plastics in a Circular Economy. In: DIRECTORATE-GENERAL, E. (ed.). European Commission.
- EU 2018. EU Strategy for Plastics in the Circular Economy. In: COUNCIL, D. O. T. E. P. A. O. T. (ed.) 2015/0276/COD. Brussels: European Commission.
- EUNOMIA 2016. Plastics in the Marine Environment: Where do they come from? Where do they go? In: EUNOMIA-MARINE-LITTER-MED.JPG (ed.). United Kingdom: Eunomia Research & Consulting Ltd.
- EUROPEAN_BIOPLASTICS 2016. Bioplastics - Facts and Figures. In: NOVA-INSTITUTE (ed.). Berlin.
- FISCHER, M. & SCHOLZ-BÖTTCHER, B. M. 2017. Simultaneous Trace Identification and Quantification of Common Types of Microplastics in Environmental Samples by

- Pyrolysis-Gas Chromatography–Mass Spectrometry. *Environmental Science & Technology*, 51, 5052-5060.
- FOTOPOULOU, K. N. & KARAPANAGIOTI, H. K. 2012. Surface properties of beached plastic pellets. *Marine Environmental Research*, 81, 70-77.
- FRIAS, J. P. G. L., OTERO, V. & SOBRAL, P. 2014. Evidence of microplastics in samples of zooplankton from Portuguese coastal waters. *Marine Environmental Research*, 95, 89-95.
- FRIES, E., DEKIFF, J. H., WILLMEYER, J., NUELLE, M. T., EBERT, M. & REMY, D. 2013. Identification of polymer types and additives in marine microplastic particles using pyrolysis-GC/MS and scanning electron microscopy. *Environmental Sciences: Processes and Impacts*, 15, 1949-56.
- GAILLARD, C., STADELMANN, P. A., PLUMMER, C. J. G. & FUCHS, G. 2004. Practical method for high-resolution imaging of polymers by low-voltage scanning electron microscopy. *Scanning*, 26, 122-130.
- GEWERT, B. 2017. *Weathering of plastic materials and identification of chemicals in their leachates* [Online]. Stockholm University. [Accessed].
- GEWERT, B., PLASSMANN, M. M. & MACLEOD, M. 2015. Pathways for degradation of plastic polymers floating in the marine environment. *Environmental Science: Processes & Impacts*, 17, 1513-1521.
- GEYER, R., JAMBECK, J. R. & LAW, K. L. 2017. Production, use, and fate of all plastics ever made. *Science Advances*, 3.
- GIGAULT, J., PEDRONO, B., MAXIT, B. & TER HALLE, A. 2016. *Marine plastic litter: The unanalyzed nano-fraction*.
- GIRÃO, A. V., CAPUTO, G. & FERRO, M. C. 2017. Chapter 6 - Application of Scanning Electron Microscopy–Energy Dispersive X-Ray Spectroscopy (SEM-EDS). In: TERESA, A. P. R.-S. & ARMANDO, C. D. (eds.) *Comprehensive Analytical Chemistry*. Elsevier.
- GOTOH, K., HIROAKI, M. & HIGASHITANI, K. 1997. *Powder Technology Handbook*, New York, Marcel Dekker Inc.
- GRASSIE, N. & SCOTT, G. 1988. *Polymer Degradation and Stabilisation*, Cambridge University Press.
- GUAITA, M., CHIANTORE, O. & COSTA, L. 1985. Changes in degree of polymerization in the thermal degradation of polystyrene. *Polymer Degradation and Stability*, 12, 315-332.
- GULMINE, J. V., JANISSEK, P. R., HEISE, H. M. & AKCELRUD, L. 2002. Polyethylene characterization by FTIR. *Polymer Testing*, 21, 557-563.
- GUTIÉRREZ-CORREA, M., LUDENA, Y., RAMAGE, G. & VILLENA, G. 2012. *Recent Advances on Filamentous Fungal Biofilms for Industrial Uses*.
- HERMABESSIERE, L., DEHAUT, A., PAUL-PONT, I., LACROIX, C., JEZEQUEL, R., SOUDANT, P. & DUFLOS, G. 2017. Occurrence and effects of plastic additives on marine environments and organisms: A review. *Chemosphere*, 182, 781-793.
- HERNANDEZ, L. M., YOUSEFI, N. & TUFENKJI, N. 2017. Are There Nanoplastics in Your Personal Care Products? *Environmental Science & Technology Letters*, 4, 280-285.

- HERRERA, M., MATUSCHEK, G. & KETTRUP, A. 2003. Fast identification of polymer additives by pyrolysis-gas chromatography/mass spectrometry. *Journal of Analytical and Applied Pyrolysis*, 70, 35-42.
- HONG, S., LEE, J., LEE, C., YOON, S. J., JEON, S., KWON, B.-O., LEE, J.-H., GIESY, J. P. & KHIM, J. S. 2016. Are styrene oligomers in coastal sediments of an industrial area aryl hydrocarbon-receptor agonists? *Environmental pollution (Barking, Essex : 1987)*, 213, 913.
- HOPEWELL, J., DVORAK, R. & KOSIOR, E. 2009. Plastics recycling: challenges and opportunities. *Philosophical Transactions of the Royal Society of London B: Biological Sciences*, 364, 2115-2126.
- HUANG, J. & TURNER, S. R. 2018. Hypercrosslinked Polymers: A Review. *Polymer Reviews*, 58, 1-41.
- HUERTA LWANGA, E., MENDOZA VEGA, J., KU QUEJ, V., CHI, J. D. L. A., SANCHEZ DEL CID, L., CHI, C., ESCALONA SEGURA, G., GERTSEN, H., SALÁNKI, T., VAN DER PLOEG, M., KOELMANS, A. A. & GEISSEN, V. 2017. Field evidence for transfer of plastic debris along a terrestrial food chain. *Scientific Reports*, 7, 14071.
- HUMMEL, D. O. 2000. *IR Hummel Infrared Industrial Polymers* John Wiley & Son.
- IBRAHIM, D., WELOOSAMY, H. & LIM, S.-H. 2015. Effect of agitation speed on the morphology of *Aspergillus niger* HFD5A-1 hyphae and its pectinase production in submerged fermentation. *World Journal of Biological Chemistry*, 6, 265-271.
- IMHOF, H. K., SCHMID, J., NIESSNER, R., IVLEVA, N. P. & LAFORSCH, C. 2012. A novel, highly efficient method for the separation and quantification of plastic particles in sediments of aquatic environments. *Limnology and Oceanography-Methods*, 10, 524-537.
- ISO13322-1 2014. ISO/TC 24/SC 24: Particle size analysis - Image analysis methods. *Part 1: Static image analysis methods*. Geneva, Switzerland: International Organization for Standardization.
- ISO16232-7 2007. ISO/TC 22/SC 34: Road vehicles - Cleanliness of components for fluid circuits. *Part 7: Particle sizing and counting by microscopic analysis*. Geneva, Switzerland: International Organization for Standardization
- ISRAELI, Y., LACOSTE, J., LEMAIRE, J., SINGH, R. P. & SIVARAM, S. 1994. Photo- and thermoinitiated oxidation of high-impact polystyrene. I. Characterization by FT-IR spectroscopy. *Journal of Polymer Science Part A: Polymer Chemistry*, 32, 485-493.
- IVAR DO SUL, J. A. & COSTA, M. F. 2014. The present and future of microplastic pollution in the marine environment. *Environmental Pollution*, 185, 352-364.
- JAMBECK, J. R., GEYER, R., WILCOX, C., SIEGLER, T. R., PERRYMAN, M., ANDRADY, A., NARAYAN, R. & LAW, K. L. 2015. Plastic waste inputs from land into the ocean. *Science*, 347, 768-771.
- JANG, Y. C. L., JONGMYOUNG; HONG, SUNWOOK; CHOI, HYUN WOO; SHIM, WON JOON; HONG, SU YEON; 2015. Estimating the Global Inflow and Stock of Plastic Marine Debris Using Material Flow Analysis: a Preliminary Approach. *Journal of the Korean Society for Marine Environment and Energy*, 18, 263-273.
- JILLAVENKATESA, A., DAPKUNAS, S. J. & LUM, L.-S. H. 2001. Particle Size Characterization. In: TECHNOLOGY, N. I. O. S. A. (ed.) *NIST Recommended Practice Guide*. Washington: NIST.

- KNIGHT, J. 1976. Mechanical shear degradation of polymers in solution: A review. Royal Aircraft Establishment Technical Report 76073.
- KOELMANS, A. A., BESSELING, E. & SHIM, W. J. 2015. Nanoplastics in the Aquatic Environment. Critical Review. *In: BERGMANN, M., GUTOW, L. & KLAGES, M. (eds.) Marine Anthropogenic Litter*. Cham: Springer International Publishing.
- KOENIG, J. L. & RAPRA TECHNOLOGY, L. 2001. *Infrared and Raman Spectroscopy of Polymers*, Shawbury, Shrewsbury, Shropshire, U.K., Rapra Technology Ltd.
- KOOI, M., NES, E. H. V., SCHEFFER, M. & KOELMANS, A. A. 2017. Ups and Downs in the Ocean: Effects of Biofouling on Vertical Transport of Microplastics. *Environmental Science & Technology*, 51, 7963–7971.
- KOSTIS, H.-N. 2009. Global map of average Sea Surface Density. *In: DENSITYMAP_2000X1000.JPG* (ed.). NASA's Scientific Visualization Studio.
- KOWALSKI, N., REICHARDT, A. M. & WANIEK, J. J. 2016. Sinking rates of microplastics and potential implications of their alteration by physical, biological, and chemical factors. *Marine Pollution Bulletin*, 109, 310-319.
- KUPTSOV, A. H. & ZHIZHIN, G. N. 1998. *Handbook of Fourier Transform Raman and Infrared Spectra of Polymers*, Elsevier.
- KUSCH, P. 2013. Identification of Organic Additives in Nitrite Rubber Materials by Pyrolysis-GC-MS. *LC-GC North America*, 31, 248-254.
- KUSCH, P. 2014. Identification of Synthetic Polymers and Copolymers by Analytical Pyrolysis–Gas Chromatography/Mass Spectrometry. *Journal of Chemical Education*, 91, 1725-1728.
- KUSCH, P. 2017. Chapter 7 - Application of Pyrolysis-Gas Chromatography/Mass Spectrometry (Py-GC/MS). *In: TERESA, A. P. R.-S. & ARMANDO, C. D. (eds.) Comprehensive Analytical Chemistry*. Elsevier.
- KWON, J. H., CHANG, S., HONG, S. H. & SHIM, W. J. 2017. Microplastics as a vector of hydrophobic contaminants: Importance of hydrophobic additives. *Integrated Environmental Assessment and Management*, 13, 494-499.
- LAMBERT, S. & WAGNER, M. 2016a. Characterisation of nanoplastics during the degradation of polystyrene. *Chemosphere*, 145, 265-268.
- LAMBERT, S. & WAGNER, M. 2016b. Formation of microscopic particles during the degradation of different polymers. *Chemosphere*, 161, 510-517.
- LARKIN, P. 2011. *Infrared and Raman Spectroscopy : Principles and Spectral Interpretation*, Saint Louis, UNITED STATES, Elsevier Science.
- LASCH, P. 2012. Spectral pre-processing for biomedical vibrational spectroscopy and microspectroscopic imaging. *Chemometrics and Intelligent Laboratory Systems*, 117, 100-114.
- LEBRETON, L. C. M., ZWET, J. V. D., DAMSTEEG, J.-W., SLAT, B., ANDRADY, A. L. & REISSER, J. 2017. River plastic emissions to the world's oceans. *Nature Communications*, 8.
- LING, S. D., SINCLAIR, M., LEVI, C. J., REEVES, S. E. & EDGAR, G. J. 2017. Ubiquity of microplastics in coastal seafloor sediments. *Marine Pollution Bulletin*, 121, 104-110.

- LITHNER, D., LARSSON, Å. & DAVE, G. 2011. Environmental and health hazard ranking and assessment of plastic polymers based on chemical composition. *Science of The Total Environment*, 409, 3309-3324.
- LOULAD, S., HOUSSA, R., RHINANE, H., BOUMAAZ, A. & BENAZZOUZ, A. 2017. Spatial distribution of marine debris on the seafloor of Moroccan waters. *Marine Pollution Bulletin*, 124, 303-313.
- LUND, J. W. G., KIPLING, C. & LE CREN, E. D. 1958. The inverted microscope method of estimating algal numbers and the statistical basis of estimations by counting. *Hydrobiologia*, 11, 143-170.
- LUONGO, J. P. 1971. Polymer Characterization by ir Spectroscopy. *Applied Spectroscopy*, 25, 76-79.
- MAILHOT, B. & GARDETTE, J. L. 1992. Polystyrene photooxidation. 2. A pseudo wavelength effect. *Macromolecules*, 25, 4127-4133.
- MASUDA, H., HIGASHITANI, K. & YOSHIDA, H. 2006. *Powder Technology Handbook, Third Edition*, CRC Press.
- MATHALON, A. & HILL, P. 2014. Microplastic fibers in the intertidal ecosystem surrounding Halifax Harbor, Nova Scotia. *Marine Pollution Bulletin*, 81, 69-79.
- MERKUS, H. G. 2009. *Particle Size Measurements: Fundamentals, Practice, Quality*, Springer Netherlands.
- MILOSEVIC, M. 2012. *Internal Reflection and ATR Spectroscopy*, Wiley.
- MISRA, A. & SHAHIWALA, A. 2014. *Applications of Polymers in Drug Delivery*, Smithers Rapra Technology.
- MORÉ-T-FERGUSON, S., LAW, K. L., PROSKUROWSKI, G., MURPHY, E. K., PEACOCK, E. E. & REDDY, C. M. 2010. The size, mass, and composition of plastic debris in the western North Atlantic Ocean. *Marine Pollution Bulletin*, 60, 1873-1878.
- MUNTEAN, S. A., KEMPER, M., VAN IJZENDOORN, L. J. & LYULIN, A. V. 2011. Roughness and Ordering at the Interface of Oxidized Polystyrene and Water. *Langmuir*, 27, 8678-8686.
- MÜLLER, F.-M. C., SEIDLER, M. & BEAUVAIS, A. 2011. Aspergillus fumigatus biofilms in the clinical setting. *Medical Mycology*, 49, S96-S100.
- NADERI, M. 2015. Chapter Fourteen - Surface Area: Brunauer–Emmett–Teller (BET) A2 - Tarleton, Steve. *Progress in Filtration and Separation*. Oxford: Academic Press.
- NAKAISHI, K., OOI, S. & KOBAYASHI, M. 2012. Effects of Container Diameter and Volume Fraction on the Sedimentation Process of Flocculated Clay Suspensions. *Nihon Reorogi Gakkaishi*, 40, 205-208.
- NASA, G. S. F. C. S. V. S. 2009. Global map of average Sea Surface Density. In: DENSITYMAP_4000X2000.JPG (ed.). Helen-Nicole Kostis.
- NAYAR, S. & CHOU, L. M. 2003. Relative efficiencies of different filters in retaining phytoplankton for pigment and productivity studies. *Estuarine, Coastal and Shelf Science*, 58, 241-248.
- NEIHOF, R. A. & LOEB, G. I. 1972. THE SURFACE CHARGE OF PARTICULATE MATTER IN SEAWATER. *Limnology and Oceanography*, 17, 7-16.
- NEWBURY, D. E. & RITCHIE, N. W. M. 2015. Performing elemental microanalysis with high accuracy and high precision by scanning electron microscopy/silicon drift detector

- energy-dispersive X-ray spectrometry (SEM/SDD-EDS). *Journal of Materials Science*, 50, 493-518.
- NIC, M., JIRAT, J., NOMENCLATURE, D. O. C., PURE, S. R. I. U. O., CHEMISTRY, A. & KOSATA, B. 2006. *IUPAC goldbook*, IUPAC.
- NOAA 1988. Experimental Demonstration of Controlled Photodegradation of Relevant Plastic Compositions under Marine Environmental Conditions. *In: COMMERCE, U. S. D. O.* (ed.). North Carolina: Northwest and Alaska Fisheries Center.
- NOAA 2015. Laboratory Methods for the Analysis of Microplastics in Marine Environment: recommendations for quantifying synthetic particles in waters and sediments.pdf. *In: MASUREA, J., BAKER, J., FOSTER, G., ARTHUR, C. & HERRING, C.* (eds.). USA: National Oceanic and Atmospheric Administration
- NODA, I., STORY, G. M. & MARCOTT, C. 1999. Pressure-induced transitions of polyethylene studied by two-dimensional infrared correlation spectroscopy. *Vibrational Spectroscopy*, 19, 461-465.
- NURUZATULIFAH, A. M., NIZAM, A. A. & AIN, N. M. N. 2016. Synthesis and Characterization of Polystyrene Nanoparticles with Covalently Attached Fluorescent Dye. *Materials Today: Proceedings*, 3, S112-S119.
- OLSETH, J. A. & SKARTVEIT, A. 1986. The solar radiation climate of Norway. *Solar Energy*, 37, 423-428.
- PAVIA, D. L., LAMPMAN, G. M., KRIZ, G. S. & VYVYAN, J. A. 2014. *Introduction to Spectroscopy*, Cengage Learning.
- PHUONG, N. N., ZALOUK-VERGNOUX, A., KAMARI, A., MOUNEYRAC, C., AMIARD, F., POIRIER, L. & LAGARDE, F. 2017. Quantification and characterization of microplastics in blue mussels (*Mytilus edulis*): protocol setup and preliminary data on the contamination of the French Atlantic coast. *Environmental Science and Pollution Research*.
- PLASTICSEUROPE 2016. An analysis of European plastics production, demand and waste data. *Plastics - the Facts*. Brussels.
- PRAVETTONI, R. 2016. Natural processes affecting the distribution and fate of plastics. *In: 32361765545_9A17376DEC_O.JPG* (ed.). GRID-Arendal and Maphoto.
- QUASCHNING, V. 2016. *Understanding Renewable Energy Systems*, Taylor & Francis.
- QUESNEL, D. J., RIMAI, R. S. & SHARPE, L. H. 2002. *Particle Adhesion: Applications and Advances*, Taylor & Francis.
- QUINN, B., MURPHY, F. & EWINS, C. 2017. Validation of density separation for the rapid recovery of microplastics from sediment. *Analytical Methods*, 9, 1491-1498.
- RABEK, J. F. 1990. *Photostabilization of polymers: principles and applications*, Elsevier Applied Science.
- REDDY, M. S., SHAIK, B., ADIMURTHY, S. & RAMACHANDRAIAH, G. 2006. Description of the small plastics fragments in marine sediments along the Alang-Sosiya ship-breaking yard, India. *Estuarine, Coastal and Shelf Science*, 68, 656-660.
- REES, O. J. 2010. *Fourier Transform Infrared Spectroscopy : Developments, Techniques, and Applications*, New York, Nova Science Publishers, Inc.

- REINEY, M. J., TRYON, M. & ACHHAMMER, B. G. 1953. Study of Degradation of Polystyrene, Using Ultraviolet Spectrophotometry. *Journal of Research of the National Bureau of Standards*, 51, 155-165.
- RENNER, G., SCHMIDT, T. C. & SCHRAM, J. 2017. Chapter 4 - Characterization and Quantification of Microplastics by Infrared Spectroscopy. In: TERESA, A. P. R.-S. & ARMANDO, C. D. (eds.) *Comprehensive Analytical Chemistry*. Elsevier.
- RIOS, L. M. & JONES, P. R. 2015. Characterisation of microplastics and toxic chemicals extracted from microplastic samples from the North Pacific Gyre. *Environmental Chemistry*, 12, 611-617.
- ROBERTSON, G. L. 2016. *Food Packaging: Principles and Practice, Third Edition*, CRC Press.
- ROCHA-SANTOS, T. & DUARTE, A. C. 2017. *Characterization and Analysis of Microplastics*, [Place of publication not identified], Elsevier.
- SEACHRIST, D. D., BONK, K. W., HO, S.-M., PRINS, G. S., SOTO, A. M. & KERI, R. A. 2016. A review of the carcinogenic potential of bisphenol A. *Reproductive Toxicology*, 59, 167-182.
- SHIM, W. J., SONG, Y. K., HONG, S. H. & JANG, M. 2016. Identification and quantification of microplastics using Nile Red staining. *Marine Pollution Bulletin*, 113, 469-476.
- SHYICHUK, A. V. & WHITE, J. R. 2000. Analysis of chain-scission and crosslinking rates in the photo-oxidation of polystyrene. *Journal of Applied Polymer Science*, 77, 3015-3023.
- SIGLER, M. 2014. The Effects of Plastic Pollution on Aquatic Wildlife: Current Situations and Future Solutions. *Water, Air, & Soil Pollution*, 225.
- SINGH, B. & SHARMA, N. 2008. Mechanistic implications of plastic degradation. *Polymer Degradation and Stability*, 93, 561-584.
- SONDI, I. & PRAVDIC, V. 1998. The Colloid and Surface Chemistry of Clays in Natural Waters. *Croatica Chemica Acta*, 71, 1061-1074.
- SONG, Y. K., HONG, S. H., JANG, M., HAN, G. M., JUNG, S. W. & SHIM, W. J. 2017. Combined Effects of UV Exposure Duration and Mechanical Abrasion on Microplastic Fragmentation by Polymer Type. *Environmental Science & Technology*, 51, 4368-4376.
- SONG, Y. K., HONG, S. H., JANG, M., HAN, G. M. & SHIM, W. J. 2015. Occurrence and Distribution of Microplastics in the Sea Surface Microlayer in Jinhae Bay, South Korea. *Archives of Environmental Contamination and Toxicology*, 69, 279-287.
- STAMM, M. 2008. Polymer Surface and Interface Characterization Techniques. In: STAMM, M. (ed.) *Polymer Surfaces and Interfaces*. 1 ed. Germany: Springer.
- STEVENS, E. S. 2002. *Green Plastics: An Introduction to the New Science of Biodegradable Plastics*, Princeton University Press.
- STRAND, J., LASSEN, P., SHASHOUA, Y. & ANDERSEN, J. H. 2013. Poster: Microplastic particles in sediments from Danish waters. *ICES Annual Science Conference*. Iceland.
- STUART, B. H. 2004. *Infrared Spectroscopy*, Hoboken, John Wiley & Sons, Incorporated.
- STUART, B. H. & ANDO, D. J. 1997. *Biological Applications of Infrared Spectroscopy*, Wiley.
- SU, L., CAI, H., KOLANDHASAMY, P., WU, C., ROCHMAN, C. M. & SHI, H. 2018. Using the Asian clam as an indicator of microplastic pollution in freshwater ecosystems. *Environmental Pollution*, 234, 347-355.

- SUHRHOFF, T. J. & SCHOLZ-BÖTTCHER, B. M. 2016. Qualitative impact of salinity, UV radiation and turbulence on leaching of organic plastic additives from four common plastics — A lab experiment. *Marine Pollution Bulletin*, 102, 84-94.
- SUTHERLAND, B. R., BARRETT, K. J. & GINGRAS, M. K. 2014. Clay settling in fresh and salt water. *Environmental Fluid Mechanics*, 15, 147-160.
- SUTHINDHIRAN, K. & KANNABIRAN, K. 2010. Diversity and exploration of bioactive marine actinomycetes in the Bay of Bengal of the Puducherry coast of India. *Indian Journal of Microbiology*, 50, 76-82.
- SØRENSEN, L., MELBYE, A. G. & BOOTH, A. M. 2014. Oil droplet interaction with suspended sediment in the seawater column: Influence of physical parameters and chemical dispersants. *Marine Pollution Bulletin*, 78, 146-152.
- TAKEDA, M., IIMURA, K., YAMADA, A. & IMAMURA, Y. 1959. Infrared Spectra of Crystalline and Amorphous Polystyrene. *Bulletin of the Chemical Society of Japan*, 32, 1150-1152.
- TAYLOR, M. L., GWINNETT, C., ROBINSON, L. F. & WOODALL, L. C. 2016. Plastic microfibre ingestion by deep-sea organisms. *Scientific Reports (Nature Publisher Group)*, 6, 33997.
- TEUTEN, E. L., SAQUING, J. M., KNAPPE, D. R. U., BARLAZ, M. A., JONSSON, S., BJÖRN, A., ROWLAND, S. J., THOMPSON, R. C., GALLOWAY, T. S., YAMASHITA, R., OCHI, D., WATANUKI, Y., MOORE, C., VIET, P. H., TANA, T. S., PRUDENTE, M., BOONYATUMANOND, R., ZAKARIA, M. P., AKKHAVONG, K., OGATA, Y., HIRAI, H., IWASA, S., MIZUKAWA, K., HAGINO, Y., IMAMURA, A., SAHA, M. & TAKADA, H. 2009. Transport and release of chemicals from plastics to the environment and to wildlife. *Philosophical Transactions of the Royal Society of London B: Biological Sciences*, 364, 2027-2045.
- THOMAS, S., GROHENS, Y. & JYOTISHKUMAR, P. 2014. *Characterization of Polymer Blends: Miscibility, Morphology and Interfaces*, Wiley.
- THOMPSON, R. C., OLSEN, Y., MITCHELL, R. P., DAVIS, A., ROWLAND, S. J., JOHN, A. W. G., MCGONIGLE, D. & RUSSELL, A. E. 2004. Lost at Sea: Where Is All the Plastic? *Science*, 304, 838.
- TIMÁR, G., BLÖMER, J., KUN, F. & HERRMANN, H. J. 2010. New Universality Class for the Fragmentation of Plastic Materials. *Physical Review Letters*, 104, 095502.
- TSUGE, S., OHTANI, H. & WATANABE, C. 2011. *Pyrolysis-GC/MS Data Book of Synthetic Polymers, Pyrograms, Thermograms and MS of Pyrolyzates*, Great Britain, ELSEVIER.
- UNEP 2010. Assessing the Environmental Impacts of Consumption and Production: Priority Products and Materials, A Report of the Working Group on the Environmental Impacts of Products and Materials to the International Panel for Sustainable Resource Management. In: HERTWICH, E., VOET, E. V. D., SUH, S., M., A. T. A. H., KAZMIERCZYK, P., LENZEN, M., MCNEELY, J. & MORIGUCHI, Y. (eds.).
- URGERT, W. 2015. *Microplastics in the rivers Meuse and Rhine: Developing guidance for a possible future monitoring program*. Master's thesis, Open University of the Netherlands.
- VAN CAUWENBERGHE, L., DEVRIESE, L., GALGANI, F., ROBBENS, J. & JANSSEN, C. R. 2015. Microplastics in sediments: A review of techniques, occurrence and effects. *Marine Environmental Research*, 111, 5-17.

- VAN CAUWENBERGHE, L., VANREUSEL, A., MEES, J. & JANSSEN, C. R. 2013. Microplastic pollution in deep-sea sediments. *Environmental Pollution*, 182, 495-499.
- VAN FRANEKER, J. A. & LAW, K. L. 2015. Seabirds, gyres and global trends in plastic pollution. *Environmental Pollution*, 203, 89-96.
- VASILE, C., PASCU, M. & LIMITED, R. T. 2005. *Practical Guide to Polyethylene*, RAPRA Technology.
- VETHAAK, A. D. & LESLIE, H. A. 2016. Plastic Debris Is a Human Health Issue. *Environmental Science & Technology*, 50, 6825-6826.
- VIGNOLA, F., MICHALSKY, J. & STOFFEL, T. 2016. *Solar and Infrared Radiation Measurements*, CRC Press.
- VROOM, R. J. E., KOELMANS, A. A., BESSELING, E. & HALSBAND, C. 2017. Aging of microplastics promotes their ingestion by marine zooplankton. *Environmental Pollution*, 231, 987-996.
- WAGNER, M. & LAMBERT, S. 2017. *Freshwater Microplastics: Emerging Environmental Contaminants?*, Springer International Publishing.
- WALLACE, W. E. & BLAIR, W. R. 2007. Matrix-assisted laser desorption/ionization mass spectrometry of covalently cationized polyethylene as a function of sample temperature. *International Journal of Mass Spectrometry*, 263, 82-87.
- WALLENBERGER, F. T. & BINGHAM, P. A. 2009. *Fiberglass and Glass Technology: Energy-Friendly Compositions and Applications*, Springer US.
- WANG, F. C.-Y. 2000. Polymer additive analysis by pyrolysis–gas chromatography: I. Plasticizers. *Journal of Chromatography A*, 883, 199-210.
- WANG, J., TAN, Z., PENG, J., QIU, Q. & LI, M. 2016. The behaviors of microplastics in the marine environment. *Marine Environmental Research*, 113, 7-17.
- WANG, Z.-M., WAGNER, J., GHOSAL, S., BEDI, G. & WALL, S. 2017. SEM/EDS and optical microscopy analyses of microplastics in ocean trawl and fish guts. *Science of The Total Environment*, 603, 616-626.
- WARD, M. 2013. *Marine Microplastic Removal Tool*.
- WARNOCK, D. W., CAMPBELL, C. K. & JOHNSON, E. M. 2013. *Identification of Pathogenic Fungi*, Chichester, UNITED KINGDOM, John Wiley & Sons, Incorporated.
- WEF 2016. The New Plastics Economy: Rethinking the future of plastics. World Economic Forum.
- WELLS, P. G., BUTLER, J. N. & HUGHES, J. S. 1995. *Exxon Valdez Oil Spill: Fate and Effects in Alaskan Waters*, ASTM.
- WESSEL, C. C., LOCKRIDGE, G. R., BATTISTE, D. & CEBRIAN, J. 2016. Abundance and characteristics of microplastics in beach sediments: Insights into microplastic accumulation in northern Gulf of Mexico estuaries. *Marine Pollution Bulletin*, 109, 178-183.
- WOODALL, L. C., SANCHEZ-VIDAL, A., CANALS, M., PATERSON, G. L. J., COPPOCK, R., SLEIGHT, V., CALAFAT, A., ROGERS, A. D., NARAYANASWAMY, B. E. & THOMPSON, R. C. 2014. The deep sea is a major sink for microplastic debris. *Royal Society Open Science*, 1.
- WOZNIAK, B. & DERA, J. 2007. *Light Absorption in Sea Water*, Springer New York.

- WRIGHT, S. L. & KELLY, F. J. 2017. Plastic and Human Health: A Micro Issue? *Environmental Science & Technology*, 51, 6634-6647.
- WRIGHT, S. L., THOMPSON, R. C. & GALLOWAY, T. S. 2013. The physical impacts of microplastics on marine organisms: A review. *Environmental Pollution*, 178, 483-492.
- WYZGOSKI, F. J., POLCE, M. J., WESDEMIOTIS, C. & ARNOULD, M. A. 2007. Matrix-assisted laser desorption/ionization time-of-flight mass spectrometry investigations of polystyrene and poly(methyl methacrylate) produced by monoacylphosphine oxide photoinitiation. *Journal of Polymer Science Part A: Polymer Chemistry*, 45, 2161-2171.
- XINGZHOU, H. 1997. Wavelength sensitivity of photo-oxidation of polyethylene. *Polymer Degradation and Stability*, 55, 131-134.
- YANG, R., ZHAO, J. & LIU, Y. 2013. Oxidative degradation products analysis of polymer materials by pyrolysis gas chromatography–mass spectrometry. *Polymer Degradation and Stability*, 98, 2466-2472.
- YOUSIF, E. & HADDAD, R. 2013. Photodegradation and photostabilization of polymers, especially polystyrene: review. *SpringerPlus*, 2, 398.
- YOUSIF, E., SALIMON, J. & SALIH, N. 2012. New stabilizers for polystyrene based on 2-N-salicylidene-5-(substituted)-1,3,4-thiadiazole compounds. *Journal of Saudi Chemical Society*, 16, 299-306.
- ZHANG, Z., GUO, K., LI, Y., LI, X., GUAN, G., LI, H., LUO, Y., ZHAO, F., ZHANG, Q., WEI, B., PEI, Q. & PENG, H. 2015. A colour-tunable, weavable fibre-shaped polymer light-emitting electrochemical cell. *Nat Photon*, 9, 233-238.
- ZIAJAHROMI, S., NEALE, P. A. & LEUSCH, F. D. L. 2016. Wastewater treatment plant effluent as a source of microplastics: review of the fate, chemical interactions and potential risks to aquatic organisms. *Water Science and Technology*, 74, 2253-2269.

Appendix

A. Supplementary information

Table A.1: Additional information about the microplastic materials provided by the suppliers.

Material	Supplier	Additional information from Supplier												
PE-10	Cospheric	Product name: Clear Polyethylene Microspheres Form: Solid Size: 3-16 μm Mass: 200 mg Bead density: 0.96 g/cm^3												
PS-10	PolySciences	Product name: Polybead® Polystyrene Microspheres Form: 2.5 % w/v suspension (DI water) with residual surfactant Size: 10.0 μm Volume: 5 mL Bead density: 1.05 g/cm^3 Coefficient of variance: $\leq 10\%$ Particles/mL: 4.55×10^7												
PE-100^a	Total (pristine pellets) CARAT (grinded material)	Product name: Lotréne® FD0270 Low Density Polyethylene Size: ~5 mm Melting point: 112 °C Tensile strength, yield (break) MD/TD: 12/12 MPa (28/24 MPa) Density (at 23 °C): 0.923 g/cm^3 Softening point: 96 °C Preparation of MP: Cryogenic grinding, size determination (sieving): <table border="1"> <thead> <tr> <th>Sieve-size (mm)</th> <th>8</th> <th>6.3</th> <th>4.5</th> <th>3.15</th> <th><3.15</th> </tr> </thead> <tbody> <tr> <td>Sieve-residue (%)</td> <td>0</td> <td>0</td> <td>0</td> <td>99.8</td> <td>0.2</td> </tr> </tbody> </table> Antioxidants and stabilizers: < 0.7 % ICP-OES elemental analysis (ppm): Ca (8), K (7), Ti (8) and Zn (20)	Sieve-size (mm)	8	6.3	4.5	3.15	<3.15	Sieve-residue (%)	0	0	0	99.8	0.2
Sieve-size (mm)	8	6.3	4.5	3.15	<3.15									
Sieve-residue (%)	0	0	0	99.8	0.2									
PS-100^a	STYRON™ (pristine pellets) CARAT (grinded material)	Product name: STYRON™ 637 Clear Polystyrene Components: 95-100 % styrene polymers, 0-5 % white mineral oil Size: ~5 mm Softening point: 207 °C Tensile strength, yield (break): 55.0 MPa (2.0 %) Density: 1.05 g/cm^3 Preparation of MP: Cryogenic grinding, size determination (sieving): <table border="1"> <thead> <tr> <th>Sieve-size (mm)</th> <th>4.5</th> <th>3.15</th> <th>2.00</th> <th>1.00</th> <th><1.00</th> </tr> </thead> <tbody> <tr> <td>Sieve-residue (%)</td> <td>0</td> <td>4.9</td> <td>95.0</td> <td>0.1</td> <td>0</td> </tr> </tbody> </table> T _g : 95 °C ICP-OES element analysis: Cu and Zn present	Sieve-size (mm)	4.5	3.15	2.00	1.00	<1.00	Sieve-residue (%)	0	4.9	95.0	0.1	0
Sieve-size (mm)	4.5	3.15	2.00	1.00	<1.00									
Sieve-residue (%)	0	4.9	95.0	0.1	0									

^a PE-100 and PS-100 was produced by grinding 5 mm pellets. Properties of both the 5 mm pellets (Total/STYRON™) and the ground material (CARAT) is included.

B. Calculations

B.1 Experimental irradiance versus annual irradiance in Trondheim

The experimental irradiance was 765 W/m^2 in the 290-800 nm region (maximum irradiance setting on the Atlas SunTest CPS+). The annual global solar insolation in Trondheim is $870 \text{ kWh/m}^2/\text{yr}$ (Olseth and Skartveit, 1986). Insolation (H) is irradiance (E_e) over a specific period of time, so the annual global solar insolation can be converted to irradiance according to Equation 4:

$$(4) \quad E_e (\text{Wm}^{-2}) = \frac{H_{h,yr} (\text{kWhm}^{-2}\text{yr}^{-1})}{24 \text{ h} \times 365 \text{ d}} \times 1000$$

Hence, the average irradiance in Trondheim ($E_{e,T}$) is:

$$E_{e,T} = \frac{870 \text{ kWhm}^{-2}\text{yr}^{-1}}{24 \text{ h} \times 365 \text{ d}} \times 1000 = 99.3 \text{ Wm}^{-2}$$

The ratio (R) of the experimental irradiance ($E_{e,E}$) and the average irradiance in Trondheim ($E_{e,T}$) is:

$$R = \frac{E_{e,E}}{E_{e,T}} = \frac{765 \text{ Wm}^{-2}}{99.3 \text{ Wm}^{-2}} = 7.70$$

A ratio of 7.70 means that 24 hours of irradiation in the Atlas SunTest equals 185 hours of average solar irradiance in Trondheim.

C. Method and method development

Table A.2: Detailed list of samples in photodegradation experiment.

Sample letter	Sample name	MP		UV exposure	Sampling day
		Type	Amount		
a	PS-10-UV t_0	PS-10	600 μ L	x	0
b	PS-10-UV t_{10}	PS-10	600 μ L	x	10
c	PS-10-UV t_{20}	PS-10	600 μ L	x	20
d	PS-10-UV t_{40}	PS-10	600 μ L	x	40
e	PS-10-UV t_{40}	PS-10	600 μ L	x	80
f	PS-10-UV control t_{40}	PS-10	600 μ L		40
g	PE-10-UV t_0	PE-10	15 mg	x	0
h	PE-10-UV t_{10}	PE-10	15 mg	x	10
i	PE-10-UV t_{20}	PE-10	15 mg	x	20
j	PE-10-UV t_{40}	PE-10	15 mg	x	40
k	PE-10-UV t_{80}	PE-10	15 mg	x	80
l	PE-10-UV control t_{40}	PE-10	15 mg		40

Table A.3: Detailed list of samples in mechanical degradation experiment, part 1/2: PS-10 and PE-10.

Sample number	Sample name	MP		Soil		Sampling day
		Type	Amount	Type	Mass	
1	PS-10-silt t_0	PS-10	600 μ L	Silt	5 g	0
2	PS-10-silt t_{20}	PS-10	600 μ L	Silt	5 g	20
3	PS-10-silt t_{40}	PS-10	600 μ L	Silt	5 g	40
4	PS-10-silt t_{80}	PS-10	600 μ L	Silt	5 g	80
5	PS-10-sand t_0	PS-10	600 μ L	Sand	5 g	0
6	PS-10-sand t_{20}	PS-10	600 μ L	Sand	5 g	20
7	PS-10-sand t_{40}	PS-10	600 μ L	Sand	5 g	40
8	PS-10-sand t_{80}	PS-10	600 μ L	Sand	5 g	80
9	PE-10-sed control t_0	PS-10	600 μ L	-	-	40
10	PE-10-silt t_0	PE-10	15 mg	Silt	5 g	0
11	PE-10-silt t_{20}	PE-10	15 mg	Silt	5 g	20
12	PE-10-silt t_{40}	PE-10	15 mg	Silt	5 g	40
13	PE-10-silt t_{80}	PE-10	15 mg	Silt	5 g	80
14	PE-10-sand t_0	PE-10	15 mg	Sand	5 g	0
15	PE-10-sand t_{20}	PE-10	15 mg	Sand	5 g	20
16	PE-10-sand t_{40}	PE-10	15 mg	Sand	5 g	40
17	PE-10-sand t_{80}	PE-10	15 mg	Sand	5 g	80
18	PE-10-sed control t_{40}	PE-10	15 mg	-	-	40

Table A.4: Detailed list of samples in mechanical degradation experiment, part 2/2: PS-100, PE-100 and sediment blanks.

Sample number	Sample name	MP		Soil		Sampling day
		Type	Amount	Type	Mass	
19	PS-100-silt t_0	PS-100	100 mg	Silt	5 g	0
20	PS-100-silt t_{20}	PS-100	100 mg	Silt	5 g	20
21	PS-100-silt t_{40}	PS-100	100 mg	Silt	5 g	40
22	PS-100-silt t_{80}	PS-100	100 mg	Silt	5 g	80
23	PS-100-sand t_0	PS-100	100 mg	Sand	5 g	0
24	PS-100-sand t_{20}	PS-100	100 mg	Sand	5 g	20
25	PS-100-sand t_{40}	PS-100	100 mg	Sand	5 g	40
26	PS-100-sand t_{80}	PS-100	100 mg	Sand	5 g	80
27	PS-100-sed control t_{40}	PS-100	100 mg	-	-	40
28	PE-100-silt t_0	PE-100	100 mg	Silt	5 g	0
29	PE-100-silt t_{20}	PE-100	100 mg	Silt	5 g	20
30	PE-100-silt t_{40}	PE-100	100 mg	Silt	5 g	40
31	PE-100-silt t_{80}	PE-100	100 mg	Silt	5 g	80
32	PE-100-sand t_0	PE-100	100 mg	Sand	5 g	0
33	PE-100-sand t_{20}	PE-100	100 mg	Sand	5 g	20
34	PE-100-sand t_{40}	PE-100	100 mg	Sand	5 g	40
35	PE-100-sand t_{80}	PE-100	100 mg	Sand	5 g	80
36	PE-100-sed control t_{40}	PE-100	100 mg	-	-	40
37	Silt blank t_{40}	-	-	Silt	5 g	40
38	Silt blank t_{80}	-	-	Silt	5 g	80
39	Sand blank t_{40}	-	-	Sand	5 g	40
40	Sand blank t_{80}	-	-	Sand	5 g	80

Table A.5: Parameters tested during the method development of pyrolysis gas chromatography – mass spectrometry analysis of microplastic samples.

Parameter	Tested settings
Sample type	<ul style="list-style-type: none"> • PS standard (Pyrola), $c = 7.5 \mu\text{g}/\mu\text{L}$ in toluene • PE-10 and PS-10 • Piece of a plastic bag ($d \approx 0.5 \text{ mm}$), PE • Piece of a plastic fork ($d \approx 0.5 \text{ mm}$), PS • Dispersants (Tween 20, Tween 80 and sodium dodecyl sulphate) • Green fluorescent microspheres (unknown), 1-5 μm
Sample preparation	<ul style="list-style-type: none"> • None • Careful melting/fixation with blow torch • Fixation with a drop of toluene ($\sim 0.5 \mu\text{L}$) <ul style="list-style-type: none"> ○ Natural evaporation (1 and 5 min) ○ Drying with blow torch
Sample amount	<ul style="list-style-type: none"> • Aqueous samples: 0.8 - 1 μL • Solids: diameters between 0.2 - 0.7 mm (10-100 μg)
Pyrolysis settings	<ul style="list-style-type: none"> • Ramp pyrolysis <ul style="list-style-type: none"> ○ 100 – 300 °C (rate: 10 mA/s) • Manual fractionation <ul style="list-style-type: none"> ○ 150 (15 s), 250 (15 s), 350 (15 s), 700 (5 s) °C ○ 150 (10 s), 250 (10 s), 350 (10 s), 700 (3 s) °C ○ 250 (5 s), 400 (5 s), 700 (5 s) °C ○ 250 (5 s), 600 (5 s) °C • Direct pyrolysis <ul style="list-style-type: none"> ○ 700 °C for 2-5 s ○ 600 °C for 5 s (Tsuge et al., 2011)
GC settings	<ul style="list-style-type: none"> • Temperature programs <ul style="list-style-type: none"> ○ Method A: 50 – 300 °C at 15 °C/min (5 min hold) ○ Method B: 60 °C (1 min hold), 60 – 100 °C at 2.5 °C/min, 100 – 300 °C at 10 °C/min (5 min hold) (Kusch, 2014) ○ Method C: 40 – 90 °C at 5 °C/min, 90 – 300 °C at 10 °C/min (5 min hold) ○ Method D: 40 °C (2 min hold), 40 – 320 °C at 20 °C/min, (13 min hold) (Tsuge et al., 2011)
MS settings	<ul style="list-style-type: none"> • Mass ranges <ul style="list-style-type: none"> ○ 41 – 600 m/z ○ 33 – 600 m/z ○ 29 – 600 m/z, 70 amu/s (Tsuge et al., 2011)

D. Results

Table A.6: MP recoveries for photodegradation experiment

Weathering time (days)	Recovery (mg)	
	<i>PE-10</i>	<i>PS-10</i>
0	11.8	3.4
10	7.6	9.0
20	9.5	11.7
40	5.1	11.3
80	9.9	8.9
Control (40)	6.6	6.5

Table A.7: MP recoveries for mechanical weathering experiment

Soil type	Weathering time (days)	Recovery (mg)				
		<i>PE-10</i>	<i>PS-10</i>	<i>PE-100</i>	<i>PS-100</i>	<i>None (blank)</i>
Silt	0	0.0 ^a	0.0 ^a	63.8	54.9	/
	20	0.4	0.0	63.2 ^b	80.1 ^b	/
	40	-	-	65.3	66.7	0.0
	80	-	-	69.7	66.1	0.0
Sand	0	2.0 ^a	0.0 ^a	85.6	68.1	/
	20	7.8	7.7	75.0	70.7	/
	40	11.7	11.1	81.5	72.7	0.0
	80	10.8	4.6	89.0	85.9	1.0 ^c
None (control)	40	13.1	10.6	86.8	69.7	/

- Not extracted due to low recoveries and insufficient separation from the silt

/ Not prepared, MP controls only at t_{40} , and silt/sand blanks at t_{40} and t_{80}

^a Whatman GF/F filter, changed to Millipore HA for remaining PE-10 and PS-10 samples

^b Recovered MP was accidentally placed in the same vial, but recoveries recorded separately

^c Sand residue

Table A.8: Substances desorbed (250 °C) from photodegraded PS-10.

t_R (min)	Abbreviation	Chemical name	Present in			
			t_0	t_{40}	t_{80}	Control (t_{40})
3.91	F ₁	Ethylbenzene			x	
6.57	O ₁	Benzoylformic acid			x	
6.84	O ₂	2,2-dihydroxy-1-phenylethanone			x	
9.55	O ₃	2,2-bisacetoxy-acetophenone			x	
9.68	O ₄	Unknown (contains oxygen)			x	
12.34	O ₅	Benzoic acid			x	
13.68	A ₁	Unknown (contains nitrogen)	x		x	
14.76	O ₆	1,2-benzenedicarboxylic acid			x	
15.86	F ₂	Biphenyl		x	x	
17.59	O ₇	Sinapyl alcohol			x	
18.61	A ₂	Diethyl phthalate			x	
19.20	A ₃	Unknown (contains fluoride)	x		x	
20.93	A ₄	Unknown (contains chloride)	x		x	

Table A.9: Polymer-characteristic pyrolysis products (600 °C) from photodegraded PS-10.

Mean t_R (min)	Abbreviation	Chemical name	Relative area (%)			
			t_0	t_{40}	t_{80}	Control (t_{40})
2,81	T	Toluene	0,46	1,08	1,57	0,40
5,21	S	Styrene (monomer)	60,3	62,8	56,3	71,5
6,40	AB	Allylbenzene	0,18	0,40	0,57	0,19
7,34	aS	α -methylstyrene	0,25	0,86	1,47	0,30
17,81	D ₁	1,2-diphenylethane	0,32	0,33	0,34	0,35
18,68	D ₂	propane-1,2-diyldibenzene	0,01	0,11	0,18	0,08
19,00	D ₃	3-butene-1,2-diyldibenzene	0,17	0,12	0,11	0,15
19,44	D ₄	propane-1,3-diyldibenzene	0,04	0,41	0,86	0,02
20,21	SS	3-butene-1,3-diyldibenzene	6,92	3,23	1,98	4,27
20,27	D ₅	1-pentene-2,4-diyldibenzene	0,14	0,28	0,24	0,13
21,31	D ₆	(E)-1-butene-diyldibenzene	0,23	0,71	1,50	0,53
22,06	D ₇	hexa-1,5-diene-2,5-diyldibenzene	0,54	0,25	0,18	0,34
27,12	SSS	5-hexene-1,3,5-triyltribenzene	24,5	19,5	18,4	17,8

Table A.10: Degradation-characteristic pyrolysis products (600 °C) from photodegraded PS-10.

t_R (min)	Abbreviation	Chemical name	Present in			
			t_0	t_{40}	t_{80}	Control (t_{40})
6.82	O ₁	Phenacylidene diacetate	x	x	x	x
12.26	O ₂	Benzoic acid			x	
12.98	O ₃	Phenoxyethene		x	x	
13.15	O ₄	3-methylbenzaldehyde		x	x	
16.62	F ₁	Diphenylmethane	x	x	x	x
18.83	F ₂	4-phenyl-tetracyclo[4.2.1.0(3,7).0(2,9)]non-4-ene	x	x	x	x
19.22	F ₃	4-ethenyl-1,1'-biphenyl	x	x	x	x
19.45	F ₄	1,1'-(1,3-propanediyl)bisbenzene			x	
20.41	F ₅	1,1'-cycloproylidenebisbenzene			x	
21.30	F ₆	1,4-diphenyl-(E,E)-1,3-butadiene			x	
23.12	O ₅	1,3-diphenyl-2-propen-1-one			x	
29.28	F ₇	[3-(diphenylmethylene)cyclopentyl]benzene		x	x	
29.54	O ₆	2-benzylidene-1,4-ethano-1,2,3,4-tetrahydroantracen-3-ol		x	x	
29.66	F ₈	[3-(diphenylmethylene)cyclopentyl]benzene		x	x	